Regulation of Actin dynamics by Formin in early *Drosophila* embryogenesis

Dissertation
for the award of the degree
"Doctor rerum naturalium"
of the Georg-August-Universität Göttingen

in the GGNB program "Genes and Development"

at the Georg-August-Universität Göttingen

Faculty of Biology

submitted by
Zhiyi Lv
born Shanxi, China

Göttingen October 2014

Thesis Committee

Prof. Dr. Jörg Großhans (Supervisor)

Department of Developmental Biochemistry , Universitätsmedizin Göttingen

Prof. Dr. Reinhard Schuh

Department of Molecular Developmental Biology, MPI for Biophysical Chemistry, Göttingen

Prof. Dr. Dirk Görlich

Department of Cellular Logistics, MPI for Biophysical Chemistry, Göttingen

Members of the Examination Board

Reviewer: **Prof. Dr. Jörg Großhans**

Department of Developmental Biochemistry , Universitätsmedizin Göttingen

Second Reviewer: **Prof. Dr. Reinhard Schuh**

Department of Molecular Developmental Biology, MPI for Biophysical Chemistry, Göttingen

Further members of the Examination Board:

Prof. Dr. Dirk Görlich

Department of Cellular Logistics, MPI for Biophysical Chemistry, Göttingen

Prof. Dr. Gregor Bucher

Department of Evolutionary Developmental Genetics, University of Göttingen

Prof. Dr. Blanche Schwappach,

Department of Molecular Biology, Universitätsmedizin Göttingen

PD.Dr. Halyna Shcherbata

Research group of Gene expression and signaling, MPI for Biophysical Chemistry, Göttingen

Date of the oral examiniation: 18.12.2014

Publication list

Shuling Yan,* **Zhiyi Lv,*** Moritz Winterhoff,* Christian Wenzl, Thomas Zobel, Jan Faix, Sven Bogdan, and Jörg Grosshans. 2013. The F-BAR protein Cip4/Toca-1 antagonizes the formin Diaphanous in membrane stabilization and compartmentalization. *J Cell Sci* 126, 1796-1805.
* equally contribution

Gummalla, M., Winkler, F., Kuenneke, L., **Lv, Z**., Zippelius, A., Aspelmeier, T., and Grosshans, J. Fluctuation analysis of centrosomes reveals a suppressive role of Kinesin-1, J Biophysics (2014), submitted

AFFIDAVIT

I hereby declare that I prepared the doctoral thesis "Regulation of Actin dynamics by Formin in early *Drosophila* embryogenesis" on my own with no other sources and aids than quoted.

_____

Zhiyi Lv
Göttingen, 29.10.2014

Table of Contents

Summery

During the development, cells have to change their shape, migrate and rearrange their internal structure properly etc. All these processes depend on actin cytoskeleton. In *Drosophila* embryonic development, the actin filaments form different structures corresponding to different developmental stages. The formin protein Dia, as an actin nucleator, plays an important role in the regulation of actin architecture.

The F-BAR protein Cip4 overexpression leads to a phenocopy of *dia* in *Drosophila* embryos, implying the interaction of these two proteins. We found that *in vitro* Cip4 inhibited Dia activity by using actin pyrene and TIRF microscopy assay, collaborated with M. Winterhoff and Prof. Dr. J. Faix.

dia mutant embryos show a defect on stabilization of membrane at furrow canals. I found that Arp2/3 complex promoted the membrane tubular extensions at furrow canals, and this effect was counteracted by Dia. Another phenotype of *dia* mutant is a defect of maintenance of membrane compartmentalization during cellularization. Using *shibire/dynamin* temperature sensitive allele, I found that sorting mechanism mediated by endocytosis and exocytosis was not essential for this process. By FRAP analysis, I could show that the difference of membrane mobility caused by F-actin accumulation contributes to the membrane compartmentalization.

I propose that Dia localizes at furrow canals and polymerizes F-actin, and F-actin stabilizes the membrane at furrow canals and maintains the compartmentalization of lateral-basal domains.

In addition, a new allele of *ced-12* was identified. Current data suggest that Ced-12/Spg provides the signal linker between centrosomes and actin caps/metaphase furrows.

List of figures

List of tables

Abbreviations

bp	base pairs
cDNA	complementary DNA
DAPI	4', 6' – Diamidino-2-phenylindole
ddH2O	double distilled water
°C	degree Celsius
DNA	deoxyribonucleic acid
DTT	1,4-dithiothreitol
Δ	deletion
E.coli	*Escherichia coli*
EDTA	ethylenediaminetetraacetic acid
FRT	flippase recognition target
FRAP	fluorescence recovery after photobleaching
GFP	green fluorescent protein
GST	Glutathion-S-transferase
g	gram(s)
h	hour(s)
IPTG	Isopropyl-β-D-thiogalactopyranoside
kb	kilobases
kDa	kiloDalton
l	litre(s)
m	milli-
µ	micro-
min	minute(s)
PCR	polymerase chain reaction
PMSF	Phenylmethylsulfonylfluorid
RNA	ribonucleic acid
rpm	revolutions per minute
RT	room temperature
SDS	sodiumdodecylsulphate
SDS-PAGE	SDS-polyacylamide gel electrophoresis
Tris	tris(hydroxymethyl)aminomethne hydrochloride

Chapter 1. Introduction

1.1   Actin polymerization regulation

Actin is one of the most abundant proteins in eukaryotic cells where it may be present at concentrations of over 100 µM (Pollard et al., 2000). Globular actin (G-actin), as a 42 KDa protein with ATPase activity, can undergo self-assembly into filamentous actin (F-actin). F-actin are two-stranded helical polymers with a diameter of 5-9 nm (Kishino and Yanagida, 1988). In the living cells, F-actin can be assembled into different structures, such as linear actin bundles, two dimensional networks, and three dimensional gel, to perform specific functions (Chhabra and Higgs, 2007).
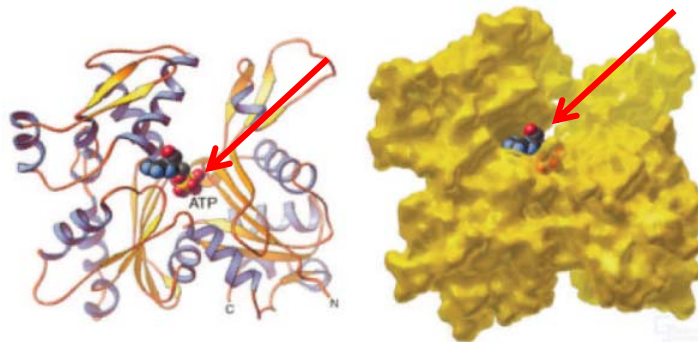
Figure 1.1 Ribbon and space-filling models of the actin molecule (Pollard and Cooper, 2009). An actin monomer is approximately pear shaped and composed of four domains with a large cleft almost bisecting the molecule. This cleft (arrow) contains the nucleotide binding site.

Actin monomers can spontaneously polymerize into filaments *in vitro*, with a relatively slow starting phase, because the dimers and trimers are very unstable. But once the short filaments have been created, actin polymerization undergoes rapidly. However, the dynamics of actin polymerization in eukaryotic cells are highly controlled by more than 100 actin-accessory proteins (Staiger and Blanchoin, 2006). The functions of these accessory proteins include maintaining actin monomer pool, controlling the length of actin filaments,

regulating the polymerization and depolymerization of F-actin, and cross-linking F-actin to bundles or networks.

Here we will focus on actin nucleation regulation.

In the initiation of actin assembly, the formation of actin dimers and trimers is kinetically unfavorable. To overcome the thermodynamic barrier, actin nucleators are required. From genetic and cell biological approach, a large number of actin nucleators are identified. These actin nucleators can be classified into 3 groups: 1) Arp2/3complex and its nucleation promoting factors (NPFs), 2) formins and 3) WH2-domain containing proteins (Campellone and Welch, 2010). These 3 classes of nucleators use different mechanism to overcome the nucleation kinetic barrier, and have distinct roles in cellular functions.
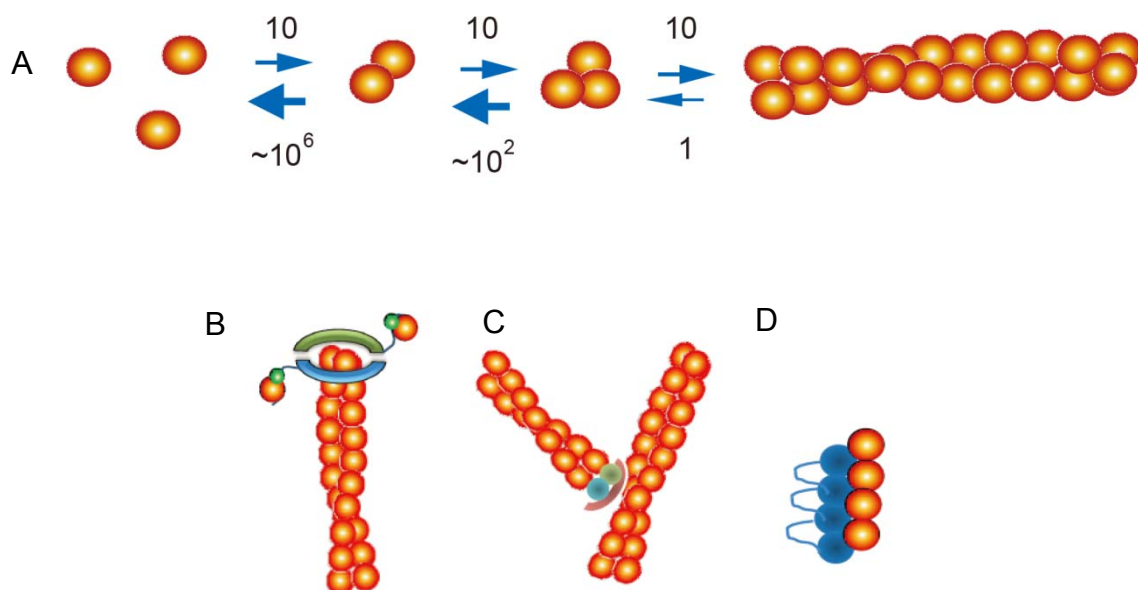
Figure 1.2 Actin nucleation regulations. (A) Spontaneous nucleation and elongation. The dimer and trimer formation is kinetically unfavorable, but the following addition of monomer is favorable (Pfaendtner et al., 2010). (B-D) The nucleators help actin to overcome the kinetic barrier. (B) Nucleation and elongation mediated by formins. Formins nucleate actin by stabilizing the dimer, allowing new monomer added to the barbed end. Formins stay associated with barbed end, recruit profilin-actin and transfer actin monomer to the barbed end. (C) Arp2/3 complex induces branch actin filament by mimicking actin barbed end. (D) Spire nucleates actin by recruiting and organizing actin monomer into short pitch, serving as a polymerization "seed".

1.1.1 The Arp2/3 complex

Arp2/3 complex (**A**ctin-**r**elated-**p**rotein 2/3) was the first identified actin nucleator. This complex is comprised of 7 subunits, which include Arp2 and Arp3, and 5 additional polypeptides, ARPC1-5. Arp2 and Arp3 proteins are about 45% identical to actin and the 3D structure is very similar to the plus end of actin itself. Actin subunits can assemble onto Arp2/3, which mimics the actin dimer, bypassing the rate-limiting step of filament nucleation. Meanwhile, ARPC2 and ARPC4 bind to the side of pre-existing actin filaments, resulting in about a 70° angle between the new and old filaments (Beltzner and Pollard, 2004; Rouiller et al., 2008).

However, the Arp2/3 complex has little activity to nucleate actin by itself. There are three contributors, which increase the complex activity: 1) F-actin binding, 2) phosphorylation of Thr and Try residues in Arp2, and 3) nucleation-promoting factors (NPFs), which is the best characterized (Campellone and Welch, 2010). Based on the mechanism involved in Arp2/3 activation, NPFs can be divided into class I and class II NPFs (Campellone and Welch, 2010).

Class I NPF includes WASP/N-WASP, WAVE/Scar, WASH, WHAMM, and JMY. The catalytic domain of Class I NPFs is WCA domain located at the C terminal. The WCA domain is comprised of 1) WH2 domain that binds to G-actin, 2) an amphipathic connector and 3) an acidic peptide that binds Arp2/3 (Rotty et al., 2013). The binding of amphipathic connector/acidic peptide to Apr2/3 changes the conformation of Arp2/3 complex, resulting in the formation of an actin barbed-end-like structure, and subsequently the new actin monomers bind to the "fake actin nuclei" and new filament forms (Rotty et al., 2013). However, WASPs are in an autoinhibition state, and small GTPase is involved in the activation of WASPs (Rohatgi et al., 1999). In addition, SH3

domain containing proteins such as NCK1 and Cip4/TOCA1, also contribute to the activation of N-WASP (Fricke et al., 2009; Tomasevic et al., 2007).

Due to lacking WCA domain and WH2 domain, the Class II NPFs cannot bind to G-actin. Instead, they can promote Arp2/3 activity by mediating F-actin binding to Arp2/3. This category includes cortactin and haematopoietic HS1 (Welch and Mullins, 2002).

1.1.2 Formins

Formins are the second family of actin nucleators recognized a decade ago in yeast (Pruyne et al., 2002; Sagot et al., 2002). All the formins share the conserved domains FH1 (Fomin-homology domain 1) and FH2 (Fomin-homology domain 2). The *Drosophila* genome contains six genes encoding proteins with FH1 FH2 domain, including *diaphanous*, *daam*, *fmnl*, *cappuccino*, *formin3* and *knittrig*/*fhos* (Lammel et al., 2014). Diaphanous (Dia) is the best characterized formin in *Drosophila*.

From *in vitro* studies, FH2 domain was shown to be sufficient for nucleation of purified actin monomers (Chesarone et al., 2010; Grosshans et al., 2005). Crystal structure study has shown that FH2 domains form a ring as a dimeric configuration. The dimer is stabilized by the binding of N-terminal lasso of each subunit to the post of the other (Xu et al., 2004). Co-crystal structure of yeast formin Bni1 with tetramethylrhodamine-actin study has shown that the FH2 bridge element binds two actin monomers in an orientation, which resembles a short-pitch actin filament, suggesting that this structure functions as a filament nucleus, and implying that the FH2 domain promotes actin nucleation via stabilization of actin dimer structure (Otomo et al., 2005). Study of biochemical properties of heterodimeric FH2 mutants revealed that the FH2 domain consists of an alternating closed-open configuration (Otomo et al., 2005). Together with the FH2-actin structure, a model of FH2 activity was proposed. In the closed conformation, both FH2 domains sit on the F-actin

barbed end tightly, blocking addition of new actin monomers. In the open state, one of the FH2 domains steps towards the barbed end and leaves space for a new actin monomer to the barbed end (Otomo et al., 2005).

The FH1 domain is involved in the acceleration of F-actin elongation. The FH1 domain binds profiling-bound actin via its proline-rich motif (Courtemanche and Pollard, 2012). Profilin-actin is the major form of actin monomers in living cells (Sagot et al., 2002). Profilin has two binding sites. One binds to the face of actin monomers opposite to the ATP-binding cleft, and the other binds to the proline-rich domain. Profilin-actin can readily add to a free barbed end but cannot add to pointed end (Kovar et al., 2006). In addition, Profilin binding to actin suppresses spontaneous nucleation (Goode and Eck, 2007). The FH1-Proflin interaction plays an important role in increasing the formin catalyzed filament elongation at the barbed end by ~10 times over the free barbed end (Paul and Pollard, 2009). Actin monomer diffusion rate is the limiting factor for the rate of actin elongation. The FH1 domain of formins can recruit Profilin-actin complex. This increases the local concentration of actin monomer at the barbed end, resulting in a fast speed elongation (Kovar et al., 2006; Romero et al., 2004). Moreover, the rate of actin filament elongation at the barbed-end increases with the number of poly-proline tracks in the FH1 domain (Courtemanche and Pollard, 2012; Paul et al., 2008).

The N terminal half of Dia is a regulatory region, including a GTPase binding domain (GBD) and Diaphanous inhibitory domain (DID) that is involved in autoinhibition. The DID domain is followed by a coiled-coil domain and a dimerization domain (DD) (Chesarone et al., 2010). In addition, the FH2 domain forms dimeric conformation without DD (Kovar et al., 2006). The function of DD still needs to be clarified. The FH1-FH2 domain is located at the C terminal region and is followed by a short peptide termed Diaphanous autoinhibitory domain (DAD) at the C terminus. DAD binding to DID inhibits the FH1-FH2 actin polymerization activity (Wallar et al., 2006). The electron microscopy and single

particle analysis of mDia1 full length protein has shown that the DAD-DID interaction makes fork-shaped N-terminal DID-CC region, and this region hangs over the ring-shaped FH2 domain, resulting in steric obstruction of actin binding to the FH2 domain (Maiti et al., 2012). In *Drosophila*, Rho1 (RhoA in mammals) binding to GBD can release the FH2 actin polymerization activity from autoinhibition (Grosshans et al., 2005; Lammers et al., 2005). Structure analysis showed that binding of DAD and RhoGTPase to GBD-DID domain is
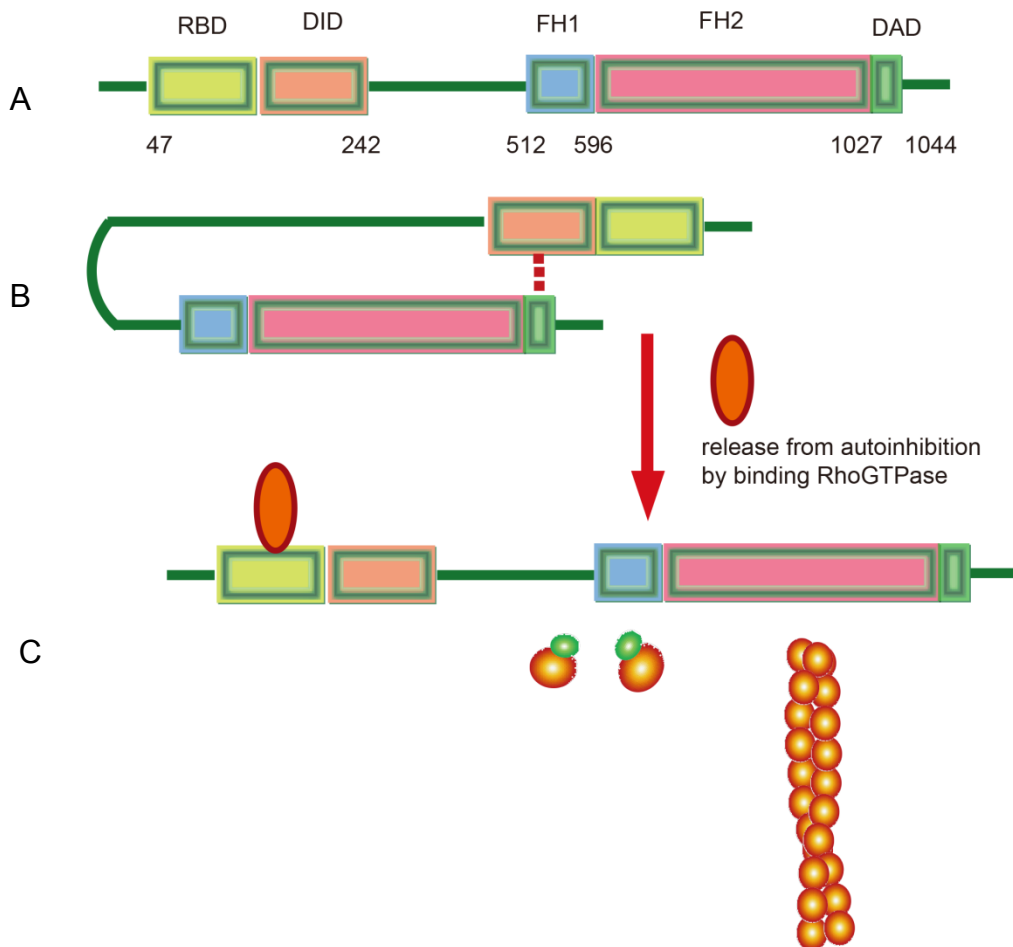
Figure 1.3 Schematic representation of domain organization and regulation of Dia. (A,B) N terminus is a regulatory domain, consisting of a GTPase binding domain and Dia inhibitory domain. The catalytic domain locates at C terminus. The FH1 domain recruits profilin-actin complex and delivers to the FH2 domain, increasing the local concentration of actin monomer. The FH2 polymerizes actin into linear filament. The Dia autoinhibition domain (DAD) mediates intramolecular interactions with the DID at N terminus to maintain formins in an autoinhibited state. (C) GTPase binding to GBD releases the autoinhibition by disrupting the interaction between DID and DAD.

mutually exclusive (Campellone and Welch, 2010). However, the FH2 domain is not fully active after RhoGTPase binding *in vitro*. This suggests that some other unknown factors are required in the activation of the FH2 domain (Grosshans et al., 2005).

An increasing number of studies point to the fact that formins often work with formin-binding nucleation-promoting-factors (NPFs) to overcome actin polymerization barriers. In *Drosophila*, there are two NPF-formin pairs: Spire-Capu (Quinlan, 2013) and APC-Dia (Jaiswal et al., 2013). Spire-Capu pair is important in oogenesis (Quinlan et al., 2005). Adenomatous polyposis coli (APC) colocalizes with Dia on the metaphase furrow in syncytial embryo and both proteins are required in metaphase furrow formation (Webb et al., 2009). APC and Dia directly interact *in vitro* and co-stimulate actin assembly, overcoming the dual barrier imposed by profilin and capping protein (Jaiswal et al., 2013). The vertebrate APC and mDia1 work similarly as the *Drosophila* APC-Dia pair. A "rocket launcher" mechanism was proposed by using color TIRF microscopy. APC and mDia1 form a ternary complex with actin monomer to initiate actin filament polymerization. Upon filament polymerization, the complexes separate. The mDia1 sits on growing barbed ends while APC remains at the site of nucleation (Breitsprecher et al., 2012).

FH1 domain is critical for recruiting profilin-actin and delivering to FH2 domain for actin polymerization. The length of FH1 domain is an important element for the speed of actin elongation mediated by formins (Courtemanche and Pollard, 2012). In addition, recent studies show that FH1 domain also plays an important role in formin activity regulation (Bilancia et al., 2014; Graziano et al., 2014; Yan et al., 2013). Enabled and Dia are important for promoting filopodia, but with different morphology and dynamics. The fine tuning of different filopodia requires the balance of activity of Enabled and Dia. This balance is achieved partially by the Enabled negatively regulating Dia. Enabled protein inhibits Dia activity via the interaction of Enabled EVH1 domain and

DiaFH1 domain (Bilancia et al., 2014). Dia-interacting Protein (DIP) is another FH1 domain binding protein. The interaction between DIP and DiaFH1 domain leads to the inhibition of mDia2, and overexpression of DIP reduces membrane integrity (Eisenmann et al., 2007).

In comparison to Dia, other formins in *Drosophila* have not been extensively characterized in cellular function or biochemical properties. Dishevelled-associated activator of morphogenesis (DAAM) is involved in the non-canonical Wnt signaling pathway in *Xenopus* gastrulation (Habas et al., 2001). In *Drosophila* DAAM is required in tracheal cuticle pattern regulation (Matusek et al., 2006). Formin3, along with FH1 and FH2 domain containing protein (FHOS/FOSD), do not show any similarity in their N terminal. Formin3 is required in F-actin assembly during *Drosophila* tracheal fusion (Tanaka et al., 2004). FHOD is involved in macrophage spreading and migration in *Drosophila* cellular immune response (Lammel et al., 2014). Cappuccino, together with another actin nucleator, WH2 domain containing protein Spire, plays an important role in oogenesis, which will be discussed later.

1.1.3 WH2 domain containing nucleator Spire

WH2 domain containing protein Spire has been identified as a novel actin nucleator (Quinlan et al., 2005). The WH2 (WASP-homology 2) domain is shared with Class I NPFs, suggesting that they are evolutionarily related. Spire has the ability to induce actin filaments when transiently expressed in fibroblast, and was predicted as a nucleation promoting factor of Arp2/3 complex because of the presence of WH2 domain (Otto et al., 2000). However, Spire could induce actin nucleation independent of Arp2/3 (Quinlan et al., 2005). It was reported that Spire-induced F-actin is linear, which excluded the possibility of Arp2/3 involvement in Spire mediated actin nucleation (Quinlan et al., 2005).

In vitro studies showed the nucleation activity of Spire based on the tandem of four WH2 domains separated by three conserved linkers L1-3, especially the WH2 domain C and D, and the linker L3 between them (Rasson et al., 2014). The electron microscopy supported a Spire-induced actin nucleation model: WH2-C and WH2-D bind actin monomers, and the linker3 coordinates the interaction between these two actin monomers to form a dimer. Then the third and fourth actin monomer are added to the dimer by WH2-B and WH2-A domain, forming a longitudinal actin oligomer, as a seed of actin nucleation (Kerkhoff, 2006).

Mutations in *spire* cause premature cytoplasmic streaming in oocyte. Embryos from *spire* homozygous females lack pole cells. Furthermore, the dorsal-ventral and the anterior-posterior axes of these embryos are affected (Theurkauf, 1994). A similar phenotype is also observed in *cappuccino* and *chickadee* (encodes profilin) mutant flies (Qualmann and Kessels, 2009; Theurkauf, 1994), indicating that Cappuccino, Profilin and Spire cooperate in actin polymerization processes. A DiaFH1FH2 coated beads assay revealed that Spire enhances actin polymerization by increasing the concentration of profilin-actin, which can be used by formin to assemble actin filaments. The synergy among Spire, Profilin and Cappuccino *in vitro* analysis mimics the function in cellular context and provides a molecular mechanism of genetic interaction between Spire, Cappuccino and Profilin in oogenesis (Bosch et al., 2007).

1.2 Actin organization in early embryogenesis of *Drosophila melanogaster*

1.2.1 *Drosophila* embryo development and actin distribution

The actin cytoskeleton in eukaryotic organisms performs a wide range of cellular processes such as cell division, cell shape change and maintenance, cell movement, endocytosis and signal transduction. Not surprisingly, it is found to play a key role in *Drosophila* early embryonic development.

After fertilization, the embryo of *Drosophila* undergoes 13 rounds of nuclear division without cytokinesis. During the first 7 mitotic cycles, the nuclei divide deep in the embryo interior. During 8 and 9 cycles, most nuclei migrate towards the embryo periphery. The yolk nuclei, which maintain their position in the deep yolk, will become polyploid and undergo apoptosis later in embryogenesis. During this stage, nuclear division is not accompanied by associated plasma membrane invagination, and the plasma membrane is underlined by a 3 μm layer of cortical F-actin (Karr and Alberts, 1986). After the ninth mitotic division, cortical migration is complete. Cortical migration is dependent on microtubule (Baker et al., 1993). Nuclei, which reach the posterior pole containing the pole plasma will form the progenitor germline cells. The somatic nuclei form a monolayer beneath the plasma membrane with a regular arrangement and then undergo another 4 cortical divisions. This developmental stage is termed syncytial blastoderm.

During cortical migration, the organization of F-actin changes dramatically. At the onset of interphase of cycle 10, F-actin is re-organized into dome-like caps that lie between the plasma membrane and the nuclei, and the plasma membrane which is above nuclei contains many protrusions. Upon entry into mitosis, the membrane invaginates between the adjacent mitotic spindles to form metaphase furrow (also termed pseudo-cleavage furrow)

which reaches about 5 µm deep. Metaphase furrows are assembled to separate spindles and ensure the appropriate division of chromosome between adjacent nuclei. When the metaphase furrows form, F-actin redistributes towards the cap margins and accumulates at the tip of the metaphase furrows. At the same time, the plasma membrane protrusions flatten, probably as a membrane source of metaphase furrow formation. By late mitosis, the metaphase furrow rapidly regresses, plasma membrane protrusions reform, and F-actin concentrate into cap structure again. The whole process is repeated through each of the four divisions (Schejter and Wieschaus, 1993). After 13 nuclear divisions, the syncytial embryos fill with 6,000 nuclei in the periphery. The plasma membrane during the syncytial blastoderm stage is polarized and consists of two domains: the apical-like domain which is above nuclei and the basolateral-like domain which is lateral to nuclei (Mavrakis et al., 2009). This syncytial blastoderm plasma membrane polarity requires F-actin organization (Mavrakis et al., 2009).

During interphase 14, the embryo undergoes a modified cytokinesis, termed cellularization, which transforms the syncytial blastoderm into the cellular blastoderm with individual cells. The developing embryo starts gastrulation stage immediately after completion of cellularization. Cellularization is accompanied by a series of morphological events including nuclear elongation, clearing cortical layer of yolk and the formation of microtubule basket structure.

The most prominent event in cellularization is the membrane invagination between the adjacent nuclei stably and ultimately forming a sheet of 40 µm tall columnar epithelium. The tip of the invaginating membrane forms a loop-like membrane structure, which is called furrow canal. Cellularization can be divided into 4 distinct stages (Lecuit and Wieschaus, 2000): Phase I takes 10 min and results in the assembly of the furrow canal. Cortical nuclei start elongation along apical-basal axis. Phase II lasts 20 min and the membrane

starts invagination, but in a very slow speed. The furrow canal stays in the position 5 µm basal to the surface of the embryo at the end of Phase II. Cortical nuclear elongation completes during this phase. In Phase III, membrane invagination accelerates, although still at a relatively slow rate. At the end of this phase, the furrow canal reaches the basal part of nuclei. In the Phase IV, the invagination speed increases dramatically and reaches the yolk. The cells are closed off basally, which results in 35-40µm tall epithelia. The transition from slow phase to fast phase is due to the completion of furrow canal assembly (Figard et al., 2013).

Prior to the membrane invagination in cellularization, cortical F-actin reorganizes. At the onset of interphase 14, F-actin transiently forms caps. However, about 10-15 min, caps resolve and F-actin marks the furrow canal. At the end of cellularization, F-actin is accumulated at sub-apical domain where adherens junctions form.

1.2.2 The function of F-actin in *Drosophila* embryonic development

The general role of the actin cytoskeleton in early embryogenesis has been studied by using specific inhibitor Cytochalasin B and Latrunculin, which disrupt the cytoskeleton structure via inhibiting F-actin polymerization. Cytochalasin B treatment leads to "nuclear fall-out" phenotype. Cortical nuclei move into the interior of syncytial blastoderm embryo. In mitosis, metaphase furrows are absent, which leads to fusion of adjacent spindles in the cortical layer (Sullivan and Theurkauf, 1995). During cellularization, Latrunculin treated embryos show defects in membrane invagination, stabilization of membrane at furrow canals, and membrane compartmentalization (Sokac and Wieschaus, 2008a).

Genetic analysis provides a deeper insight into the function of F-actin. Mutations in Arp2/3 complex result in disruption of metaphase furrow and

defect in actin cap expansion (Stevenson et al., 2002; Zallen et al., 2002). *SCAR/WAVE* mutant embryo shows a similar phenotype with *Arpc1*, a subunit of Arp2/3, but *WASP* null mutant doesn't show obvious defects (Zallen et al., 2002), suggesting that in *Drosophila* early embryogenesis Arp2/3 complex activator is SCAR/WAVE, rather than WASP.

Sponge, as a non-canonical Rac Guanine nucleotide exchange factor (GEF), is required for the formation of actin caps and metaphase furrows (Biersmith et al., 2011; Postner et al., 1992). Sponge belongs to Dreadlocks (DOCK) protein family, and consists of SH3 domain, Dock homology 1 and 2 domain and proline-rich domain (Biersmith et al., 2011). The most closely related protein in *Drosophila* is Myoblast city (Mbc), which is involved in myoblast fusion (Biersmith et al., 2011; Geisbrecht et al., 2008). Sponge cannot activate Rac/RhoGTPs, unless it is bound to Elmo (Côté and Vuori, 2007). The Elmo proteins lack catalytic activity, and seem to be scaffold proteins (Abu-Thuraia et al., 2014). Interaction between Elmo and DOCK proteins is involved in lymphocyte migration, cell invasion in mammals (Stevenson et al., 2014) and are essential for the central nervous system development in *Drosophila* (Biersmith et al., 2011). However, the detail mechanism underlying the interaction of Sponge and Elmo is less clear.

Dia is required for the formation of metaphase furrows and cellularization furrows. In *dia* germline clone embryos, multinuclear cells form due to the lack of actin-based metaphase furrows (Grosshans et al., 2005). Electron microscopy showed furrow canals are enlarged and filled with large cytoplasmic blebs, which suggests that the membrane in furrow canal is less stable (Grosshans et al., 2005).
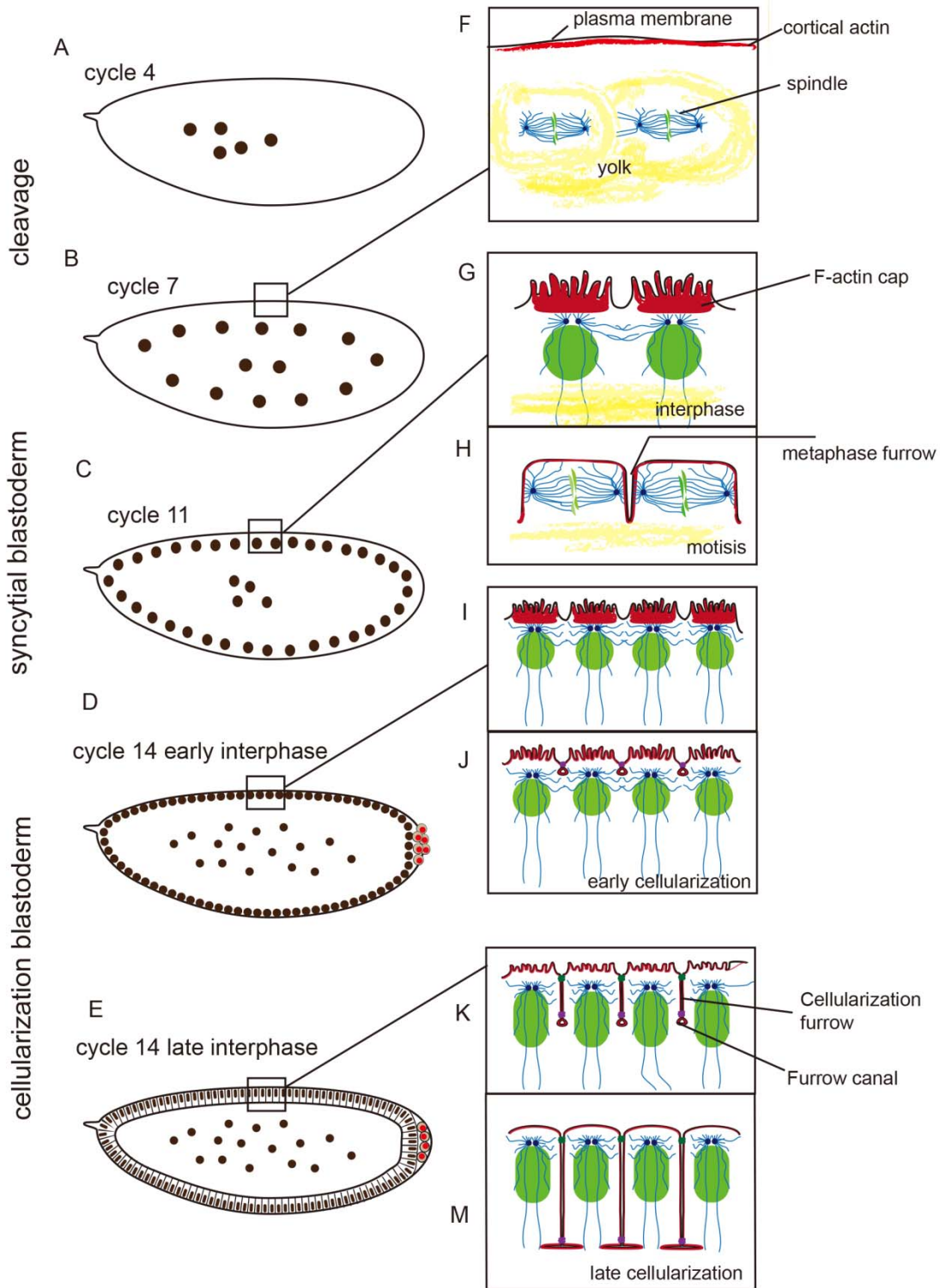
Figure 1.4 Schematic representation of Drosophila early embryogenesis and actin cytoskeleton. Modified form S. Acharya (S. Acharya PhD dissertation, 2014) (A-E) Representative stage of early embryogenesis. (F) Actin forms a cortical layer beneath the membrane in pre-syncytial stage embryo. (G) The surface is thrown into a series of protrusions in the interphase of syncytial blastoderm. At the same time, actin forms dome-like caps

between plasma membrane and nuclei. (H) Upon entry into mitosis, the protrusions flatten and actin cap dissolves and marks metaphase furrows. (I-J) At the beginning of interphase 14, the cap forms for a short time and disassembles after a few minutes, and is enriched at the furrow canal. (K) Actin is enriched at the furrow canal throughout the cellularization process. (M) At end of cellularization, actin-myosin at the furrow canal start contracting laterally, enclosing each nucleus, resulting in blastoderm cells.
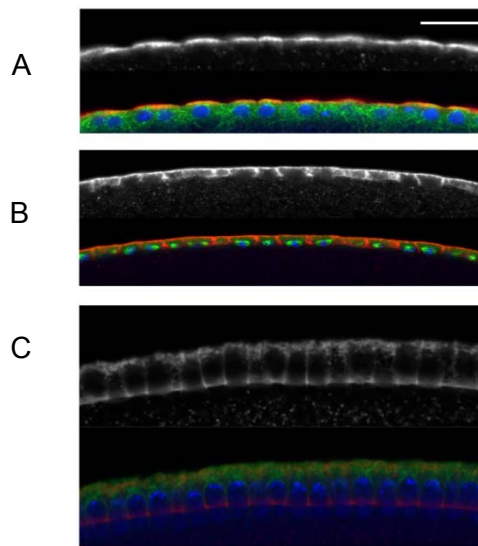
Figure 1.5 Confocal images to show actin organization in different stages. (A) Actin caps in interphase of syncytial blastoderm stage. (B) Actin caps dissolve and concentrate at metaphase furrow. (C) Actin is enriched at the tip of invaginating membrane through the course of cellularization. Red is actin stained by phalloidin-Alexa568, and green is microtubule stained by monoclonal antibody, and blue is DNA staining. Scale bar: 10 µm.

1.3 BAR domain proteins: a linker between membrane modeling and actin dynamics

The shape of cell membranes reflects their physiological function. The membrane system shows a highly dynamic nature in the living cell. Membrane remodeling plays an important role in many biological processes, including infection and immune responses, cell division and axonal pathfinding (Fricke et al., 2010). In those processes, force generation is essential to allow the cell to change the membrane shape. One of the systems most commonly used to generate force is actin cytoskeleton (Suetsugu and Gautreau, 2012).

Regulation of actin dynamics and the connection of actin and membrane is of great importance in those biological processes.

Over the last decade, the *Bin/Amphiphysin/Rvs* (BAR) proteins were reported as important regulators that couple actin dynamics and membrane remodeling (Farsad et al., 2001; Peter et al., 2004). Crystal structure studies have shown that BAR domains are composed of three anti-parallel coiled-coil helices, which make the BAR protein homodimerized and form a crescent-shaped surface (Frost et al., 2009) (http://www.bar-superfamily.org/). The crescent-shaped surface is covered by positively charged amino acid residues, which allow the BAR domain to directly interact with negatively charged membrane lipids. Based on the amino acid sequence, BAR domain proteins are divided into three classes, BAR, F-BAR and I-BAR domain proteins (Suetsugu and Gautreau, 2012).

BAR and F-BAR domains form a concave membrane binding surface, while I-BAR domain is referred to as inverse BAR due to the convex lipid binding surface and its ability to induce protrusions (Qualmann et al., 2011). These curved lipid binding surfaces are used in sensing and inducing membrane curvatures. Some BAR domain proteins can form amphipathic α-helices at the N terminus (together with BAR domain termed N-BAR domain). The amphipathic α helices insert into the leaflet of bilayer as a "wedge" causing membrane bending, and the helix intercalation may increase the binding of BAR domain to the curved membrane, further stabilizing the curvature (Mattila et al., 2007).

The F-BAR domain was initially characterized as a Fes/CIP4 homology domain (FCH) plus the following CC domain (Itoh et al., 2005). The F-BAR domain is sufficient to deform liposomes *in vitro* (Itoh et al., 2005). The F-BAR domain dimers can form macromolecules wrapping around a curved membrane by associating with each other via end-to-end and lateral interactions

(Qualmann et al., 2011). Using this mechanism the F-BAR domain stabilizes the membrane curved structure, and generates the force to make the curved membrane invagination, forming a tubular structure with a specific diameter (Frost et al., 2007).

The presence of Src Homology 3 (SH3) domain at C terminal of F-BAR protein mediates binding to Dynamin and WASP/WAVEs (Dawson et al., 2006). Dynamin is essential for membrane scission during endocytosis, which suggests F-BAR domain proteins play an important role in this process (Arasada and Pollard, 2011). WASP/WAVEs are regulators of actin-nucleation Arp2/3 complex as mentioned previously. Besides Cdc42 and Rac, SH3 domain binding contributes the activation of WASP/WAVEs (Suetsugu and Gautreau, 2012). Cip4, as an SH3 domain containing protein, binds to proline-rich domain (PRD) of WASP, resulting in the activation of actin nucleation. *In vitro* studies have shown F-BAR proteins bind directly to N-WASP and activate actin polymerization when bound to liposome (Chitu and Stanley, 2007). Cip4 is also able to form a complex with WAVE/Scar during endocytosis, and the interaction was found in *Drosophila* (Fricke et al., 2009), *C.elegans* (Giuliani et al., 2009) and vertebrates (Roignot et al., 2010).
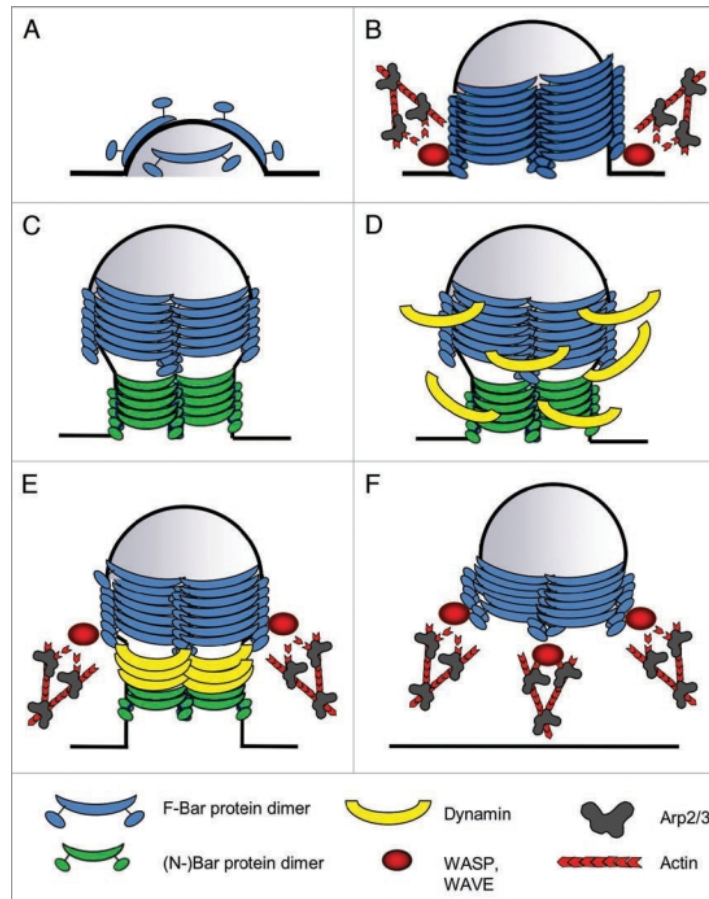
Figure 1.6 Schematic representation of the role of BAR protein during endocytosis. (Fricke et al., 2010) (A) F-BAR proteins bind to and induce the membrane curvature. (B) F-BAR proteins form oligomers by lateral/tail-to-tail interaction, and the oligomers of F-BAR proteins form a helical coat around the membrane, together with actin filaments, generating force for membrane invagination. (C) Other BAR proteins with smaller diameter are recruited and associate with the neck of the tubule, narrowing the neck. (D) F-BAR proteins recruit Dynamin with their SH3 domain. Dynamin pinches off the neck of vesicle by GTP hydrolysis. (E) Scission by Dynamin. During this process, actin polymerization mediated by Arp2/3 is involved. (F) After the scission, WASP/WAVE associates to membrane via interaction with F-BAR protein, and polymerize the actin filament to push the vesicle into the depth of the cell.

BAR domain proteins provide the link between membrane and actin cytoskeleton. BAR proteins are involved in endocytosis (Figure 1.6). BAR proteins bind to plasma membrane and generate curvature. Subsequently, other BAR proteins are recruited and form a homo-oligo or hetero-oligo complex. Meanwhile, NPFs are recruited and promote actin polymerization by activation of Arp2/3. The actin filaments generate the force to push the

membrane invagination. Dynamin pinches off the invaginating membrane, forming an endocytic vesicle which will be pushed inside of the cell by actin filaments.

Fomin binding protein 17 (FBP17) was found as a binding partner to the mouse Formin1 (Chan et al., 1996). This protein belongs to F-BAR family proteins. Cip4 is a paralog of FBP17 in *Drosophila*. However, the physiological function of Cip4 to Dia is not known.

1.4 Aim of the work

This work focuses on the actin organization in *Drosophila* early embryonic development. We studied the mechanism of Dia function in membrane compartmentalization and the interaction between Dia and the F-BAR protein Cip4. In addition, we cloned a new allele of *ced-12*, which is essential for actin cap and metaphase furrow formation in the syncytial blastoderm.

Chapter 2. Materials and Methods

2.1 Materials

2.1.1 Chemicals Regents

All chemicals were purchased from Sigma-Aldrich (Steinheim, Germany), AppliChem GmbH (Darmstadt, Germany), Carl ROTH (Karlsruhe, Germany) unless otherwise mentioned.

2.1.2 Antibiotics

Antibiotics	Stock concentration	Working concentration
Ampicillin	100mg/ml	100-200µg/ml
Geneticin (G418)	75 mg/ml	75 µg/ml

2.1.3 Enzymes

All restrict enzymes were purchased from Fermentas and New England Biolabs.

The other enzymes used in this study were:

-Taq DNA polymerase and Pfu DNA polymerase (prepared in the lab)

-Long PCR Enzyme Mix (Fermentas)

-Protease K (Roche)

-T4 DNA ligase (Fermentas)

-PreScission protease (gift form Prof. J Faix)

-Lysozyme (AppliChem)

2.1.4 Primary antibodies

The information of primary antibodies used in this study was in the following list.

Table 2.1 Primary antibodies used in this study

antibody	Raised in	Dilution and working concentration		Source
		immunostaining	Western blot	
Amph*	Guinea pig	1:1000	-	Lab Grosshans
Dlg	Mouse	1:00 (~0.4µg/ml)	-	Hybridoma bank 4F3
Dia*	Rabbit	1:1000	1:5000	Lab Grosshans
Dia*	Guinea pig	1:1000	1:5000	Lab Grosshans
Slam*	Rabbit	1:5000	1:5000	Lab Grosshans
α-Tubulin	Mouse	1:5000 (7µg/ml)	1:50000 (0.7µg/ml)	Hybridoma bank B512
γ-Tubulin	Mouse	1:5000	-	Sigma T6557
Krüppel*	Guinea pig	1:1000	-	Prof. E. Wimmer
Even-skipped*	Guinea pig	1:1000	-	Lab Grosshans
Phospho-Histone H3(S10)	Mause	1:5000 (0.2µg/ml)	-	Millpore
Ced-12*	Guinea pig	1:1000	1:3000	Prof. Geisbrecht
Sponge*	goat	1:1000	1:1000	Prof. Geisbrecht
Vasa	Rat	1:100(1.6µg/ml)	-	Hybridoma bank anti-vasa

* serum

2.1.5 Other reagents used in immunostainings

Secondary antibodies were used in a final concentration of 4 µg/ml (Invitrogen).

GFP-Booster Atto 488, in a final concentration of 2µg/ml (Chromotek).

DAPI (4",6"-Diamino-2-phenylindole): DNA staining, in a final concentration of 0.4 µg/ml (Sigma-Aldrich)

Phalloidin-Alex 488: used for actin staining, in a final concentration of 6 nM (Molecular Probes)

Mounting medium: Aquapolymount (Polysciences, Eppelheim)

2.1.6 Other reagents used in western blot

IRDye-800CW and IRDye-680 secondary antibodies were purchased from LI-COR Biotechnology and used at a dilution of 1:20000 (0.05 µg /ml).

2.1.7 Buffers

All buffers were prepared according to Sambrook and Russel, 2001 unless otherwise stated.

1) Buffers for DNA extraction from adults flies:

Homogenisation buffer   10 mM Tris/HCl pH7,5
                                   60 mM NaCl
                                   10 mM EDTA

2) Buffer for Immunostaining and western blot:

PBS   130 mM NaCl
                                   7 mM Na2HPO4
                                   3 mM NaH2PO4
                                   pH 7.4

PBST   0.1% Tween 20 in PBS

Embryo fixation solution   4.5 ml 1X PBS
                                   0.5 or 1 ml Formaldehyde (37%)
                                   5 ml Heptane

Immunostaining blocking buffer   5% BSA in 1X PBS

Western blot blocking buffer	5% milk powder in 1X PBS
Wet transfer buffer	25 mM Tris 175 mM Glycine 20% Methanol

3) Buffer for Mini prep of plasmid DNA:

Solution I	50 mM Tris/HCl, pH 8.0 10 mM EDTA
Solution II	1% SDS 0.2M NaOH
Solution III	3 M Potassium acetate Adjusted to pH 5.4 with acetic acid

4) Buffer for GST-Tag protein purification:

Lysis buffer	50 mM Tris/HCl pH 8.0 150 mM NaCl 1 mM DTT
Wash buffer	50 mM Tris/HCl pH 8.0 500 mM NaCl 1 mM DTT
Elution buffe	50 mM Tris/HCl pH 8.0 150 mM NaCl 10 mM Glutathione (freshly added from 100 mM stock stored at -20°C) 1 mM DTT
Storage buffer	20 mM HEPES pH 8 150 mM NaCl, 0.5 mM DTT, 60% Glycerol for -20 °C storage

All buffers were filtered prior to use

5) His-tag protein purification under native conditions:

Lysis buffer	20mM Na-Phosphate pH 8.0

| | 500 mM NaCl |
| | 20mM Imidazol |

Wash buffer	20 mM Na-phosphate pH 8
	500 mM NaCl
	40 mM imidazol

Elution buffe	20 mM Na-phosphate pH 8
	500 mM NaCl
	250 mM imidazol

Storage buffer	20 mM HEPES pH 8
	150 mM NaCl,
	0.5 mM DTT,
	60% Glycerol for -20 °C storage

All buffers were filtered prior to use

6) Buffer for protein coupling to CNBr beads:

| Wash buffer for CNBr beads | 1 mM HCl |

| Coupling buffer | 100 mM NaHCO3/NaOH pH 8.3 |
| | 300 mM NaCl |

| Blocking buffer | 0.1 M Tris/HCl pH 8.0 |

Wash buffer I	0.1 M Na-acetate
	0.5 M NaCl
	pH adjusted to 4.0

Wash buffer II	0.1 M Tris/HCl
	0.5 M NaCl
	pH adjusted to 8.0

7) Buffer for affinity purification of antibodies:

| Wash buffer | 1X PBS |
| | 300 mM NaCl |

| Elution buffer (Low pH) | 50mM Glycine |
| | pH adjusted to 2.5 |

Elution buffer (High Salt)	4 M $MgCl_2$
	50 mM Tris/HCl pH 7.5

Neutralisation buffer   1M Tris/HCl pH 11.0

20% Sodium Azide (NaN3)

8) *Buffer for making a poly-L-proline Sepharose column for purification of profilin:*

10X Quenching buffer	1 M NaCl
	1 M glycine
	100 mM Tris pH 7.5

Storage buffer	10 mM Tris pH 7.5
	50 mM KCl
	1 mM EDTA
	0.002% Sodium Azide

9) *Buffer for profilin purification:*

P buffer	30 mM Tris pH 8.0
	100 mM KCl
	100 mM Glycin
	2 mM EDTA
	5 mM Benzamidin
	1 mM DTT
	0.1% PMSF

Elution buffer	30% DMSO in P buffer

Storage buffer	P buffer with 60% Glycerol for -20 °C storage

All buffers were filtered prior to use

10) *Buffer for immunoprecipitation:*

RIPA buffer	10 mM Tris/HCl pH 7.5
	150 mM NaCl
	0.1% SDS
	1% TritonX 100
	1% Deoxycholate
	5 mM EDTA
	2 mM PMSF (freshly added)
	1X Roche protease inhibitor cocktail (freshly

added)

11) Buffer for fractionation:

Lysis (and wash) buffer   50mM Tris pH 7.5
                                    75mM NaCl
                                    1mM $MgCl_2$
                                    0.05% NP-40
                                    1mM DTT
                                    2mM PMSF (freshly added)
                                    1X Roche Protease inhibitor cocktail (freshly added)

2.1.8 Kits

MiniElute Gel extraction Kit Quiagen, Hilden

Plasmid Midi Kit Nucleobond AX Macherey-Nagel, Düren

In-fusion HD cloning kit Clontech

2.1.9 Column materials for protein purification

GSTrap HP column   GE Healthcare Life Sciences

HisTrap HP column   GE Healthcare Life Sciences

CNBr activated Sepharose 4B   GE Healthcare Life Sciences

PD-10 desalting columns   GE Healthcare Life Sciences

2.1.10 Bacterial cell lines

Following strains of *E.coli* were used:

DH5α for molecular cloning:

F– Φ80*lac*ZΔM15 Δ(*lac*ZYA-*arg*F) U169 *rec*A1 *end*A1 *hsd*R17 (rK–, mK+) *pho*A *sup*E44 λ– *thi*-1 *gyr*A96 *rel*A1

BL21(DE3) was used for protein expression:

F– *omp*T *hsd*SB(rB–, mB–) *gal dcm* (DE3)

2.1.11 fly stocks

Table 2.2 Fly stocks used in this study

Stock name	Genotype	source/ lab collection number
oregon-R	+/+	A401
w	w	A101
yw	yw	A102
dia^{sy5}/CyO	w ; al dp b pr dia[SY5] Frt[2L]{neoR} / CyO, hs-hid{w+}	H037
dia^{sy5},117GFP/CyO	w ; GFP117{w+} dia[SY5] Frt[2L, neoR] / CyO	H018
UASp-GAP43-venus	w[*]; P{w[+mC]=UASp-Venus.GAP43}10	Bloomington Drosophila Stock Center
shibire	w shi[1] / FM6, y B	A119
UASp-Cip4GFP	w ; Sp / CyO ; UASp-Cip4GFP{w+}	Dr. Sven Bogdan (Yan et al., 2013)
mat67;15	w; tub-Gal4-VP16{w+}[67] ; tub-Gal4-VP16{w+}[15]	B101
Flp122; ovo^{D}2L	hs-Flp[122]; ovoDFrt2L[40A]/If/CyO, hs-hid{w+}	Maintained in the lab
ΔCip4	ΔCip4/ΔCip4	Dr. Sven Bogdan (Yan et al., 2013)
dia^{sy5}/CyO; ΔCip4	w ; al dp b pr dia[SY5] Frt[2L]{neoR} / CyO, hs-hid{w+}; ΔCip4/ΔCip4	Generated by Grosshans

arp3/TM6B	w[1118]; P{w[+mC]=EP}Arp3[EP3640]/TM6B, Tb[1]	Dr. Sven Bogdan (Yan et al., 2013)
UASp-GFPDia6	w ; Sp / CyO, nlsGFP ; UASp-GFPdia[6]	Dr. Christian Wenzl
UASp-GFPDia10	w ; Sp / CyO, nlsGFP ; UASp-GFPdia[10]	
UASp-GFPDia21	w ; Sp / CyO, nlsGFP ; UASp-GFPdia[21] / TM3, Sb	
UASp-GFPDia26	w ; UASp-GFPdia[27] / CyO, nlsGFP ; Dr / TM3, Sb	
UASp-GFPDia27	w ; UASp-GFPdia[26] / CyO, nlsGFP	
2L367	w ;2L367, al dp b pr Frt[40A]{neoR} / CyO, hs-hid{w+}	K110 (Vogt et al., 2006)
Utrophin-GFP	w; sqh-Utr::GFP/CyO	Prof. T. Leciut (Levayer et al., 2011)
membrane 4XGFP	117-GFP; Spider-GFP	Deqing Kong

Table 2.3 Fly stocks generated in this study

Palmitoylated-YFP-X	UASp-Palmitoylated-YFP/FM7
Palmitoylated-YFP-II	UASp-Palmitoylated-YFP/CyO
Palmitoylated-YFP-III	UASp-Palmitoylated-YFP/TM3
GFP-SAS6	Sp/CyO; GFP-SAS6/TM6c
2L367; GFP-SAS6	2L367/ CyO; GFP-SAS6/TM6c
GAP43-venus	Sp/CyO; tub-Gal4-VP16{w+}[15],UASp-GAP43-venus

2L367; GAP43-venus	2L367/CyO; tub-Gal4-VP16{w+}[15],UASp-GAP43-venus
GFPlinkerDia	UASp-DialinkerGFP/FM7
DialinkerGFP2	UASp-DialinkerGFP2/TM3
DialinkerGFP9	UASp-DialinkerGFP9/FM7
DialinkerGFP11	UASp-DialinkerGFP11/TM3
DialinkerGFP27	UASp-DialinkerGFP27/FM7
DialinkerGFP; dia^{sy5}/CyO	UASp-DialinkerGFP; dia[SY5] Frt[2L]{neo}, matGAL4[67]{w+}
dia^{sy5}; GFPlinkerDia	w ; dia[SY5] Frt[2L]{neo}, matGAL4[67]{w+} ; UASp-GFPlinkerdia / TM3, Sb
UASp-Cip4GFPΔSH3	W; UASp-Cip4GFPΔSH3{w+}
Flp122; ovo^{D}2L; ΔCip4	hs-Flp[122]; ovoDFrt2L[40A]/If/CyO, hs-hid{w+}; ΔCip4/ΔCip4

Fly stocks from Bloomington Drosophila Stock Center used for complement test in this study:

Rab6^{D23D}, Aats, Ced-12^{c06760}, Mt2, Pex19, Prd, CG14946, Df(2L)BSC208, Df(2L)BSC209, Df(2L)ED8142, Df(2L)BSC214, Df(2L)BSC213, Df(2L)BSC145, Df(2L)BSC241, Df(2L)BSC244, Df(2L)ED761, Df(2L)ED775, Df(2L)BSC277, Df(2L)BSC892, Df(2L)BSC159, Df(2L)BSC812, Df(2L)BSC243, Df(2L)BSC826, Df(2L)BSC891, Df(2L)BSC407, Df(2L)Exel6031, Df(2L)Exel6033.

2.1.12 Oligonucleotides used in this study

All oligonucleotides used in this study were ordered from Eurofins genomics.

Table 2.4 Oligonucleotides used in the study

Oligo No.	sequence 5'-> 3'	Description
ZL01	CGCGGTACCATGGTGAGCAAGGGCGAGGAGCTGT	Forward primer for cloning of GFP-Linker into pBSKII with KpnI
ZL02	CGCGAATTCGACCGGAGCTGCCAGAGC	Reverse primer for cloning of GFP-Linker into pBSKII with EcoRI
JG336	AAGAAGGAGATATACCATGAGCTGGCAAGATTATGTG	Foward primer for InFusion cloning of Profilin into pET15b with NcoI
ZL03	ATGGCTGCTGCCCATGCTAGTACCCGCAAGTAATC	Reverse primer for InFusion cloning of Profilin into pET15b with NcoI
ZL04	GGCCATGGGAGGATCACTCAATCTCAGCCGGGCCGAG	Foward primer for InFusion cloning of Cip4ΔFBARΔSH3/Cip4ΔFBAR into pGEX-6OH with BamHI
ZL05	GATGAGATCTGGATCCTAAGCATAGAGCGTGATCTC	Reverse primer for InFusion cloning of Cip4ΔFBAR into pGEX-6OH with BamHI
ZL06	GATGAGATCTGGATCTCACGATGCGGCCGCATTAAG	Reverse primer for InFusion cloning of Cip4ΔFBARΔSH3 into pGEX-6OH with BamHI
ZL07	GGGACAACTGAACGAGTCGG	Cip4 Sequence primer
ZL08	CTGGTGGCCGTCGGCACTTGGC	Cip4 Sequence primer
ZL09	TAGTGGATCTGGATCCATGCTGTGCTGCATCAGAAG	Foward primer for InFusion cloning of Palmitoylated EYFP into pUASp with BamHI
ZL10	CGAGGTCGACTCTAGATTACTTGTACAGCTCGTCCAT	Reverse primer for InFusion cloning of Palmitoylated EYFP into pUASp with XbaI
ZL11	ACTCTAGGCTCTAGGATAAC	Foward primer for nest PCR of Palmitoylated EYFP from UBb5 plasmid
ZL12	GTTATCTCGAATCGCGCGTT	Reverse primer for nest PCR of Palmitoylated EYFP from UBb5 plasmid

30

ZL13	GGCTACGGCCTGCAGTGC	Palmitoylated EYFP sequence primer
ZL14	CTTGAAGTCGATGCCCTT	Palmitoylated EYFP sequence primer
ZL15	GAGGATCCTTACTTGTACAGCTCGTCC	Reverse primer for cloning of Linker (Right part)-GFP into pBSKII with BamHI
ZL16	GCTCTAGAGGCTCTGGCAGCTCCGGTGGCATGGTGAGCAAGGGCGA	Forward primer for cloning of Linker(Right part)-GFP into pBSKII with XbaI
ZL17	GCCTCTAGAGCTCTGAAAATAAAGGTTTTCCGCGGAGCCTAGAACCT	Reverse primer for cloning of Dia-Linker (left part) into pBSKII with XbaI
ZL18	TAGCGGCCGCATGTCTCGTCACGAGAAACG	Forward primer for cloning of Dia into pBSKII with NotI
ZL19	TCCCAGTCACGACGTTG	pSKII Sequence primer
ZL20	TGAGCACCACGTTCAGAC	Dia sequence
ZL21	ATGGAGGAGTTCTTTGCG	Dia sequence
ZL22	CTGACCCTGAAGTTCATC	GFP sequence

2.1.13 Plasmids

Table 2.5 Plasmids were used in this study

Name	Description	Source
pET-15b	Protein expression in *E.Coli*	Novagen
pUASp	Making transgenic flies based on P element insertion	Lab of Grosshans
Delta2-3 Turbo	Transposes vector for making transgenic flies based on p element insertion	Lab of Grosshans
pUASp-attB	Making transgenic flies with attB/phi-C31 system	Lab of Grosshans
pBS (SK-)-Dia (EST)	Dia cDNA clone	Lab of Grosshans

pBS (SK-)-Chic (EST)	Drosophila profilin cDNA clone	Lab of Grosshans
pQE-ZZ-DiaC	DiaC expression in *E.Coli*	Lab of Grosshans
pQE-ZZ-DiaN	DiaN expression in *E.Coli*	Lab of Grosshans
pGEX6P2-CIP4 FL	Expression of GST-CIP4FL in *E.Coli*	Dr. Sven Bodgan
pGEX6P2-CIP4ΔSH3	Expression of GST-CIP4ΔSH3 in *E.Coli*	(Yan et al., 2013)

Table 2.6 Plasmids were generated in this study

Name	Description
pET-profilin	Expression of Drosophila profilin in *E.Coli* without any tag
pGEX60H-Cip4ΔFBAR	Expression of GST-CIP4ΔFBAR in *E.Coli* GST-tag fused on N-terminal of Cip4ΔFBAR
pGEX60H-Cip4ΔFBARΔSH3	Expression of GST-CIP4ΔFBARΔSH3 in *E.Coli* GST-tag fused on N-terminal of Cip4ΔFBARΔSH3
pGEX60H-Cip4-SH3	Expression of SH3 domain in *E.Coli* GST-tag fused on N-terminal of SH3 domain
pUASp-GFP-linker-Dia	Making transgenic flies with GFP-linker-Dia; GFP fused on N-terminal of Dia
pUASp-Dia-tev-linker-GFP	Making transgenic flies with GFP-linker-Dia; GFP fused on C-terminal of Dia
pUASp-palmitoylated-YFP	Making transgenic flies with palmitoylated-YFP which labeled the membrane
pUASp-attB-Cip4ΔSH3	Making transgenic flies overexpressing Cip4ΔSH3

2.1.14 Microscopy

Zeiss Stemi 2000 (Carl Zeiss), Leica MZ125 (Leica), Microinjection microscope (Carl Zeiss), LSM 780 (Carl Zeiss), Zeiss Axiovert 200 M Ultra-view spinning Disc confocal microscope   (Carl Zeiss), Zeiss Axioplan 2 Fluorescence microscope (Carl Zeiss)

2.1.15 Other reagents and materials

-Histone-Alexa488 for injection   Life technologies

-Complete Mini (EDTA-free) Protease Inhibitor Cocktail   Roche

-Aquapolymount   Polysciences, Inc

-Coverslips Menzel

-Glass slides   Thermo Scientific

-Fly vials   Greiner

-Glass pipettes (25ml, 20ml, 10ml, 5ml)   Silber Brandt

-Pasteur pipettes   Brandt

-Glass homogenizer B. Braun Biotech International

-Petri dishes   Greiner

-Pipet-aid   Drummond

-Micropipettes (1000µl, 200µl, 20µl, 2µl) Gilson

-Micropipette tips (1000µl, 200µl, 20µl, 2µl)   Eppendorf

-Eppendorf tubes (1.5ml, 2ml, 5ml)   Eppendorf

-PCR tubes Brand, Wertheim

-Falcon tubes (50 ml, 15 ml) BD Falcon

-Protein condensator   Vivaspin sartorius

-Dialysis tube   ROTH

-10S and 3S VoltaLef Halocarbon oil Lehmann & Voss & Co.

-Buchner funnel

-C 10/10 Column   GE Healthcare Life Sciences

2.1.16 Other equipment

-Äkta pure   GE Healthcare Life Sciences

-Odyssey CLx Infrared imaging system   LI-COR Biosciences

-Thermal Cycler Bio-rad

-Needle puller   P-87 Flaming/Brown Micropipette Puller-Sutter Instrument Co

-Sonicator   Sonifier Cell Distuptor Branson Ultrasonics

-Microfluidizer   EmulsiFlex-C5, Avestin

-Microinjector   FemtoJet - Eppendorf

-Western-Blot   Trans-blot SD Semi-Dry Transfer Cell - BIO-RAD

-Homogeniser   Dounce

-Pump P-1   Pharmacia Biotech

2.1.17 Softwares

Adobe Photoshop CS6 and Adobe Illustrator CS6 from Adobe were used for picture arrangement. FIJI (NIH) was used for measurement gray value in FRAP experiments. Zen 2012 (Carl Zeiss) was used for taking picture with LSM780. Lasergene (GATC biotech) was used for DNA plasmids editing. Microsoft excel and Microsoft word (Microsoft) were used for calculation and editing. Zotero (Roy Rosenzweig Center for History and New Media) was used for management of literatures.

2. 2 Methods

2.2.1 DNA methods

2.2.1.1 Standard methods in molecular biology

All the molecular cloning methods were carried out according to Sambrook and Russel, 2001, unless otherwise stated.

2.2.1.2 Isolation of DNA form adult flies

About 200 flies were anesthetized on ice and transferred to a mortar with liquid nitrogen and grinded with a pestle grinder until the flies became to a homogenous powder. The powder was transferred to a cooled Dounce homogenizer containing 5 ml of homogenization buffer. After grinding with a few strokes, debris were removed by centrifuge at 1000 rpm for 1 min. The supernatant was transferred to a new tube. After centrifugation at 8000 rpm for 5 min, the nuclei were in the pellet. The pellet was resuspended in 0.5 ml homogenization buffer, and incubated at 37°C for 45 to 60 min after proteinase K (final concentration of 100 µg/ml) and 50 µl of 10% SDS were added and mixed well by swirling and rocking.

0.5 ml phenol/chloroform was added and mixed for 5 min. The sample was centrifuged at 13,000 rpm for 5 min. The upper phase was transferred to a new Eppendorf tube. This step was repeated to remove protein completely. 0.5 ml of Chloroform was added to this and mixed well. The sample was centrifuged again at 13,000 rpm for 5 min. The upper phase was again transferred to a fresh Eppendorf tube. NaCl was added to a final concentration of 200 mM and mixed well. Two volumes of 100% ethanol was added and mixed by gentle swirling. The DNA appeared at the interface as a clump. The DNA pellet was precipitated by centrifugation of 13000 rpm for 5 min. The pellet was washed in

80% ethanol and then 100% ethanol. Supernatant was discarded and pellet dried in the Speedvac. The dried pellet was resuspended in 0.5 ml of TE buffer.

2.2.1.3 Polymerase chain reaction (PCR)

PCR were carried out using Taq or Pfu DNA polymerase which were generated in the lab. The following reagents were mixed for the standard PCR:

50-200 ng DNA template,

0.5 µM forward and reverse primers,

50 µM dNTP (each),

10X PCR buffer (depending on the polymerase),

1-2 units (per 50 µl of reaction) Taq or Pfu polymerase.

The PCR were done using the following conditions:

Step 1 (Initial denaturation): 95°C - 2 min

Step 2 (Denaturation): 95°C - 30 sec

Step 3 (Annealing): 50-60°C - 1 min

Step 4 (Elongation): 72°C - 1 min/Kb to be amplified

Repetition of steps 2 to 4 for 20-35 times

Step 5 (Final elongation) 72°C – 10 min

2.2.1.4 In-fusion cloning

In-fusion cloning was carried out according to the manufacturer's instructions.

2.2.1.5 DNA sequencing

DNA sequencing was carried out with the sequencing facility at the Department of Developmental Biochemistry, GZMB, University of Göttingen. Sequencing samples were prepared according to the instructions.

2.2.2 Protein purification

2.2.2.1 Preparation of Poly-L-proline column

3 g of dry CNBr-activated-sepharose beads were swelled in 30 ml of 1 mM HCl for 15 min. The beads were washed on a sintered glass filter funnel with about 600 ml of 1 mM HCl and subsequently washed by coupling buffer.

0.25 gm of poly-L-proline was dissolved in 20 ml ice-cold ddH$_2$O. The poly-L-proline solution was added to 50% slurry of activated Sepharose with stirring and followed by 2-hour stirring at room temperature and overnight stirring at 4°C. 10X quench buffer was added to the slurry beads. The resin was washed with 2 L dd H$_2$O in sintered glass filter funnel and store in 1X storage buffer. The resin was poured into the C10/10 column and washed by 6 M urea, H$_2$O, 20 % ethanol and again H$_2$O.

2.2.2.2 Purification of Profilin

pET-Profilin was transformed into *E.Coli* BL21(DE3). The expression of profilin was induced when the OD$_{600}$ reading of the culture reached at 0.6. 0.2 mM of IPTG was added for the induction. After 4 hours at 37 °C induction, the cells were harvested by centrifuging at 5000rpm for 30 min.

The cells were resuspended in P buffer and incubated with 1mg/ml lysozyme and a pinch of DNase for 30 min on ice. The cells were then lysed using either microfluidizer or sonifier (4X1min, output level 5, 40% duty cycle). The soluble part was obtained by centrifuging twice at 15,000 rpm for 20 min each to remove the insoluble fraction. The clear supernatant (soluble fraction) was passed through the prepared a Poly-L-proline column (equilibrated with P buffer before use) by P-1 pump at the speed of 1 ml/min and the flow through was reloaded once. The column was washed with 10 X column volume and eluted with elution buffer. The protein solution was precipitated by ammonium

sulfate (final concentration of 2.4 M) at 4°C. The protein pellet was collected by centrifugation 15K for 40 min at 4°C, and dissolved in 0.5 ml P buffer. The protein solution was applied to gel filtration with Superdex75 (16/60) to get rid of the remaining DMSO and salt. After gelfiltration, the protein was concentrated with vivaspin 15 (MW5000). The protein was stored in P buffer with 60% glycerol at -20°C.
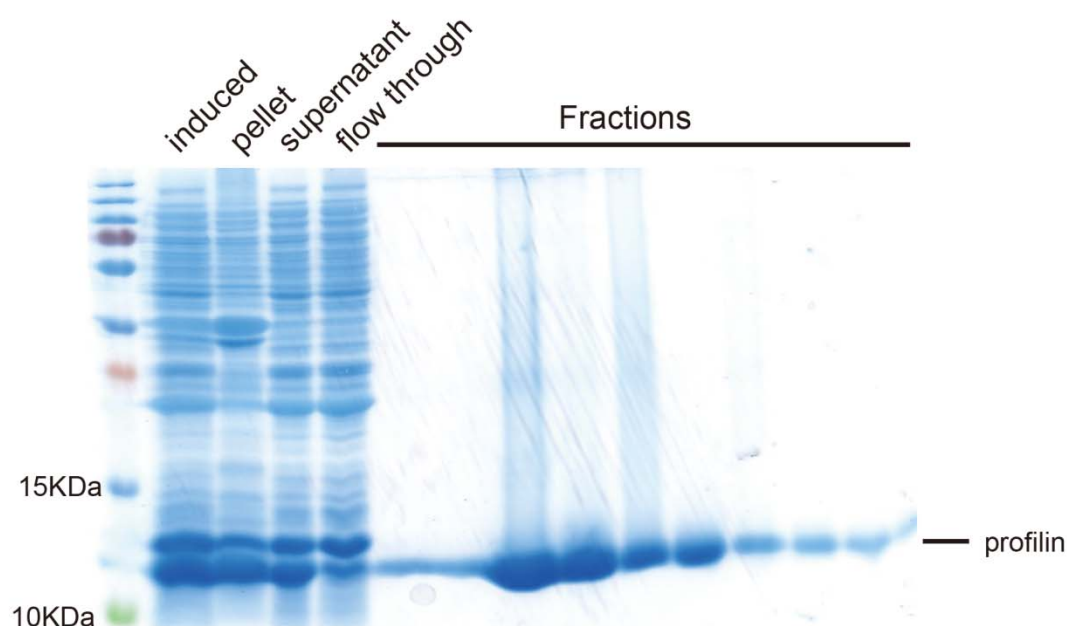

Figure 2.1 Purification of profilin using poly-L-proline column. SDS-PAGE showing samples from different steps of profilin purification. Half of profilin remained in the pellet after lysing cells. After binding to the poly-L-proline column, the profilin band is lighter than input (supernatant). The protein was eluted from the column and precipitated by $(NH_4)_2SO_4$ and went through gelfilteration. After concentration, the protein was stored in-20°C.

2.2.2.3 Purification of His-tag proteins

Expression of ZZ-DiaN–His6X(1..511) and ZZ-DiaC-His6X (512..1091) were induced by adding 0.1 mM IPTG at OD_{600} of 0.6 and incubated at 37°C for 4 hours. The cells were harvested by centrifuge and lysed in His-tag protein lysis buffer as described previously. The supernatant was applied to a Nickel-Sepharose prepacked column (HisTrap HP column 1 ml) using Äkta pure

system. After washing with approximately 10 ml of wash buffer, the protein was eluted with elution buffer. Since the eluted protein solution contained high concentrated imidazole, buffer exchanging was done immediately using PD10 desalting column, and the protein was concentrated using vivaspin and stored in storage buffer at -20°C.

2.2.2.4 Purification of GST-tag proteins

Expression of GST-Cip4 (1..631), GST-Cip4ΔSH3(1..565), GST-Cip4ΔFBAR (190..631), GST-Cip4ΔFBARΔSH3 (190..565), GST-SH3 (564..631) were induced and the cells harvested, lysed as described previously, but in the GST-tag protein lysis buffer. The supernatant was applied to a Glutathione Sepharose prepacked column (GSTrap HP column) using Äkta pure system. After washing with approximately 10 ml of wash buffer, the protein was eluted with elution buffer. After buffer exchange, the protein were concentrated and kept at -20°C. Alternatively, the GST tag were cleaved using PreScission protease as following described.

2.2.2.5 Cleavage of GST-Tag using PreScission protease

GST-Cip4 and GST-Cip4ΔSH3 were transferred tin the dialysis bag with PreScission protease. The storage buffer without glycerol was used as dialysis buffer. The volume of dialysis buffer was 100X of the protein solution volume. Dialysis buffer was changed three times and each dialysis duration was more than 3 hours. Dialysis was done at 4°C. After dialysis, the glutathione was gone from the dialysis bag and GST-tag was already cut off by PreScission protease. Subsequently the protein solution was passed through GSTrap HP column, and the free GST tag bond to column and Cip4/Cip4ΔSH3 went through. The flow through was collected, concentrated and stored in storage buffer at -20°C.
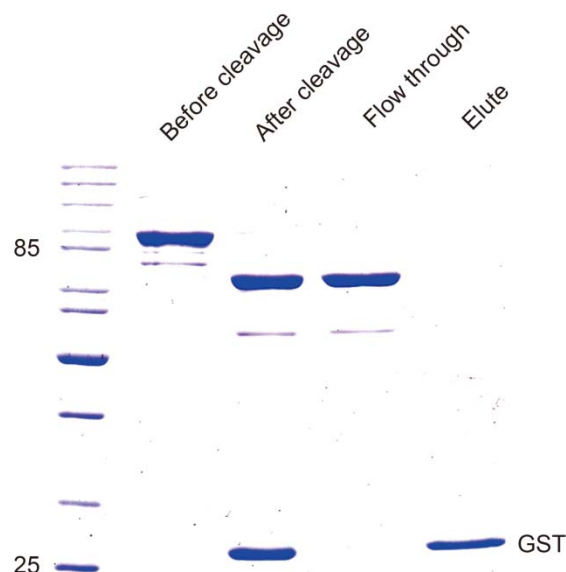
Figure 2.2 Cleavage of GST-Cip4 using PreScission protease. SDS-PAGE showing the efficient cleavage. GST tag was removed by passing through Glutathione column. The flow through was collected. After concentrating with vivaspin, the protein was stored in storage buffer at -20°C

2.2.3 Affinity purification of antibodies

2.2.3.1 Preparation of affinity column using the CNBr-activated Sepharose beads

1 g of dry CNBr-sepharose 4B (activated) beads were swelled in 10 ml of 1 mM HCl for 15 min. The beads were washed on a sintered glass filter with about 200 ml of 1 mM HCl. The beads were transferred to falcon tube and washed with coupling buffer for 3 times. The purified protein (10 mg) was diluted in coupling buffer, and added to the beads in a 1:2 gel:buffer ratio. The mixture was rotated for 3 hours at room temperature. After making the beads settle down, the supernatant was discarded and the beads was washed with 5X volume of coupling buffer to remove excess protein. The beads were resuspended and poured into the C10/10 column. The column was washed with five cycles of alternating low and high pH buffers (Buffer I and Buffer II). Then the column was washed with five column volumes of PBS. The column was stored at 4°C.

2.2.3.1 Affinity purification of antibodies against Dia C terminal and N terminal fragment

The serum was centrifuged twice at 15,000 rpm for 20 min each at 4°C. The cleared serum was then applied to the column at a flow rate of 0.5 mg/ml by P1 pump. The flow-through was reloaded to the column again. The flow-through was collected and saved. The column was washed by ten column volumes of PBS + 500 mM NaCl and then with PBS + 1 M NaCl. The elution was taken in the order of High salt, low pH and high pH elution buffer. For collecting low pH and high pH elution, 100 µl of neutralization buffer was added to the collection tubes in advance and 900µl fractions were taken from elution.

A280 absorption was taken for each fraction, and peak fractions from the same elution were pooled together. The purified antibodies were buffer-exchanged to PBS using PD-10 column and concentrated to 5 mg/ml. Na-Azide was added to 0.02% to the antibodies and they were stored at 4°C.

2.2.4 Binding test

The expression of GST-Cip4 was induced as describe previously. The cells pellet were resuspended using lysis buffer and aliquoted in Eppendorf 1.5ml tube (equal to 50 ml culture). The suspended cells were lysed by sonifier (3X10s, output level 4, 40% duty cycle). After centrifugation at 14,000 rpm at 4 °C for 15 min, the supernatant was transferred to a new tube. 100 µl of GST-Cip4 supernatant was added to 100 µl PBST-pre-washed Glutathione beads. Additional lysis buffer was added to make the volume up to 0.5 ml. After 1 hour incubation at 4 °C, the beads were washed by lysis buffer containing PMSF (final concentration 0.5 mM). The beads were divided into 5 fractions, and purified DiaC and DiaN were added in each tube according the required concentration. Lysis buffer was added to each tube to make up the volume of

0.25 ml. After 1 hour incubation at 4 °C, the beads were pelleted using centrifuge with 500 g for 3 min. The supernatant was transferred to a new tube and centrifuged at 14,000 rpm for 2 min to get rid of the remaining beads, and the new supernatant was taken as unbound fraction. The beads were washed by lysis buffer containing PMSF for 3 times, and laemmli buffer was added to the beads as bound fraction. SDS-PAGE was performed. GST expressed sample were used parallel in this assay as control.

2.2.5 Western blot

Embryos were staged from 1.5 to 3 hours on apple-juice agar plates and dechorionated in 50% Klorix bleach for 90 seconds. The dechorionated embryos were collected into a Eppendorf tube and weighed. The weight of the embryos was determined (~1mg =100 embryos). The embryo was snap frozen in liquid nitrogen. The embryo were homogenized in 1X Lämmli buffer with the volume to make the final concentration 20 embryos/μl. The sample was heated to 95°C for 5 min and centrifuged at 14,000 rpm for 1 min. The supernatant (protein extracts) corresponding to 10-30 embryos were loaded on the SDS-PAGE. The proteins from the gel were transferred onto a nitrocellulose membrane using a semi-dry transfer for 1 hour at 60 V/gel. The membrane was blocked in 5% milk powder in PBST (fresh made) for at least 30 min and incubated with primary antibody either overnight at 4°C or 2 hours at room temperature. The membrane was rinsed with PBT for three times and 4X15 min PBST washing followed. The membrane was incubated with secondary antibody for 1 hour at room temperature, protected from light. The membrane was rinsed in PBST for three times and washed with PBST for 4X15 min. The bands were detected using the Odyssey CLx Infrared Imaging system.

2.2.6 Immunoprecipitation

Protein A beads were washed with PBS. After 1 hour incubation with rabbit DiaC antibody (antisera and purified antibodies) at 4 °C, the beads were washed with PBS for three times and kept on ice. The staged embryos were collected on the apple juice plate, and dechorionated with bleach, then weighted and frozen in liquid nitrogen. The embryos were homogenized in PIPA buffer using Dounce homogenizer. 1 ml RIPA buffer were required for 100mg embryo. The lysate was centrifuged at 14,000 rpm at 4°C for 15 min. The supernatant was added to the antibody-loaded beads as Input and rotated on a wheel for 2 hours at 4°C. The beads were centrifuged with 500 g for 5 min. The supernatant was taken as unbound sample. The beads were washed with RIPA buffer for three times. 2X laemmli buffer was added to the beads and boiled for 5 min. The supernatant was taken after centrifugation at 14,000 rpm for 1 min as bound sample. According to (1µg=100embryos), the Input, (~10 embryos), unbound (~10 embryos) and bound (~500 embryos) samples were loaded on SDS-PAGE and followed by western blot.

2.2.7 Fractionation of embryos

The dechorionated wild type embryos were homogenized in fractionation buffer using Dounce homogenizer. The lysate was considered as total fractions. The lysate was centrifuged at 2500 rpm for 5 min at 4°C for two times to precipitate the nuclei. Supernatant was transferred into a new Eppendorf tube and centrifuged at 14,000 rpm for 15 min at 4°C. The lipid layer was removed by an aspirator. The clear supernatant (cytoplasmic fraction) was transferred to a new Eppendorf tube. The pellet (membrane fraction) was washed with fractionation buffer for 3 times. The total, cytoplasm, membrane fraction samples were added 2X laemmli buffer and heated 95 °C for 5 min and loaded on a

SDS-PAGE, followed by western blot detection. α-Tubulin was also detected as loading control.

2.2.8 Generation of *dia^sy5* and *Ced-12^2L367* germline clone

The germline clone was performed following the instruction by Chou and Perrimon (Chou and Perrimon, 1992) with minor modifications. The heat shock for inducing flippase was performed at 37°C for 60min per day for two days (24-48 hr and 48-72 hr) after hatching.

2.2.9 Generation of transgenic fly

The transgenic flies were generated with either P-element transposon system or an attB/phi-C31-based integration system (Bischof et al., 2007; Bownes et al., 1990). The generation process was followed standard protocol (Wenzl et al., 2010) (http://wwwuser.gwdg.de/~jgrossh/method).

2.2.10 Mapping of unknown mutants with meiosis recombination and deficiency

Meiotic recombination mapping was used to narrow down the suspicious mutant region. Frt2L2R{w+}/*al dp b pr* Frt2L, 2L367 virgins were collected. The heterozygous for the chromosome carrying 2L367 mutant and recessive markers and the Frt2L2R{w+} recombined during meiosis and various classes of recombinant chromosomes went to the female egg and detected by crossing with *al dp b pr Bl c px sp*/SM1 males. The position of mutation was determined according to the proportion of different recombinant chromosomes. To get the finer localization of mutant, the complement test with deficiencies was done.

For the complement test with deficiencies, the mutant virgins were crossed with the males containing the molecular defined deficiencies on II chromosome. If the mutant/deficiency progenies are viable and fertile, then the mutant is out of

this deficiency region. If the mutant/deficiency progenies couldn't be found, i.e. the deficiency cannot complement the mutation, it means the mutation is located within the region of the deficiency. The deficiency region covers several genes. In order to know which gene is mutated in the mutant line, the complement test with specific genes which were in the suspicious deficiency region was carried out. The cross strategy is the same as above. If the mutated gene cannot complement the original mutant, it means they are the same gene.

2.2.11 Embryo fixation and immunostaining

The embryo fixation and immunostaining process were followed standard protocol (Wenzl et al., 2010) (http://wwwuser.gwdg.de/~jgrossh/method).

2.2.12 Injection of CK666 and Histone-Alexa488

CK666, Arp2/3 inhibitor, was dissolved in DMSO. WT and dia germline clone embryos were dechorionated, dried in a desiccation chamber for 10 min, covered with halocarbon oil and injected posteriorly with desired concentration of CK666. DMSO was injected as control. After injection, the embryos were incubated for ~10 min and subsequently fixed. The vitelline membrane was removed manually. The embryos were collected in Eppendorf tube, washed by methanol and kept -20°C.

To track the cell cycle, Histone-Alexa488 was injected into the WT and *2L367* germline clone embryos with the final concentration of 2 mg/ml. The preparation of embryos was described above. After covered with halocarbon oil, Histone-Alexa488 was injected posteriorly. The fluorescent movie was recorded at the spinning disc microscope with a 25X oil objective.

45

2.2.13 Induction of shibire phenotype

Embryos from *shibire* heterozygous or homozygous females were collected, kept at 32°C in a water bath for 30 minutes after dechorionation. The embryos were fixed as described previously.

2.2.14 Live imaging

Embryos were dechorionated, lined up, glued on to a coverslip and covered with halocarbon oil. Fluorescent live-images were taken either at the LSM with a 63X oil or glycerol objective or at the spinning disc with a 40X oil objective. Differential interference contrast microscopy movie was recorded at the spinning disc microscope with a 25X oil objective.

2.2.15 Fluorescence recovery after photobleaching (FRAP)

In order to check turnover rate of Dia-GFP on membrane, bleaching of UASp-Dia-GFP under the driven of Maternal GAL4 was carried out in a given area using 100% laser power and 50 iterations at a scan speed of 5.

For examining the membrane property during cellularization, the furrow and furrow canal labeled by GAP43-venus, palmityolated-YFP and 117GFP in wild type and *dia* germline clone background was bleached. From the surface view a range of Z-stacks were used to track the invaginating furrow canal during cellularization. The 100% laser power and 50 iterations were used for bleaching, and the recording speed was at 5 or 6 depending on how many z-stacks were taken. The other approach was doing FRAP from side view. In this case, the glycerol objective was used. The measurement was done with FIJI.

Chapter 3. Results

3.1 Actin polymerization activity of Dia is suppressed by Cip4

3.1.1 Approaches to identify the potential Dia interactor

The activity of Dia is tightly regulated in eukaryotic cells. The intramolecular interaction between DID and DAD makes Dia in an autoinhibited state in the cytosol (Chesarone et al., 2010). The activation of Dia is achieved by binding of a RhoGTPase to GBD that relieves the autoinhibition via interrupting the interaction between DID and DAD. Meanwhile Dia is recruited to the membrane by RhoGTPase or other factors (Chesarone et al., 2010). However, *in vitro* studies showed that RhoGTP in a physiological concentration cannot fully reconstitute the release of Dia autoinhibition (Grosshans et al., 2005; Li and Higgs, 2003), suggesting that additional factors are involved in activating Dia *in vivo*.

Dia localizes at the membrane, especially is enriched at the furrow canal in the cellularization stage of *Drosophila* embryo (Figure 3.1). However, by western blotting of fractionation of same stage embryos, I could show that the majority of Dia is in the cytosol; only a small fraction shows up in the embryo membrane extraction (Figure 3.2). The cytoplasmic Dia is considered to be inactive, since Dia is recruited to membrane when it is active (Chesarone et al., 2010).
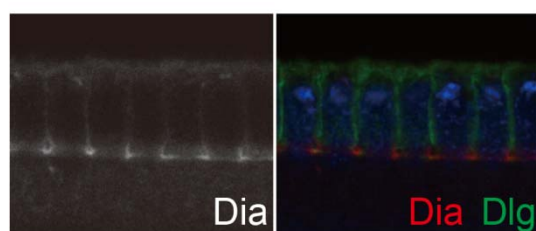
Figure 3.1 Dia localizes at the membrane. Immunostaining of Dia in cellularization stage of *Drosophila* embryo. Dia localizes at membrane, and is enriched at the furrow canal.
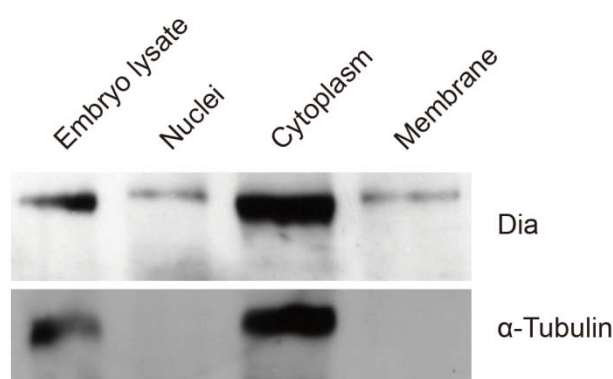

Figure 3.2 The majority of Dia is in cytosol. Fractionation shows distribution of Dia in the embryo. Only small portion is attached with membrane, while a large amount of Dia is in cytosol. The absence of α-tubulin in the membrane fraction indicates that the membrane fraction is not contaminated by cytoplasmic fraction. 30 embryos were loaded in each lane.

To identify those unknown factors, I planned to use immuno-precipitation to pull down Dia and the associated protein complex, followed by Mass-Spectrum analysis. The membrane fraction of Dia will be used as a starting material for immuno-precipitation. In our lab we have rabbit and guinea pig source serum against Dia C terminal fragment (termed DiaC in the following text) which works nicely in immunostaining. However, in the western blotting, rabbit source serum shows a stronger background (Figure 3.3 A). On the other hand, DiaC is conserved in the formin family. In an attempt to get a more specific antibody, I used Dia N terminal fragment (termed DiaN in the following text) as the antigen to immunize rabbit and guinea pig. However, no specific bands were detected using DiaN serum both from guinea pig and rabbit (Figure

3.3 A). To remove the background, affinity purification of DiaC rabbit serum was employed (Figure 3.3 B). The background was reduced after affinity
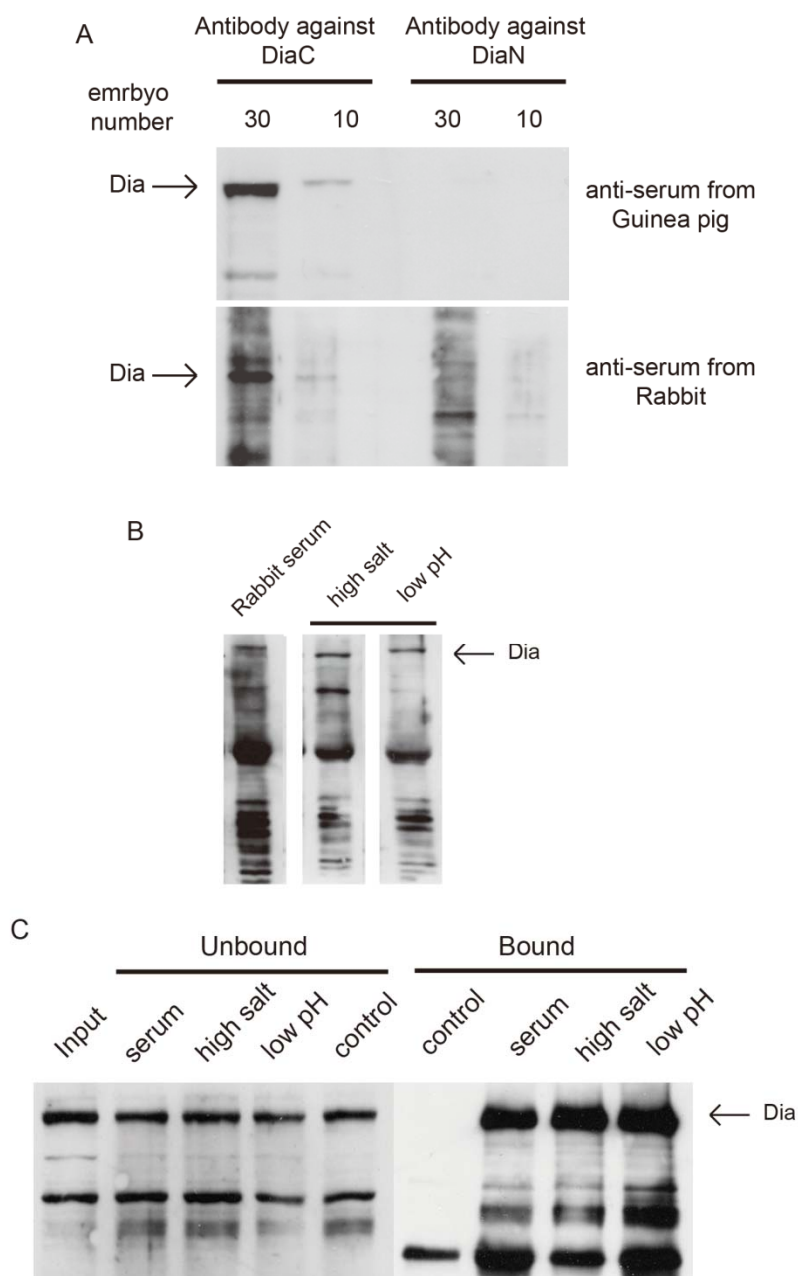

Figure 3.3 Western blot and immune-precipitation by Dia andtibodies. (A) Dia can be detected by DiaC antibodies raised in guinea pig and rabbit, and guinea pig antibody preforms better in western blot. However, DiaN antibodies couldn't detect Dia band. (B) After affinity purification of DiaC rabbit serum, the unspecific bands are reduced. (C) Dia can be pulled down with serum and purified antibody. Detected by GP antibody. Empty beads were used as a control.

purification, though there were still some unspecific bands detected. Endogenous Dia was immuno-precipitated using those antibodies (Figure 3.3C). The purified antibodies can be used in large scale immune-precipitation and mass spectrometry which will be done in the future.

The other approach for Dia IP is using GFP binder to pull down Dia-GFP complex from Dia-GFP transgenic fly embryos. Five UASp-GFP-Dia lines were generated by Dr. Christian Wenzl in our lab previously (Figure 3.4 and 3.5). However, the expression level when driven by maternal GAL4 is much higher than endogenous level (Figure 3.5 B). I checked the localization of GFP-Dia using live imaging. Nuclear exclusion of GFP-Dia was observed in these embryos. UASp-GFP-Dias were introduced in dia^{sy5}, matGal4 flies by crossing. After inducing the germline clones of dia^{sy5} by Flipase-Frt system, the ectopic GFP-Dia can partially rescue dia^{sy5} with a rescue rate of ~50%.

Figure 3.4 Schematic representation of GFP-Dia constructs. The GFP with flexible linker was added at C or N terminal of Dia

In order to get a better transgenic fly in terms of expression level and rescue capability, we did another round of making transgenic fly. We reasoned that the GFP at N-terminal could affect the Dia protein folding, resulting in a failure to rescue completely. A flexible linker with the amino acid sequence of AAAGSTGSGSSG was introduced between GFP and Dia. However, the linker did not show any improvement (Figure 3.5).

A

GFP-Dia 6   10   21

26   27

GFP-linker-Dia

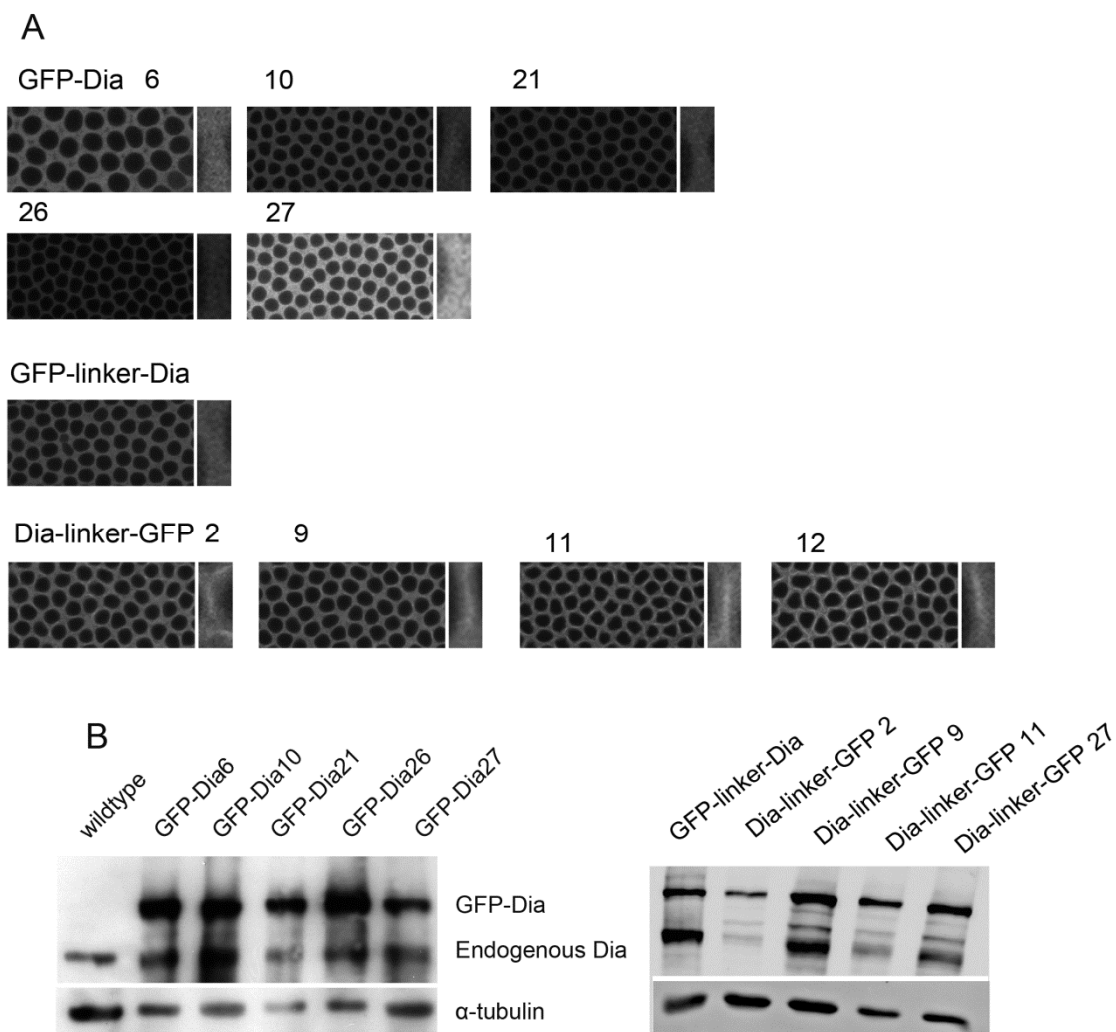Dia-linker-GFP 2   9   11   12

B

Figure 3.5 The localization and expression level of GFP-Dia in 10 lines (A) Live images of different GFP-Dia lines. Addition of GFP with linker at C terminal improves the localization of GFP-Dia. The cell border was shown in high magnification. All images were taken with the same settings. (B) Western blot showed that the level of GFP-Dia is much higher than endogenous level. 15 embryos were loaded in each line. Tubulin is detected as loading control.

It was previously found in our lab that N terminal fragment of Dia is responsible for protein localization. Adding extra amino acid at the N terminal may have an effect on the localization function. To overcome this problem, GFP tag was translocated at the C terminal fragment of Dia with the flexible linker. Meanwhile, a TEV cleavage site was also introduced between the linker and Dia. Four lines were generated after plasmid injection; two lines are with the pUASp-Dia-tev-linker-GFP insertion into the X chromosome and the other two

lines are into the third chromosome. Membrane localization of Dia-GFP could

be observed, though there was still nuclei exclusion distribution (Figure 3.5).

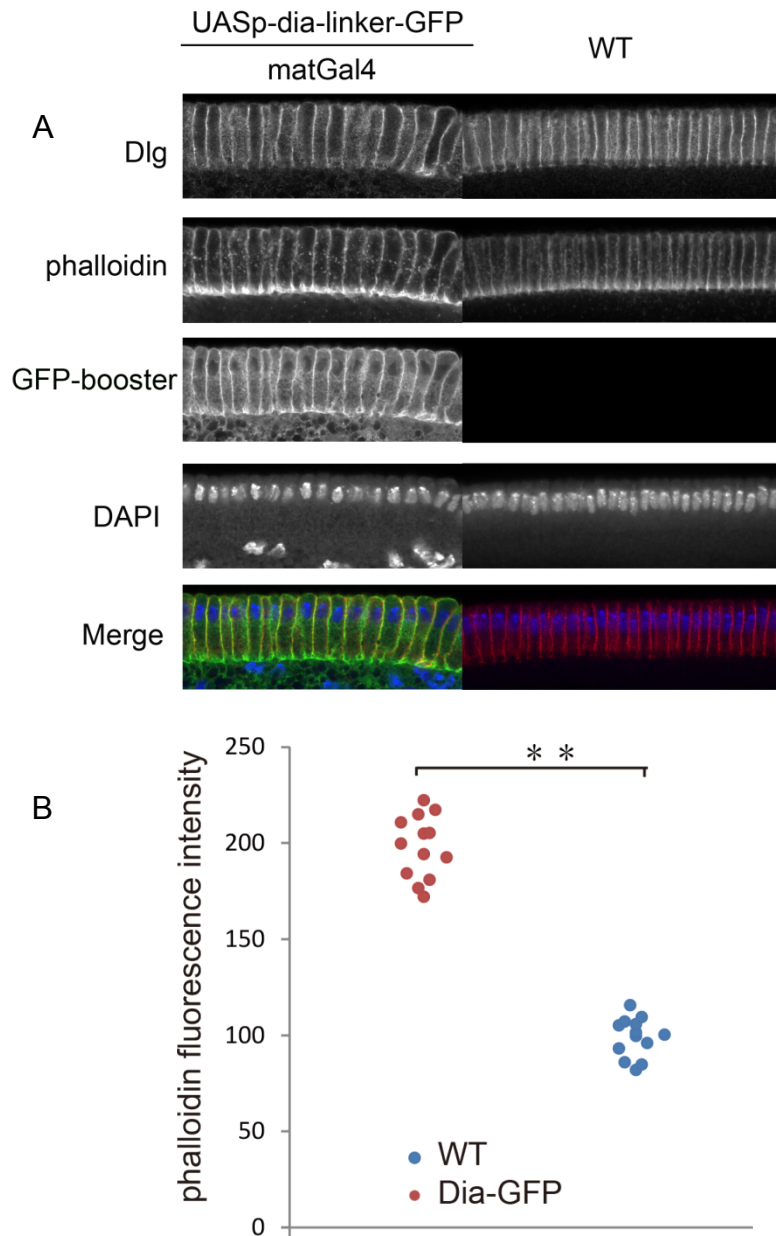In the fixed sample, F-actin intensity in Dia-GFP is higher than wild

Figure 3.6 The ectopic Dia-GFP induces F-actin polymerization. (A) Dia-GFP and WT embryos were stained in the same tube, and were distinguished by GFP booster signal. The phalliodin fluorescence intensity is much higher in Dia-GFP embryos than in wild type embryos, indicating the ectopic Dia-GFP can induce F-actin polymerization. (B) Quantitative analysis of phalliodin fluorescence intensity in wild type and Dia-GFP embryo.

type embryo which was stained in the same Eppendorf tube, suggesting the activity of ectopic Dia-GFP in the embryo even though without extra Rho activity (Figure 3.6). However, the rescue rate is not improved (Table 3.1).

Table 3.1 The rescue rate of different transgenic Dia-GFP construct

Dia-GFP construct	da^{sy5}, matGal4 67; UASp-GFP-Dia	UASp-DialinkerGFP; dia^{sy5}, matGal4 67	UASp-Dia-linker-GFP; dia^{sy5}, matGal4 67
Rescue rate	~50% (Courtesy: Dr. Christian Wenzl)	~48% n=130	~49% n=89

In order to check Dia mobility at the membrane, FRAP analysis was done using Dia-linker-GFP embryos. The signal on the membrane recovered within the range of minute. Compared with other membrane associated proteins, such as Slam and PDZ domain containing protein, Dia showed faster mobility (Acharya et al., 2014).
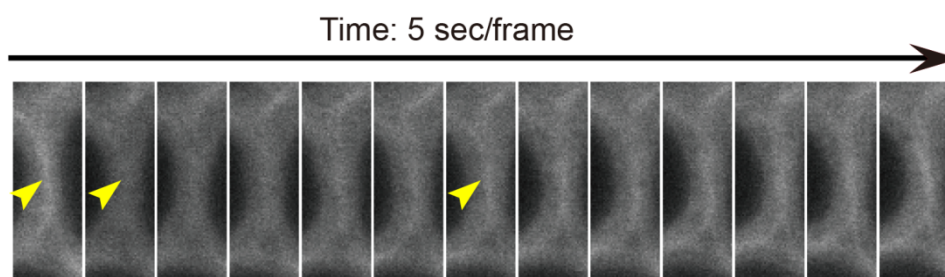

Figure 3.7 Mobility of Dia is fast. Dia-GFP is enriched at the membrane, as indicated by yellow arrows. The first image was taken before bleach, and the second was taken immediately after bleach. The cytoplasmic signal is hardly bleached, because of the fast exchange in cytoplasm. But the membrane signal completely disappeared after bleaching (the second yellow arrow). The following images were taken every 5 sec, and the signal on the membrane recovered in less than 1 min (the third yellow arrow).

3.1.2 Cip4 is an interactor of Dia

S. Bogdan and colleagues (Yan et al., 2013) found Cip4 and Dia can form a complex in S2 cells, which was shown by Co-immuno-precipitation. To confirm this result, binding assay was performed with purified proteins. Dia C terminal half and N terminal half were purified as indicated (Figure 3.8 and 3.9). Cip4 binds to DiaC with a KD of ~100 nM (Figure 3.10).
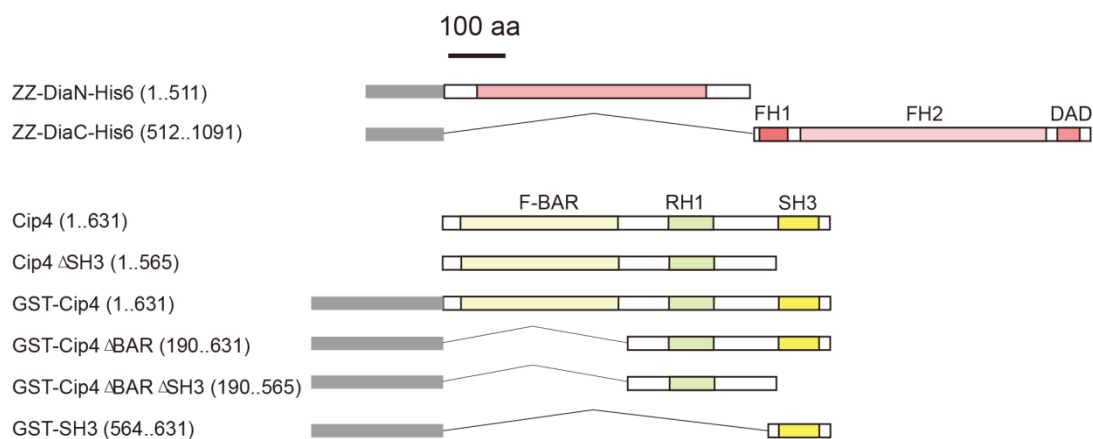

Figure 3.8 Schematic representation of proteins purified in this study.
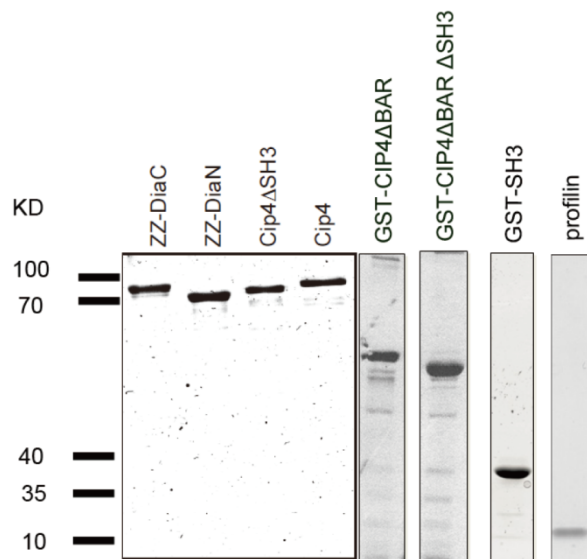

Figure 3.9 Purified proteins used in this study. The samples were loaded on SDS-gel and stained with Coomassie Blue.

Tabel 3.2 Purified proteins in this study

| Protein	Total amount of LB culture	Column	yield
ZZ-DiaC-Hisx6	3 l	HisTrap HP column (1 ml)	~10 mg
ZZ-DiaN-Hisx6	3 l	HisTrap HP column (1 ml)	~10 mg
Cip4	0.5 l	GSTrap HP column (1 ml)	~1 mg
Cip4ΔSH3	0.5 l	GSTrap HP column (1 ml)	~1 mg
GST-Cip4ΔFBAR	0.5 l	GSTrap HP column (1 ml)	~1.8 mg
GST-Cip4ΔFBARΔSH3	0.5 l	GSTrap HP column (1 ml)	~1.1 mg
GST-SH3	0.5 l	GSTrap HP column (1 ml)	~1.8 mg
Profilin	1 l	poly-L-proline column	~20 mg
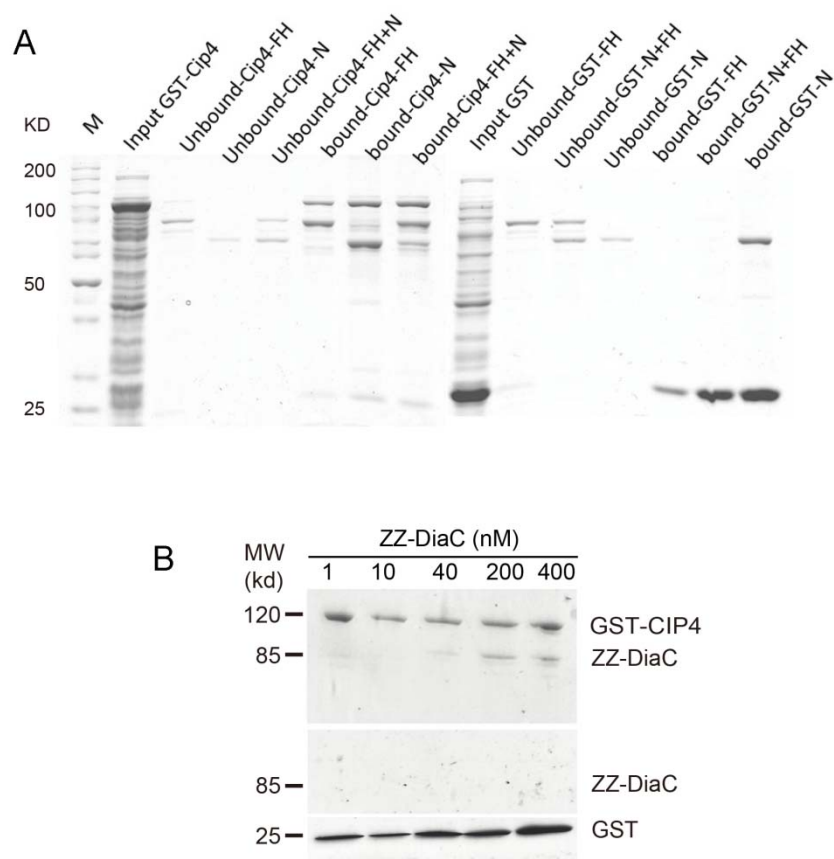
Figure 3.10 Physical interaction between Cip4 and Dia. (A) The binding of Dia to Cip4 was detected by binding assay. DiaC, rather than DiaN, could bind to Cip4. (B) Different amount of DiaC were added to GST-Cip4 or GST beads. SDS-Gels were stained with Coomassie Blue.

3.1.3 Cip4 inhibits Dia actin polymerization activity in Pyrene assay

(Pyrene assay was done by M. Winterhoff in Prof. J. Faix lab)

Next, we wondered whether the binding of Cip4 show some effect on Dia actin polymerization activity. Pyrene assay was employed to test the actin polymerization activity of Dia. Compared with dDia1 P2 (*dictyostelium* formin with two poly-proline stretches), ZZ-DiaC showed stronger actin polymerization activity (Figure 3.11 A). In the titration experiment, a series of ZZ-DiaC dilution from 0.125 nM to 1 µM was used. 2.5 nM of ZZ-DiaC was found to be sufficient for polymerizing actin filaments. This is similar to the actin polymerization activity of mDia1 (Li and Higgs, 2003) (Figure 3.11 B, C and D).
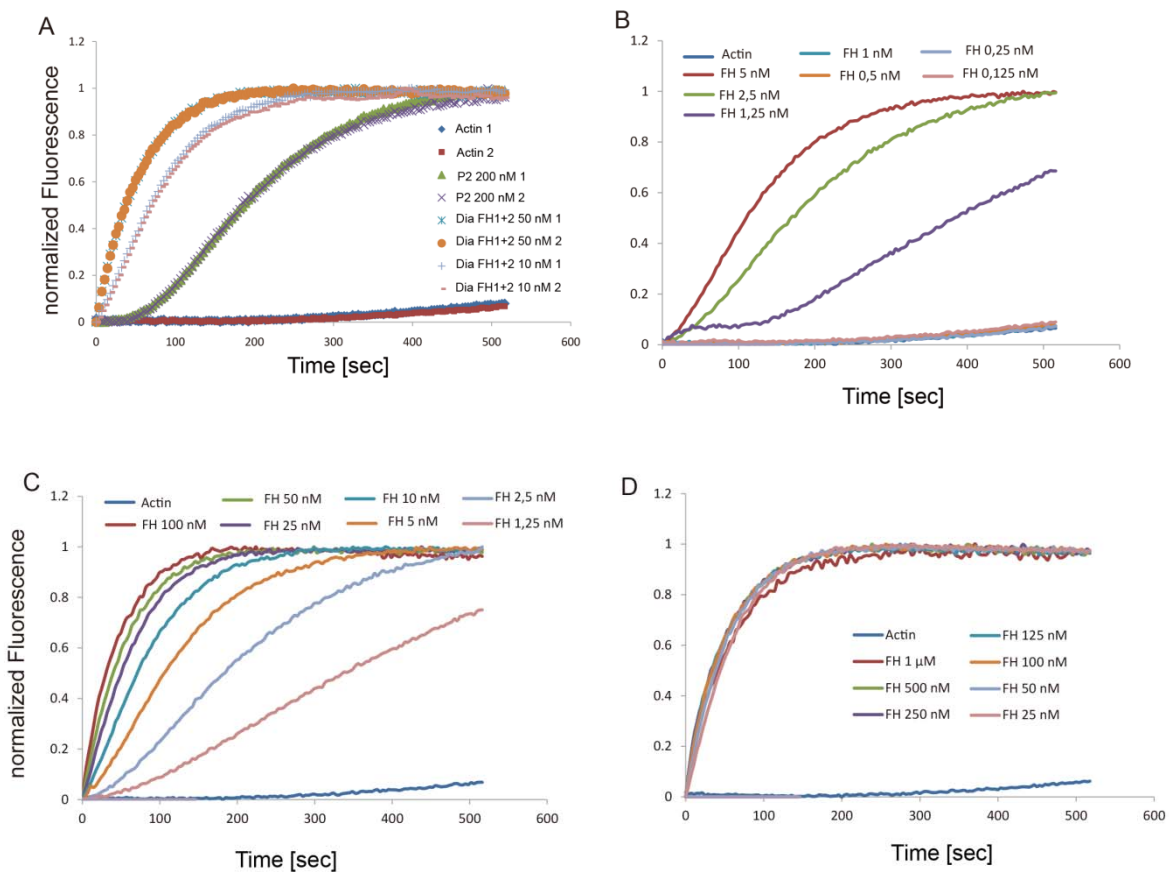

Figure 3.11 Dia is a strong actin nucleator shown in Pyrene assay. (A) Dia showed strong actin nucleation activity compared with P2. (B-D) Dia induced actin polymerization at indicated concentrations. 2.5 nM Dia (green line in B) could induce sufficient actin filaments which can be detected by Pyrene assay.

It has been reported that the activity of Dia is inhibited by the intramolecular interaction of DID and DAD domains as mentioned previously (Campellone and Welch, 2010). Theoretically, DiaN inhibits DiaC activity in the ratio of 1:1. However, in the titration inhibition assay, we found 10X more DiaN was needed for the inhibition (Figure 3.12). One possibility is that ZZ-DiaN may be not stable in lower concentration. After dilution, ZZ-DiaN lost the inhibition activity in a few minutes (data not shown).

To test whether Cip4 was able to affect actin assembly, we added increasing amounts of purified Cip4 protein to 10 nM ZZ-DiaC in the actin pyrene assay. We could show that Cip4 inhibited Dia activity in a concentration dependent manner (Figure3.12). 100 nM (10X more than DiaC) of Cip4 is sufficient for inhibition. 200 nM of Cip4 inhibited DiaC activity more efficiently, almost comparable to autoinhibition.
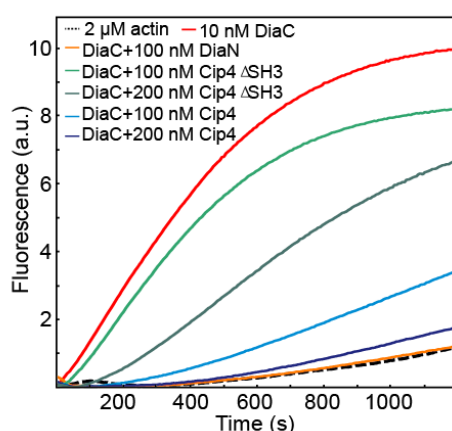

Figure 3.12 Cip4 inhibits Dia actin polymerization activity. Polymerization of actin (2 mM, 10% pyrene-labelled) in the presence or absence of DiaC, DiaN, Cip4, Cip4ΔSH3 at the concentrations indicated. Cip4 inhibits Dia actin polymerization in a concentration-dependent manner. However, Cip4ΔSH3 couldn't inhibit Dia activity as effective as by Cip4. Normalized curves are shown.

It was reported that SH3 domain could bind to proline-rich domain and the binding is involved in many cellular process (Aspenström, 2014). S. Bogdan and colleagues (Yan et al., 2013) showed that in S2 cells, the interaction of FH1 domain (proline-rich domain) and SH3 domain is crucial for colocalization of Dia

and Cip4 in the cell periphery. So we tested whether SH3 domain is necessary in the inhibition effect of Cip4. In the pyrene assay, Cip4ΔSH3 couldn't inhibit DiaC activity as efficiently as Cip4 full-length.

Next we checked if SH3 domain itself is sufficient to inhibit Dia activity. GST-SH3 domain was purified and used in actin pyrene assay. It was shown that GST-SH3 could inhibit DiaC activity. However, this inhibition needs higher molar excess of GST-SH3 (Figure 3.13).
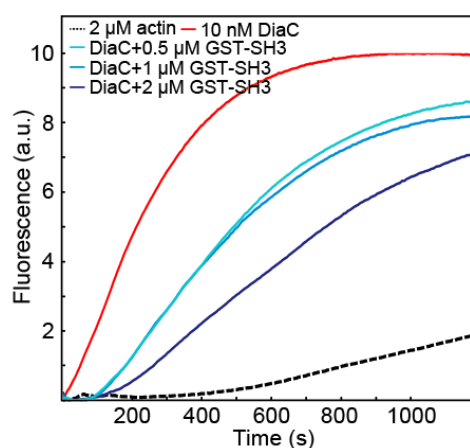

Figure 3.13 GST-SH3 is sufficient for inhibiting Dia activity. GST-SH3 can inhibit actin polymerization activity of Dia, but a relatively high concentration of GST-SH3 is needed.

3.1.4 Cip4 inhibits Dia actin nucleation activity shown by TIRF microscopy

(TIRF microscopy assay was done by M. Winterhoff in Prof. J. Faix lab)

Pyrene assay is a bulk polymerization assay, which cannot distinguish the actin nucleation and elongation activity. However, it was reported that Dia has both activities (Campellone and Welch, 2010). In order to test whether the inhibition is due to a reduced nucleation activity, Total Internal Reflection Fluorescence (TIRF) microscopy was used in this study. As shown in Figure 3.14, the single actin filament could be observed using TIRF microscopy and it was shown that DiaC has a strong actin polymerization activity. Here the

number of actin filaments was used as the representative of the nucleation activity.
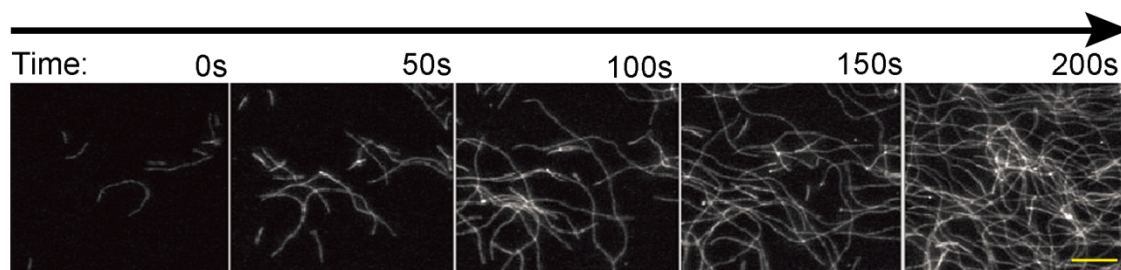

Figure 3.14 Single actin filament observed with TIRF microscopy. In the course of time, the number and the length of actin filaments are growing in the present of Dia and profilin. Scale bar: 20µm

10 nM ZZ-DiaC nucleated approximately three times more filaments compared to the actin control (Figure 3.15). Consistent with the pyrene assay, the nucleation activity of DiaC was strongly inhibited by Cip4. Addition of a tenfold molar excess of Cip4 reduced the number of filaments comparable to the actin control (Figure 3.15). Cip4ΔSH3 showed a weaker inhibitory effect than full-length Cip4, once more demonstrating the importance of the SH3 domain for the Cip4-Dia interaction (Figure 3.15).

3.1.5 Cip4 inhibits actin elongation activity of Dia

Next, we tested whether elongation activity is also affected by Cip4. The rate of actin filament growth was measured using TIRF microscopy. Actin elongation activity mediated by Dia is largely dependent on binding of actin-profilin to FH1 domain. Purified *Drosophila* profilin was used in the following experiments. In order to allow usage of relatively high concentrations of Cip4 comparable to profilin-actin complex, the F-BAR domain was deleted since full-length Cip4 formed aggregates above 500 nM at the conditions of the actin polymerization assays (Figure 3.16). In pyrene assays with DiaC and profilin, Cip4ΔBAR as well as GST-SH3 inhibited actin polymerization (Figure 3.17).

A

| 1.3 µM actin | + 200 nM Cip4 | + 200 nM Cip4ΔSH3 |
| + 10 nM DiaC | + 10 nM DiaC
+ 200 nM Cip4 | + 10 nM DiaC
+ 200 nMCip4ΔSH3 |

B

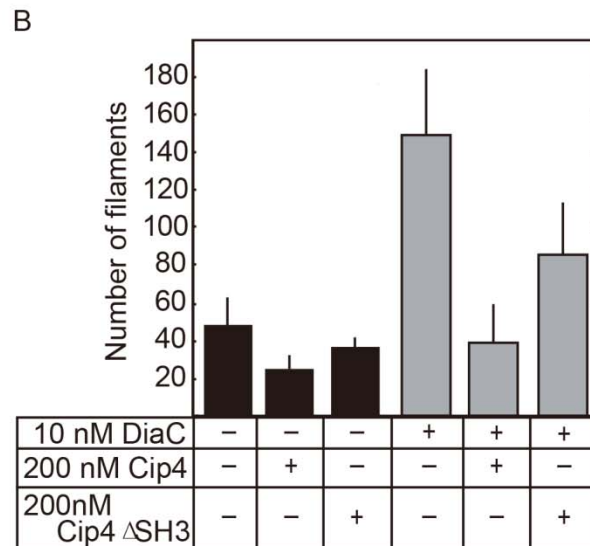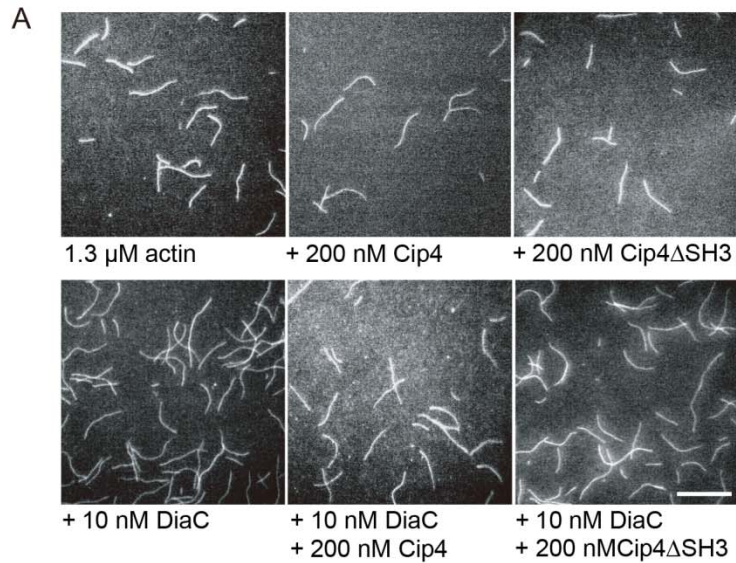|						
10 nM DiaC	−	−	−	+	+	+
200 nM Cip4	−	+	−	−	+	−
200nM Cip4 ΔSH3	−	−	+	−	−	+

Figure 3.15 Cip4 inhibits Dia actin nucleation activity shown in TIRF assay. The number of filaments is reduced by addition Cip4. Cip4ΔSH3 showed a weaker inhibition, which is consistent with pyrene assay, suggesting that inhibition is dependent partially on SH3 domain. (A) TIRF images scale bar: 20µm. (B) Quantification of filaments number.

Notably, the inhibitory effect by the GST-SH3 domain was stronger in the presence of profilin compared with the absence of profilin, which supports a competition between profilin–actin and Cip4-SH3 for interaction with Dia-FH1.

I tried to carry out the *in vitro* competitive binding assay using purified proteins. However, I couldn't get DiaC-Cip4-profilin complex in the bound

fraction. The interaction between profilin and poly-proline domain is weak (KD=~50 mM) (Perelroizen et al., 1994) and therefore couldn't be detected by Pulldown assay.

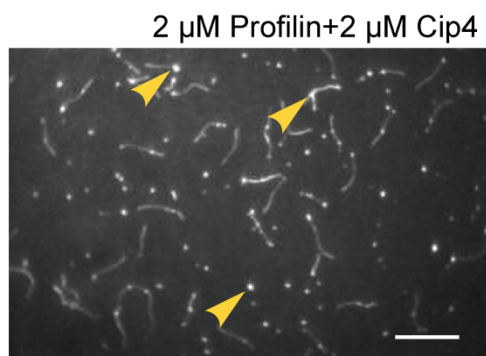**2 µM Profilin+2 µM Cip4**

Figure 3.16 TIRF image showing actin aggregation caused by high concentration of Cip4. 2 µM of Cip4 protein was added. The bright points indicated by yellow arrows are actin aggregation. Scale bar: 20 µm
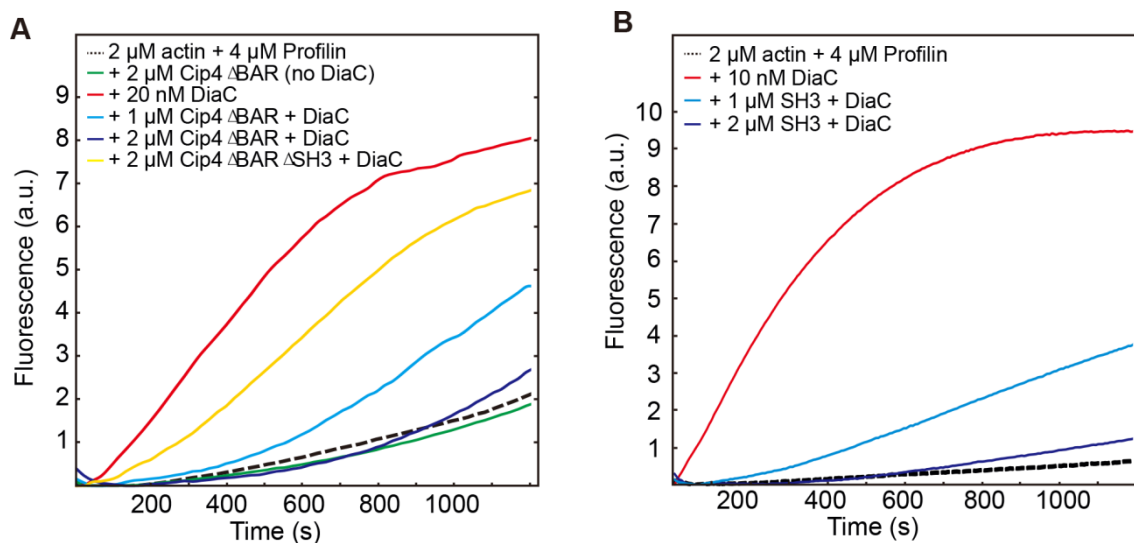

Figure 3.17 Actin polymerization shown in pyrene assay in present of profilin. Consistent with previous assay, Cip4 inhibits Dia activity, and SH3 domain is sufficient for inhibition.

In the TIRF assay, we analyzed the filament elongation rate in the absence or presence of different proteins (Figure 3.18). In the presence of profilin, DiaC increased 10-fold barbed-end elongation with a speed of 140 subunits/second, compared with the actin control elongation speed of 12 subunits/second (Table 3.3 and Figure 3.18). In the presence of profilin and

Cip4ΔBAR, most filaments grew with a speed of ~11 subunits/second, which is close to actin control speed. However, there were about 10% filaments which were identified as fast-growing filaments elongating with ~90 subunits/second.
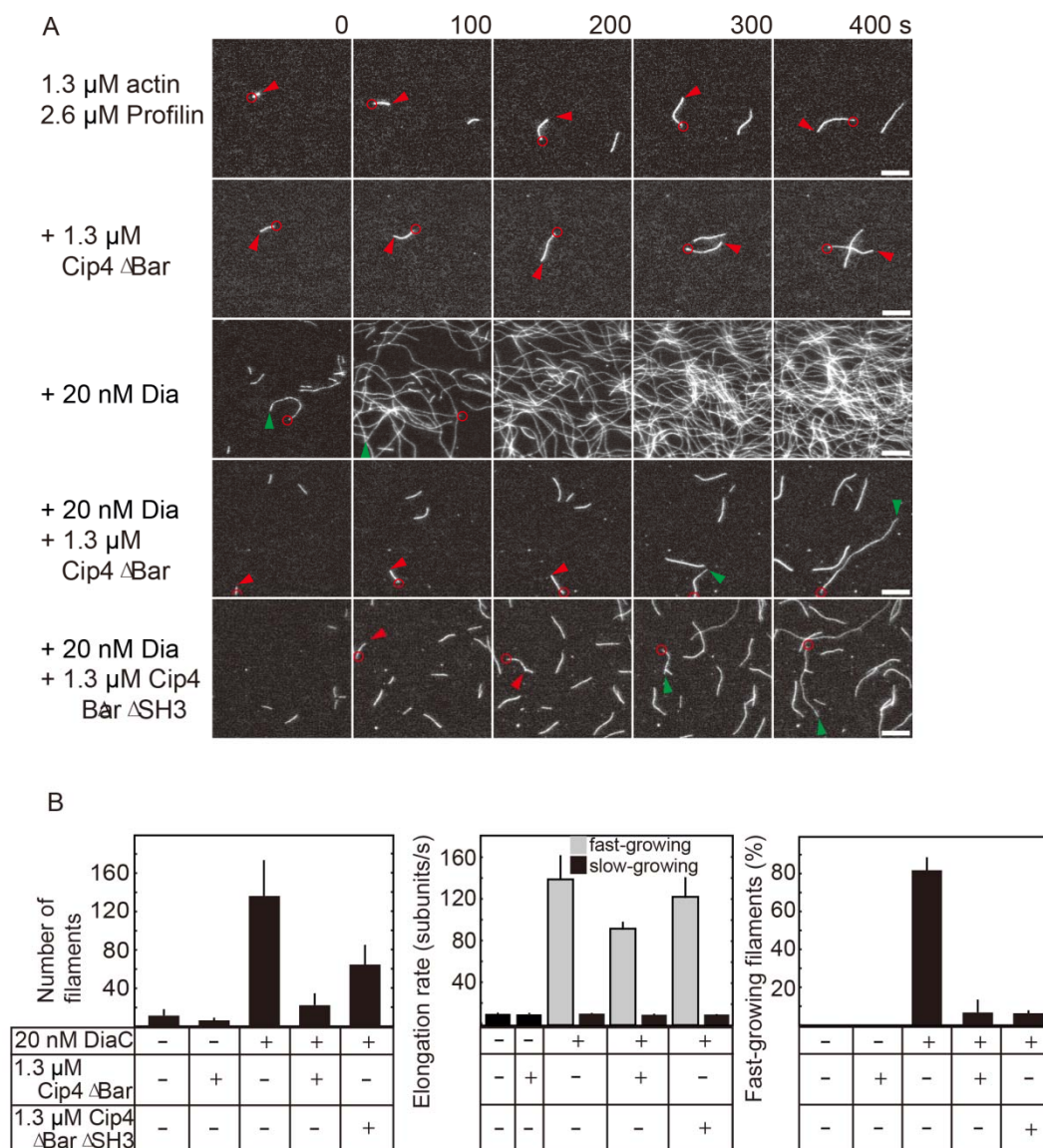

Figure 3.18 Cip4 reduced the actin filament elongation rate in present of profilin and Dia. (A) TIRF microscopy images were taken at indicated time points. Besides the reduced number of actin filaments due to inhibition effect of Cip4, the rate of elongation is also reduced. Cip4ΔSH3 doesn't show the elongation rate inhibition effect. Scale bar: 10 μm (B) Quantification of the number and elongation rate of actin filaments.

The reduction of fast elongation rate implied that Cip4 binding interferes with the elongation activity of Dia. However, Cip4ΔFBARΔSH3 could not reduce the

rate of fast filament elongation as effect as Cip4ΔFBAR. These observations indicate that Cip4 interferes with both Dia activities.

Table 3.3 Numbers and elongation rate of actin filaments

Reaction conditions	Number of filaments		Fast-growing filaments			Elongation rate in subunits/s	
	N	S.D.	P (in %)	S. D.		v	S. D.
1,3 µM actin + 2,6 µM Profilin	11,5	6,66	0	0		11,71	1,77
+ 1.3 µM Cip4DBar	6,66	3,51	0	0		10,75	0,82
+ 20 nM DiaC	136,67	37,90	81,53	6,66	fast-growing	138,78	23,09
					slow-growing	11,07	1,32
+ 20 nM DiaC + 1.3 µM Cip4DBAR	22,8	12,56	6,45	7,00	fast-growing	91,99	7,62
					slow-growing	11,15	0,56
+ 20 nM DiaC + 1.3 µM Cip4DBarDSH3	65	20,74	6,16	1,69	fast-growing	122,04	19,99
					slow-growing	10,05	1,26

3.2 Dia is essential in membrane compartmentalization during cellularization

Since complete loss-of-function of Dia prevents oogenesis(Castrillon and Wasserman, 1994), I used a weak allele *dia^sy5* to study the role of Dia in cellularization in the following experiments (Figure 3.19). Embryos of *dia^sy5* germline clone show multinuclear cells in the cellularization stage, due to the lack of metaphase furrow (Grosshans et al., 2005) (Figure 3.20).
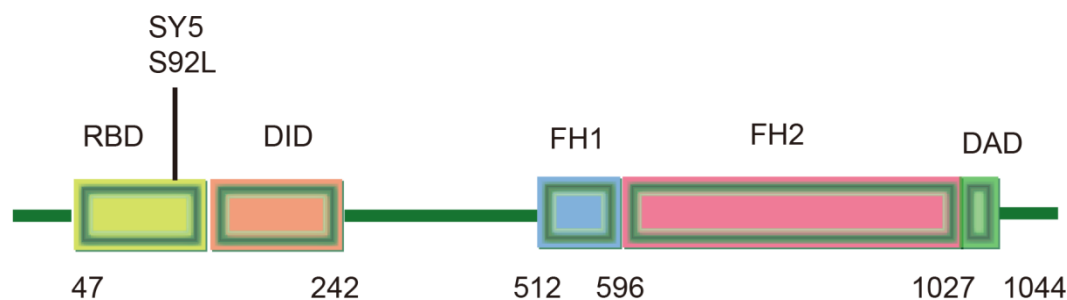
Figure 3.19 Schematic representation of *dia^sy5* allele used in this study. *dia^sy5* was generated by chemical mutagenesis. Point mutation leads to changing of the 92 amino acid from Ser to Leu in Rho-binding domain.
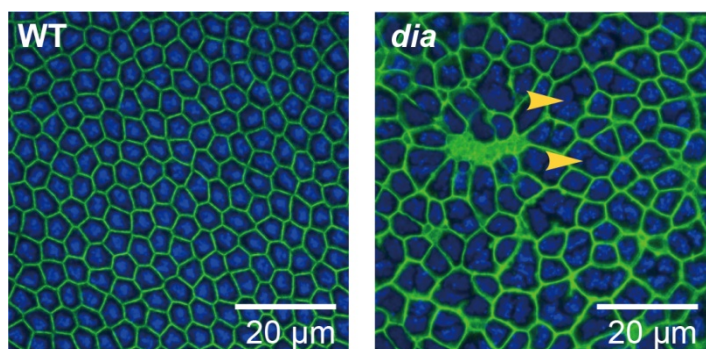

Figure 3.20 *dia^sy5* leads the typical *dia* phenotype. In *dia^sy5* germline clone embryo, multinuclei cell form as indicated by yellow arrow, due to the lack of metaphase furrow.

3.2.1 Lateral marker proteins are not excluded from the furrow canal in *dia* mutant

During the initial phase of cellularization, the basal and lateral domains of plasma membrane are established and maintained (Lecuit and Wieschaus, 2000). Patj and Slam exclusively localize at the furrow canal, whereas Discs-large (Dlg) specifically localizes at the lateral membrane domain. RhoGEF2, Dia, F-actin are enriched at furrow canal (Figure 3.21 A and B). However, the lateral membrane marker Dlg spread into the furrow canal and overlapped with Slam in *dia* germline clone embryos. The mislocalizition of Dlg can be found all through cellularization process (Figure 3.21 B and C). Moreover, Slam, the protein marker for furrow canal remains strictly at basal

domain, suggesting Dia is not required for maintaining the furrow canal, but essential for exclusion of lateral membrane protein from the furrow canal, and defining or maintaining the separation of lateral and basal domain.
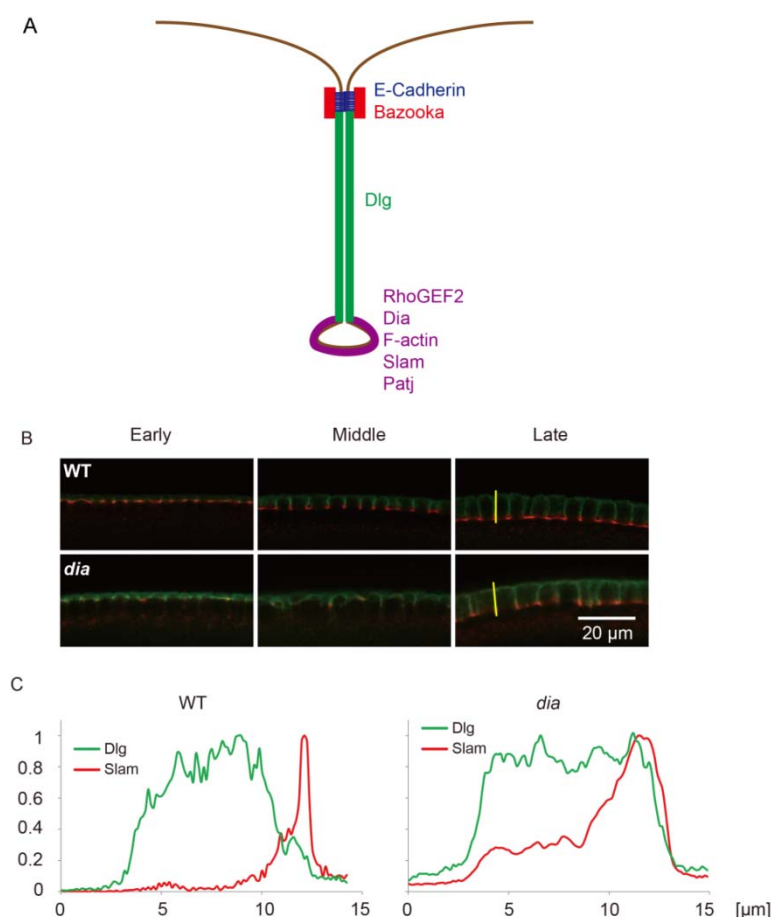

Figure 3.21 Dia is important for lateral-basal polarity. (A) Schematic representation for the membrane domain separation during cellularization. Bazooka and E-Cadherin localize at the sub-apical domain to assemble adherens junctions. Dlg exclusively localizes at the lateral domain of membrane. Patj, Slam localize at furrow canal exclusively and RhoGEF2, Dia, F-actin localize at the membrane but are enriched at the furrow canal. A sharp boundary forms between lateral and basal domain. (B) Immunostaining of Dlg (green) and Slam (red) in wild type embryo, showing a clear boundary. The boundary is missing in *dia* mutant embryo. (C) Profile plot was done along the invagination membranes, indicated in B by yellow bar in wild type and *dia* embryo, respectively.

3.2.2 Persistent tubular membrane invaginations in *dia* mutants

In the beginning of cellularization, the invaginating plasma membrane is highly dynamic, which can be seen as long tubular extensions stained by N-BAR protein Amphiphysin (Sokac and Wieschaus, 2008a) (Figure3.22 A). After 5-10 min, F-actin accumulates at the furrow canal and the tubular extensions disappear. It has been reported that cytochalasin treatment leads to persisting long tubular extensions even in the late stage of cellularization,
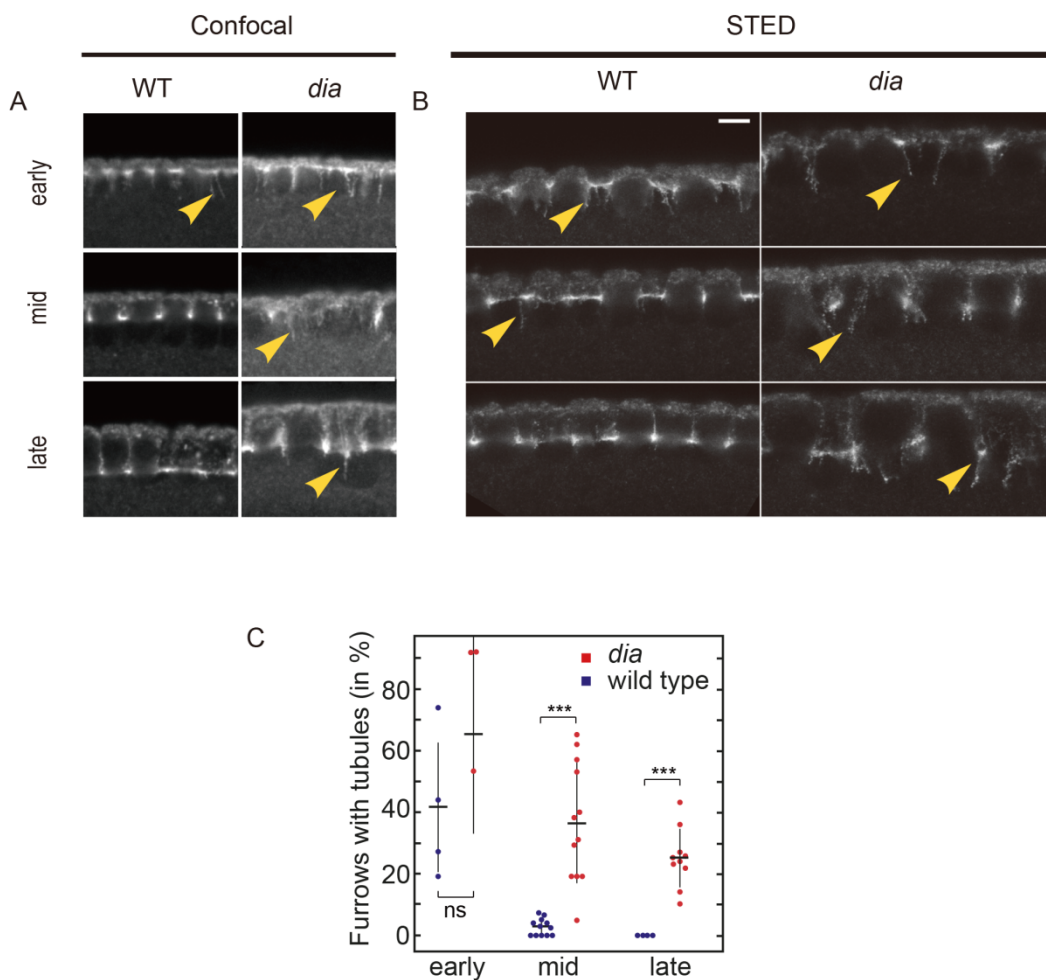

Figure 3.22 Dia is essential for membrane tubular extension suppression. (A) Conventional confocal images for different stages of embryos as indicated, showing tubular extension stained with Amph. (B) STED microscopy images showing the same pattern of Amph staining dots in tubular structure in wild type and dia mutant embryo (Courtesy: Dr. Christian Wenzl). (C) Statistics of furrow with tubular extensions in wild type and *dia* mutant embryo.

suggesting that F-actin is required for the stabilization of furrow canal (Sokac and Wieschaus, 2008a).

The Amph staining in *dia* germline clone embryos showed a similar phenotype to cytochalasin treatment embryos, and the tubular extension persists through the cellularization process (Figure 3.22). In wild type embryos, the Amph tubules were only observed in cellularization early stage; in the middle and late stage, almost no Amph tubules could be found. In contrast, around 70% and 30% furrow canals were associated with Amph tubules in middle and late stage in *dia* germline clone embryos, respectively (Figure 3.22). These data suggest that Dia is required in suppression of tubular extensions after the furrow canal has formed.

3.2.3 Cip4 protein antagonizes Dia function during cellularization

As shown previously, Cip4 binds to Dia and inhibits its actin polymerization activity. I also tested whether Cip4 interfered with Dia physiological function *in vivo*. Cip4 localizes at the membrane including furrow canal during cellularization (Figure 3.23). Cip4 deficient embryos develop normally, suggesting that a redundant pathway of Cip4 exists.
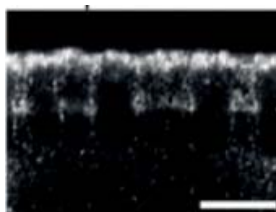

Figure 3.23 Cip4 localizes at the membrane(Courtesy: Dr. Shuling Yan). Imuunostaining with Cip4 antibody staining at cellularization stage. scale bar: 10μm

I generated *dia ΔCip4* double mutant embryos. Similar to *dia* mutant embryos, the lateral marker Dlg spread into the furrow canal, and tubular extensions were observed in late stage (Figure 3.24). In the double mutant embryo, I didn't see any enhancement or suppression of *dia* phenotype.

Secondly, UASp-Cip4-GFP transgenic flies were generated. Overexpression of Cip4-GFP driven by maternal GAL4 leads to a phenocopy of *dia* germline clone embryo. Lateral marker Dlg overlaps with Patj at the furrow canal and multi-nuclear cells form due to the lack of invaginating furrow (Figure 3.25). The counteracting behavior of Dia against Cip4 is dependent on the latter's SH3 domain. To confirm the role of SH3 domain *in vivo*, UASp-Cip4ΔSH3-GFP transgenic flies were generated. The overexpression of Cip4ΔSH3-GFP didn't show any defects in cellularization (Figure 3.26).
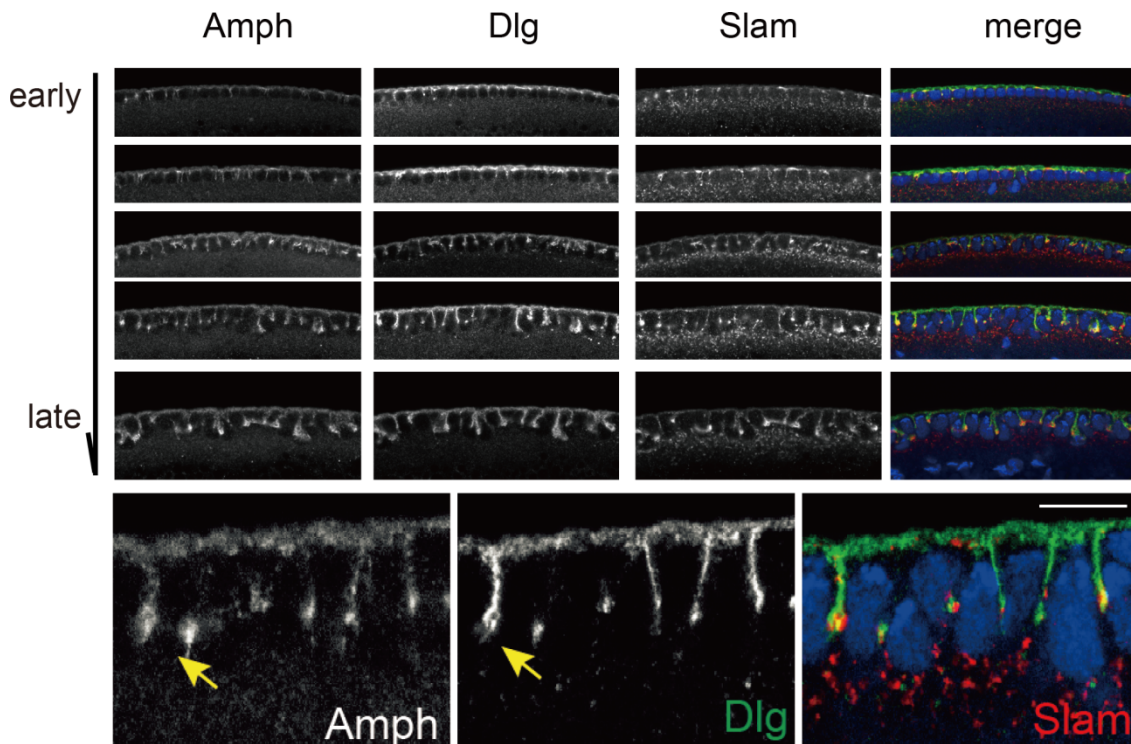

Figure 3.24 *dia ΔCip4* double mutant embryo doesn't show any enhancement or suppression of *dia* phenotype. Double mutant embryos were stained with indicated antibodies. In the double mutant embryos, Dlg spreads into furrow canal; and tubular extension stained with Amph is observed in late stage. scale bar: 10μm
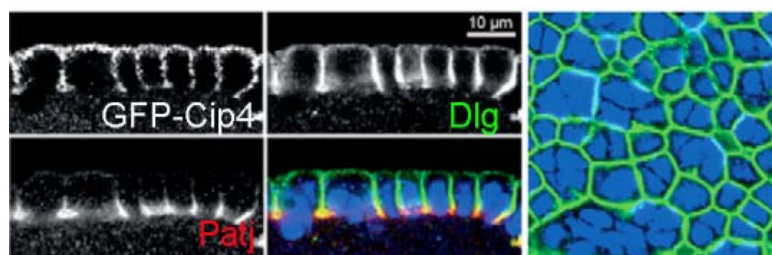
Figure 3.25 Cip4 overexpression leads to a phenocopy of *dia* (Courtesy: Dr. Shuling Yan). The overexpressed Cip4 localizes at membrane. Dlg spreads into furrow canal and colocalizes with Patj. Due to lack of metaphase furrow, multinucleated cells form.
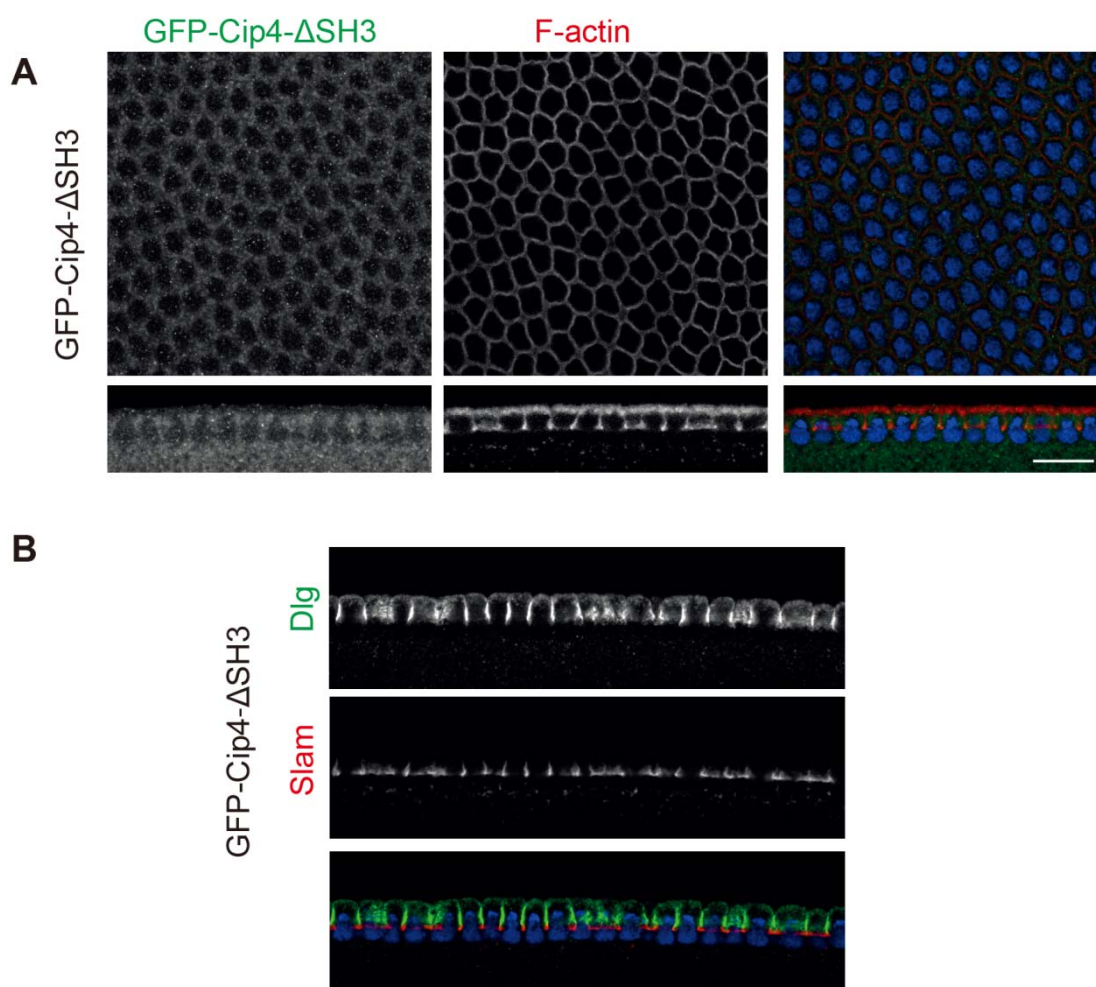

Figure 3.26 Cip4ΔSH3 over-expression does not induce cellularization defects. GFP-Cip4ΔSH3 embryo was fixed and stained with indicated antibodies. (A) Contrast with GFP-Cip4, GFP-Cip4ΔSH3 shows the nuclear exclusion rather than membrane localization. The F-actin organization is not disturbed. (B) The localization of Dlg and Slam are the same as in wild type embryos. Scale bar: 10μm

These data suggest that overexpression of Cip4 can antagonize Dia *in vivo* and this activity of Cip4 depends on its SH3 domain.

3.2.4 Role of Arp2/3-dependent F-actin at the furrow canal

It has been reported that Cip4 promotes Arp2/3 activity for actin polymerization (Fricke et al., 2009). I wondered whether Arp2/3-dependent F-actin is involved in antagonism of Cip4 and Dia. However, *arp3* germline clone embryos couldn't develop to cellularization stage (Leibfried et al., 2013). CK666 is a small molecule that can inhibit Arp2/3 activity specifically (Hetrick et al., 2013). CK666 was injected in Utrophin-GFP emrbyos. Utrophin is an F-actin binding protein, and Utrophin-GFP is used for F-actin labelling for live imaging (Levayer et al., 2011). The fluorescence was reduced after injection (Figure 3.27).
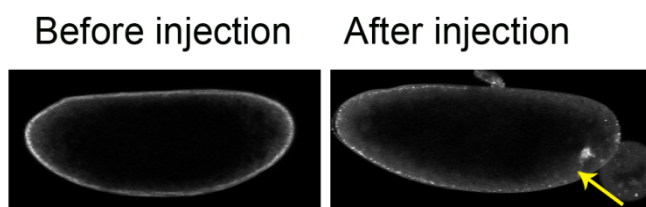

Figure 3.27 CK666 injection reduces the Utrophin-GFP signal in embryo. The injection site was indicated by yellow arrow. The GFP signal was reduced in the posterior of embryo compared with the anterior half embryo.

Next I injected CK666 in wild type and *dia* germline clone embryos. Injection of CK666 at the onset of cellularization suppressed the membrane tubular extensions at furrow canals in wild type. In contrast, injection CK666 in *dia* germline clone embryos didn't lead to the reduced number of tubular extensions. To confirm the role of Arp2/3 in producing membrane tubular extensions, I also checked the embryos from *arp3*/+ female. The *arp3*/+ flies can survive but only have one copy of *arp3* gene, and the embryo from these flies are only loaded with a reduced number of *arp3* gene products compared with wild type. In these embryos, the number of membrane tubular extensions was significantly reduced. These data show that Arp2/3 promotes formation of tubular extensions, and Dia counteracts this activity (Figure 3.28)
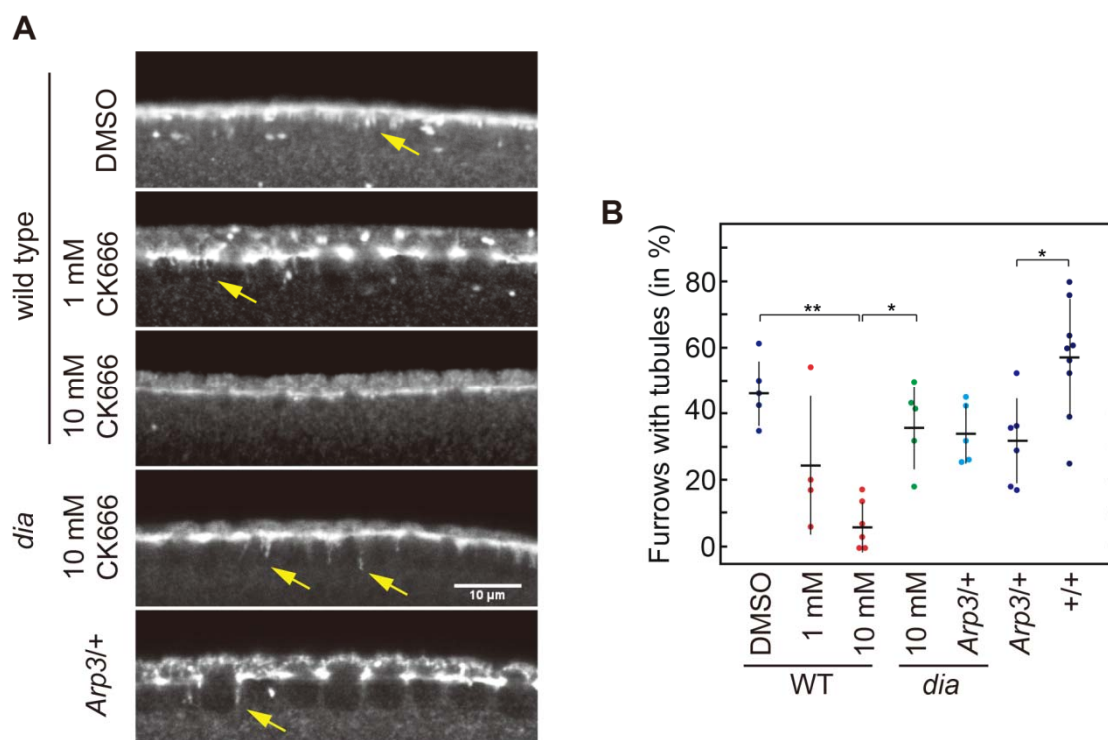
Figure 3.28 Arp2/3-dependent F-actin promotes tubular extension. (A) At the onset of cellularization, the number of Amph tubules is reduced in CK666 injected and *Arp3/+* embryo, indicating Arp2/3 promotes tubular extensions. However, CK666 injection couldn't reduce the tubular number in *dia* embryos, suggesting that Dia counteracts the promoting membrane extension activity of Arp2/3. (B) Quantification of furrows with tubular extensions.

3.3 The mechanism of lateral-basal domain separation

3.3.1 Basal junction and endocytosis are not involved in domain separation

The polarity of epithelia is maintained during the course of cellularization. As shown in Figure 3.21, there is a very sharp boundary between lateral and basal domain in epithelia. However, this polarity is missing in *dia* embryos. In order to understand the mechanism of the lateral-basal boundary maintenance, two aspects were examined: 1) sorting mechanism by endocytosis and exocytosis and 2) F-actin-dependent resistance of membrane lateral diffusion. I began with examining the first possibility. Dynamin is a GTPase essential for scission during endocytosis. Endocytosis in the embryos was perturbed by

using a temperature-sensitive allele of dynamin, *shibire* (*shi^TS*). The Amph-positive tubular extensions are longer in the embryos from *shibire* female due to reduced activity of Dynamin (Sokac and Wieschaus, 2008a).
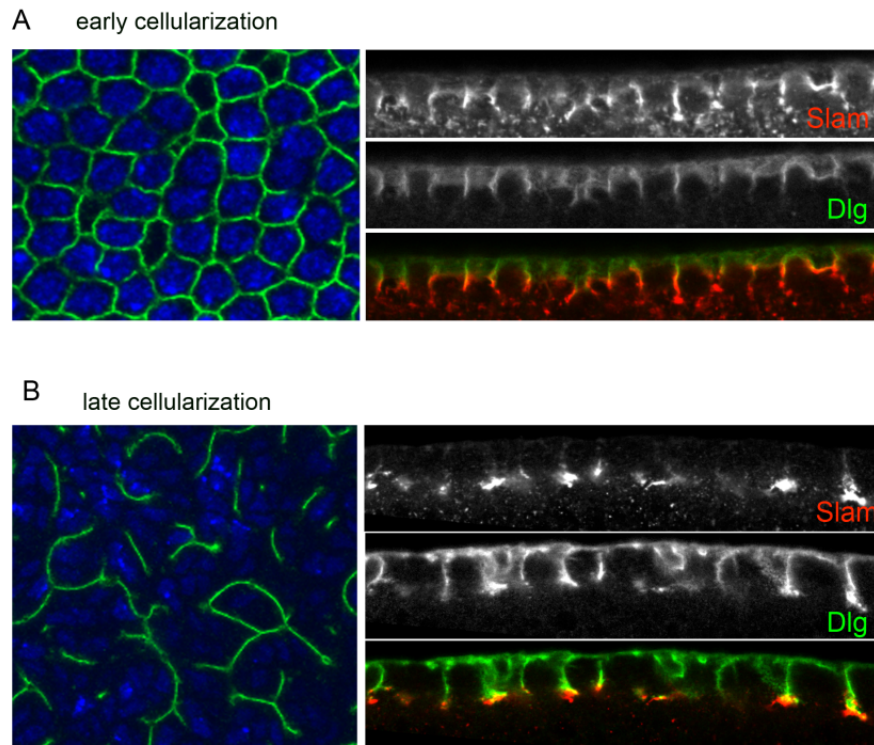
Figure 3.29 Sorting mechanism is not essential for lateral-basal domain separation. *shibire* phenotype is induced at 32 °C at the early(A) and late(B) cellularization. The domain separation is not defective.

At the restrictive temperature (32 °C) *shibire* showed multi-nuclear cell and breaking of cell border which is a typical phenotype of *dynamin* (Georgiou et al., 2008) (Figure 3.29). Nevertheless the boundary between lateral and basal domain was maintained. This data argue against that the sorting mechanism mediated by endocytosis and exocytosis is involved in domain separation.

3.3.2 Dia mediated F-actin is important for the basal-lateral domain separation

Dia loss-of-function (*dia* germline clone) embryos show furrow canal compartmentalization defects, which allows us to predict that F-actin is essential for furrow canal establishment and maintaining the lateral-basal domain boundary. But the difference in the property of membrane caused by endogenous F-actin is not clear in *Drosophila* cellularization process.

In order to check the turnover rate of membrane in lateral domain and basal domain, I did FRAP experiments performed in palmitoylated-YFP and GAP43-Venus embryos. Both fluorescence markers label the plasma membrane including furrow canals.

The palmitoylated-YFP signal is enriched at membrane, but the cytosol also shows some YFP fluorescence signal, implying that the localization of palmitoylated-YFP is in equilibrium between cytosol and plasma membrane. The fluorescence recovered after bleaching within a range of minute, and I couldn't detect the difference between the recovery rate of palmitoylated-YFP in the lateral domain and the furrow canal, implying the possibility that the F-actin coated furrow canal may not be able to block the protein exchange between plasma membrane and cytosol. The same experiment was repeated using GAP43-Venus embryo. GAP43 is attached to membrane by two palmitoyl tails. Consistent with the result from palmitoylated-YFP FRAP, the recovery rate between lateral and furrow canal membrane were the same (Figure 3.30).

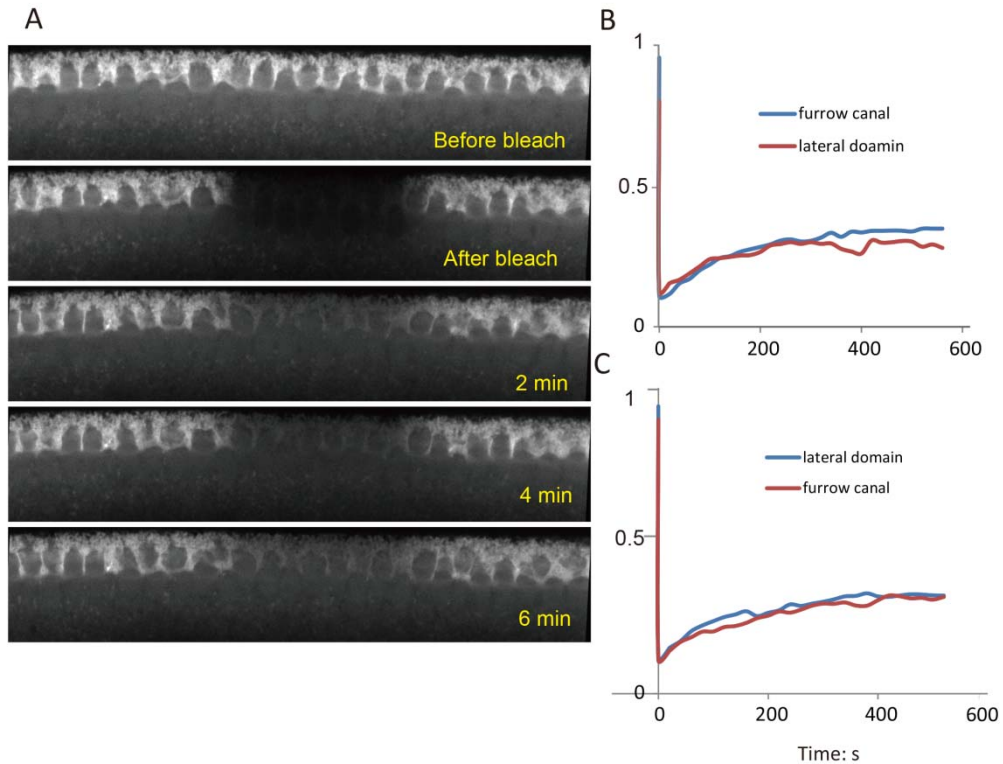Then I switched to GFP labeled membrane integrated protein 117 and

Figure 3.30 The turnover rate of membrane associated protein doesn't show difference between basal and lateral domain. (A) FRAP experiments were done using GAP43-venus embryo. (B) Two independent measurements of fluorescence intensity showed the protein fluorescence from both domains recovered at the same speed.

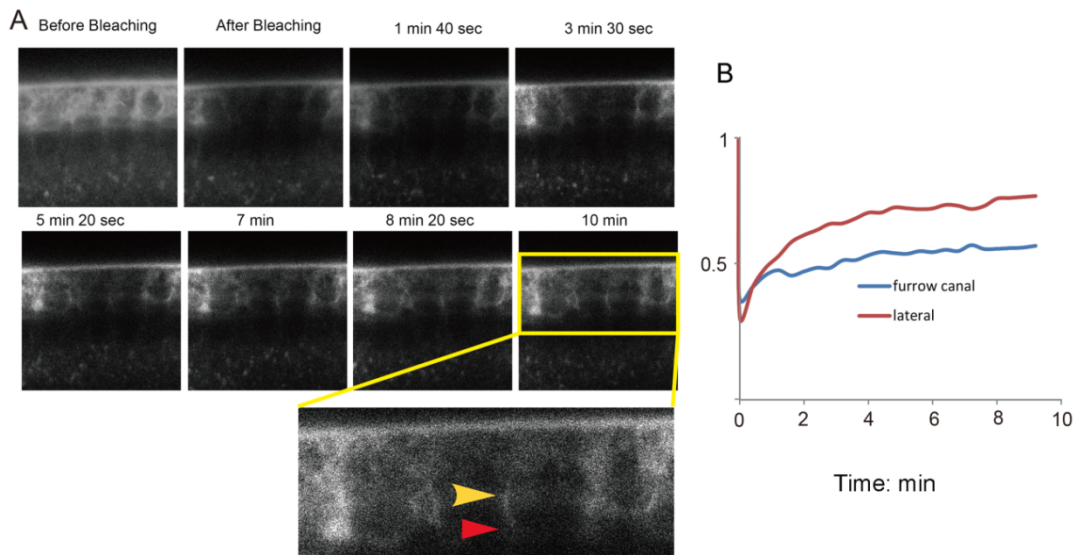**Figure 3.31 The membrane integrated proteins turnover rate are different between lateral and basal domain.** (A) FRAP experiments were carried out using 117-GFP;Spider-GFP embryo. The proteins in lateral domain diffuse faster than the one at the furrow canal. Yellow arrow marks the lateral domain, and red arrow marks the furrow canal. (B) Measurement of fluorescence intensity at lateral and basal domain, respectively.

74

spider embryos and the FRAP experiment showed that the recovery rate in the lateral membrane was faster than the furrow canal. This data implied that the membrane integrated proteins in the lateral domain can diffuse along the membrane more easily than in the furrow canal, and the proteins in the lateral domain cannot diffuse into the furrow canal due to the furrow canal F-actin enrichment.

To test this hypothesis, I checked the furrow canal membrane recovery rate in *dia* germline clone embryo. Consistent with our hypothesis, the fluorescence at furrow canals recovered faster in *dia* germline clone embryo than in wild type embryo (Figure 3.32). These data implied that F-actin plays an important role in the maintenance of lateral-basal boundary. In an attempt to get a proper quantitative analysis, more measurements are needed.
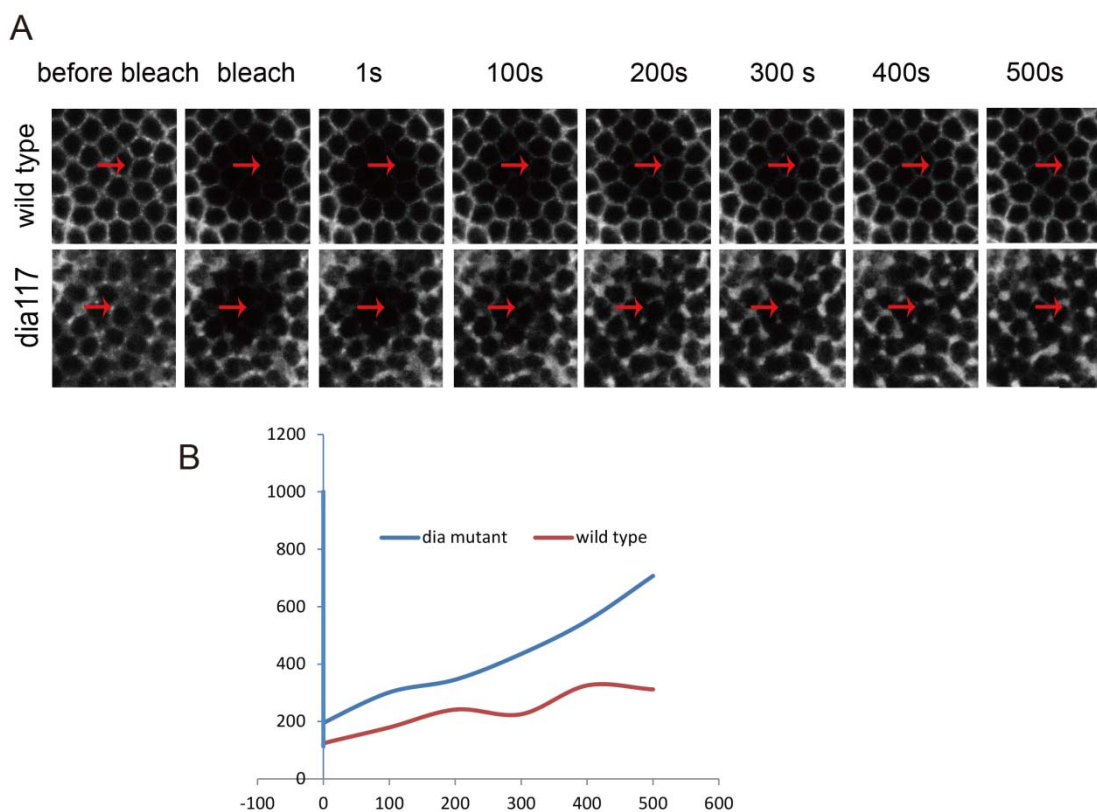

Figure 3.32 The mobility of integrated protein 117 is faster in *dia* embryo (A) The fluorescence recovered faster after bleaching in *dia* embryos than in wild type embryos. (B) Measurement of fluorescence intensity in *dia* and wild type embryos.

3.4 Characterization of a novel allele of Ced-12/ELMO

2L367 was identified in our lab with its defects in blastoderm formation and F-actin organization from a large collection of mutations in germline clones with essential functions for early development (Vogt et al., 2006). Here I analyzed the detailed phenotype of 2L367 and mapped the gene mutated in this line.

3.4.1 Cellularization defect in 2L376

Time-lapse movies by Differential Interference Contrast (DIC) microscopy showed that 2L367 embryos form a blastoderm, go through the 13 nuclear divisions, pause the cell cycle but fail to cellularize properly (Figure 3.33). The details of membrane invagination during cellularization were examined by fluorescence imaging using GAP43-Venus in 2L367 background emrbyo (Figure 3.34). The membrane could invaginate at the onset of interphase 14, but couldn't finish cellularization properly.

3.4.2 Cell cycle defect in 2L367

I wondered whether the cell cycle is affected in 2L367. Histone-Alexa488 was injected in wild type and 2L367 embryos. The mitosis in 2L367 had a longer time than wild type (Figure 3.35). The nuclear-fall-out phenotype was observed in the late cycles in 2L367 embryos (Figure 3.35). Consistent with Histon-Alexa488 fluorescence time-lapse movie, immunostaining of the marker for mitosis phosphorylated Histone3 in 2L367 also showed unsynchronized cell cycle (Figure 3.36).

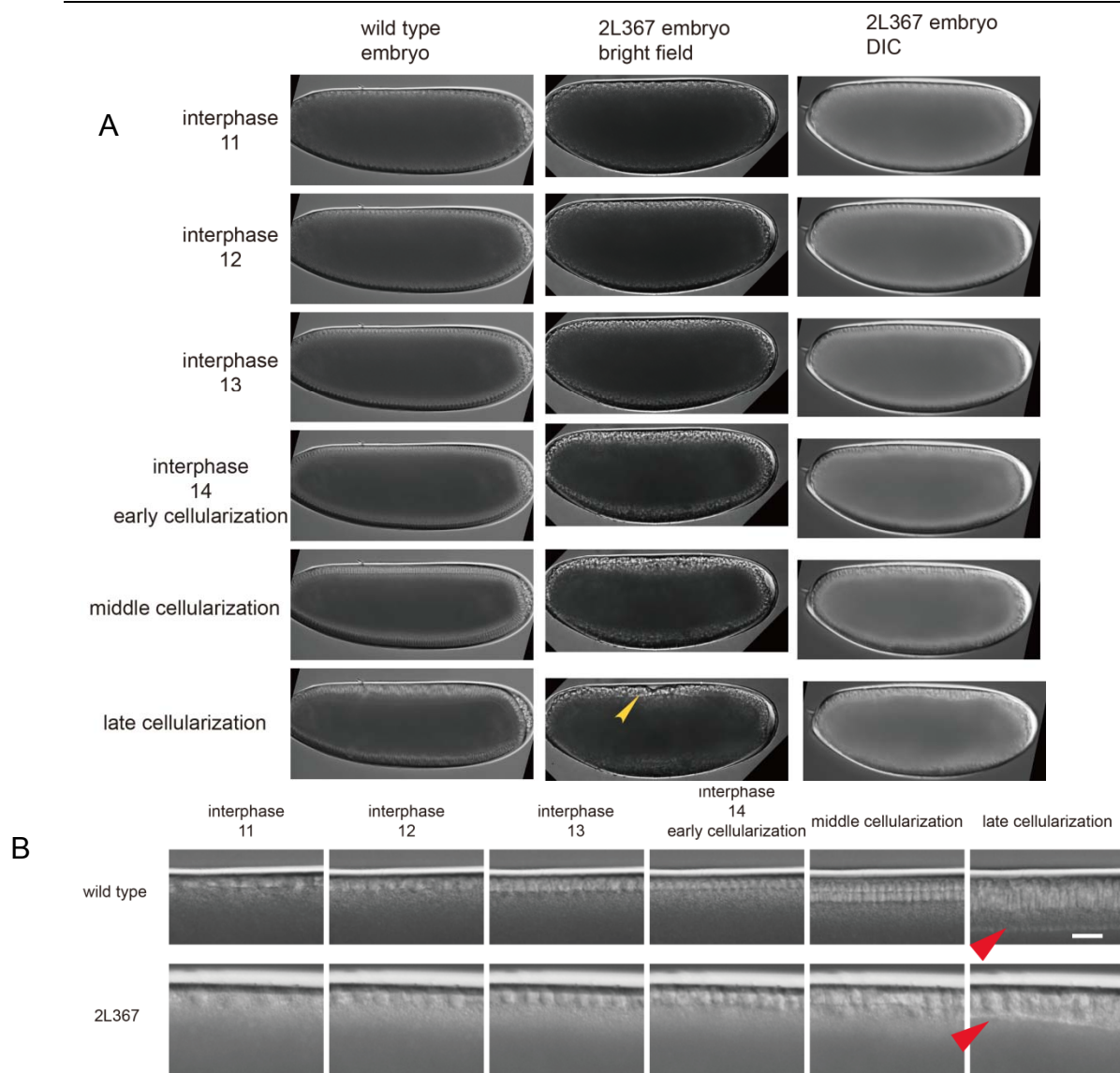**Figure 3.33. Live image of 2L-367 germline clone embryo.** (A) The whole embryo was shown with bright field and Differential Interference Contrast microscopy. The 2L367 embryo can undergo the nuclear division and form syncytial blastoderm, but couldn't cellularize properly. (B) The cortical of embryo is shown in high magnification. Arrow shows the tip of membrane invagination. Scale bar: 10 μm
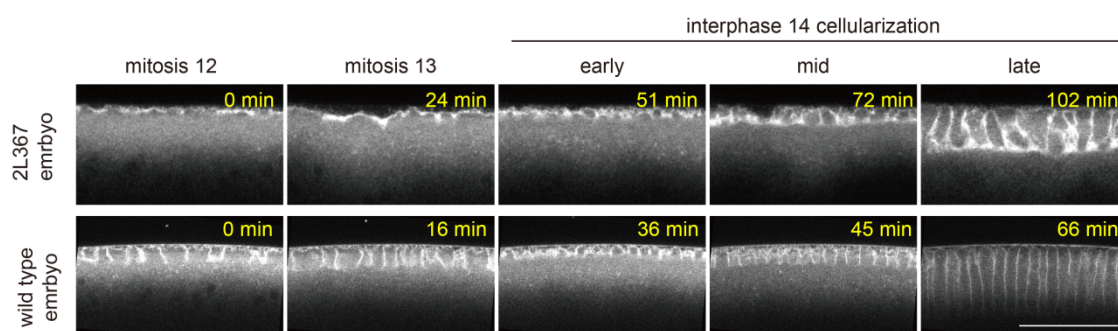
Figure 3.34 metaphase furrow and cellularization defects in 2L367 embryo. Time lapse images of GAP43-venus in wild type and 2L367 embryo. The metaphase furrow in mitosis is not visible and the length of cellularization furrow is shorter in 2L67 embryo. Scale bar: 50 µm

Figure 3.35 Cell cycles are prolonged in 2L367 mutant. Time lapse images after injection of Histone-Alexa488 to wild type and 2L367 embryos. Cell cycle is defined with the nuclei number. Nuclear fall-out phenotype is observed in 2L367.
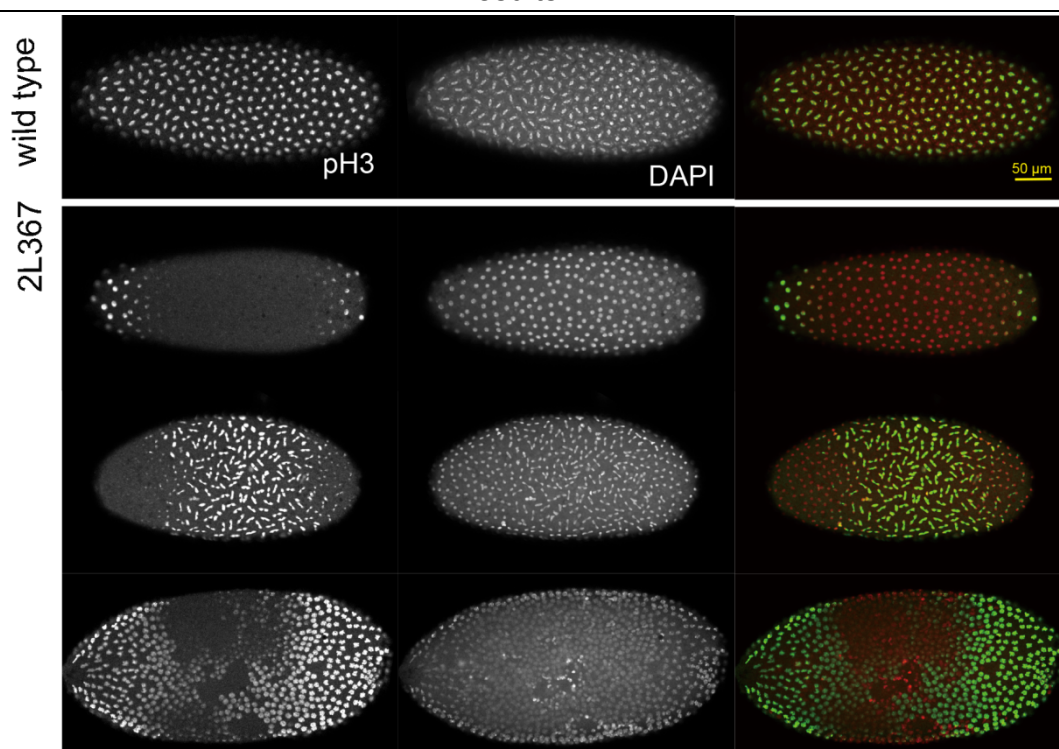
Figure 3.36 Unsynchronized cell cycle in 2L367 embryo. Phospho-HistoneH3 (pH3) is a specific marker for the mitosis and stains the condensed chromatin just before chromosomal segregation. The staining of pH3 shows uneven distribution across the 2L367 embryo.

3.4.3 Actin organization defect in 2L367

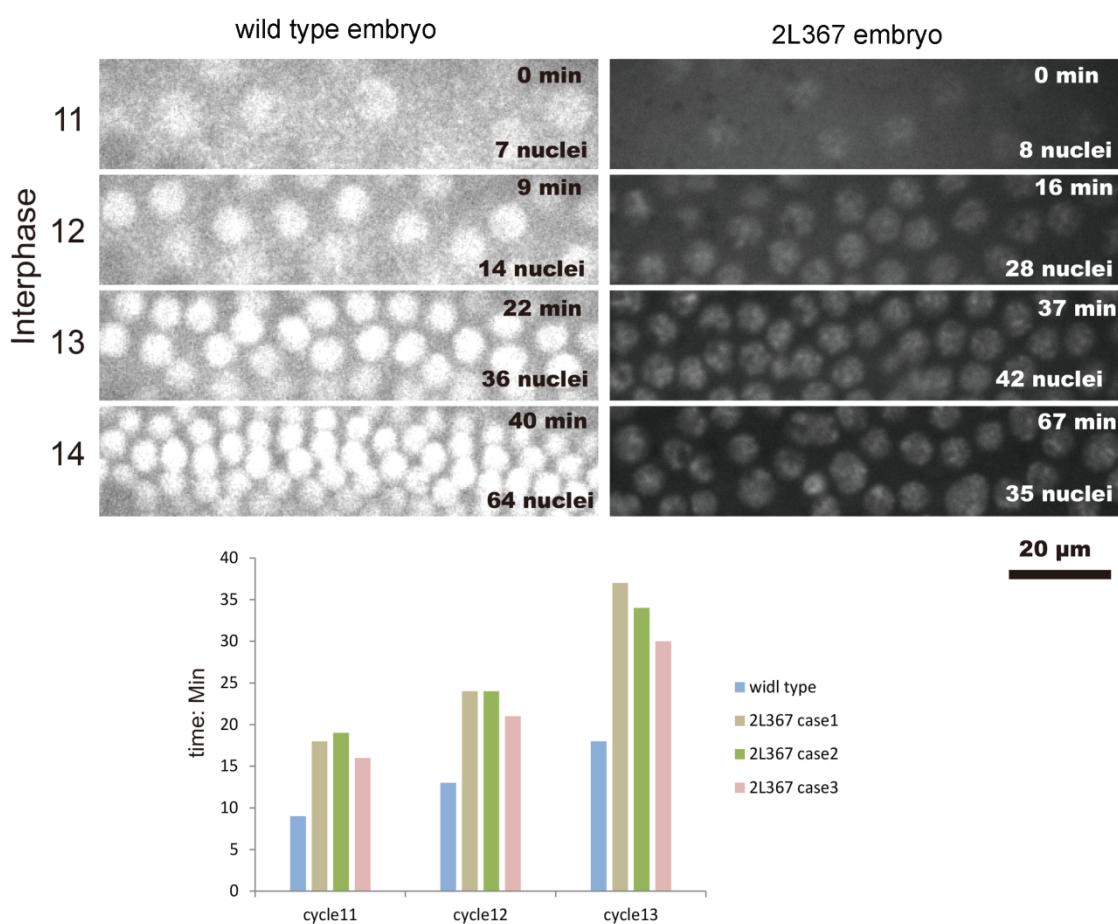During the interphase in syncytial blastoderm, the actin forms a cap structure above the nuclear and the centrosome. Upon entry into mitosis, the actin caps dissolve and localize at metaphase furrows. However, in 2L367 mutant, those actin based structures couldn't be observed (Figure 3.37). The centrosome is considered to be sufficient to induce actin cap formation and metaphase furrow (Schejter and Wieschaus, 1993). So the localization of centrosomes was examined. However, the centrosome localization is not disrupted in 2L367 mutant (Figure 3.38). These data suggest that the gene mutated in this line may be involved in controlling actin polymerization and in the linkage between centrosome and F-actin cap/metaphase furrow actin remodeling.

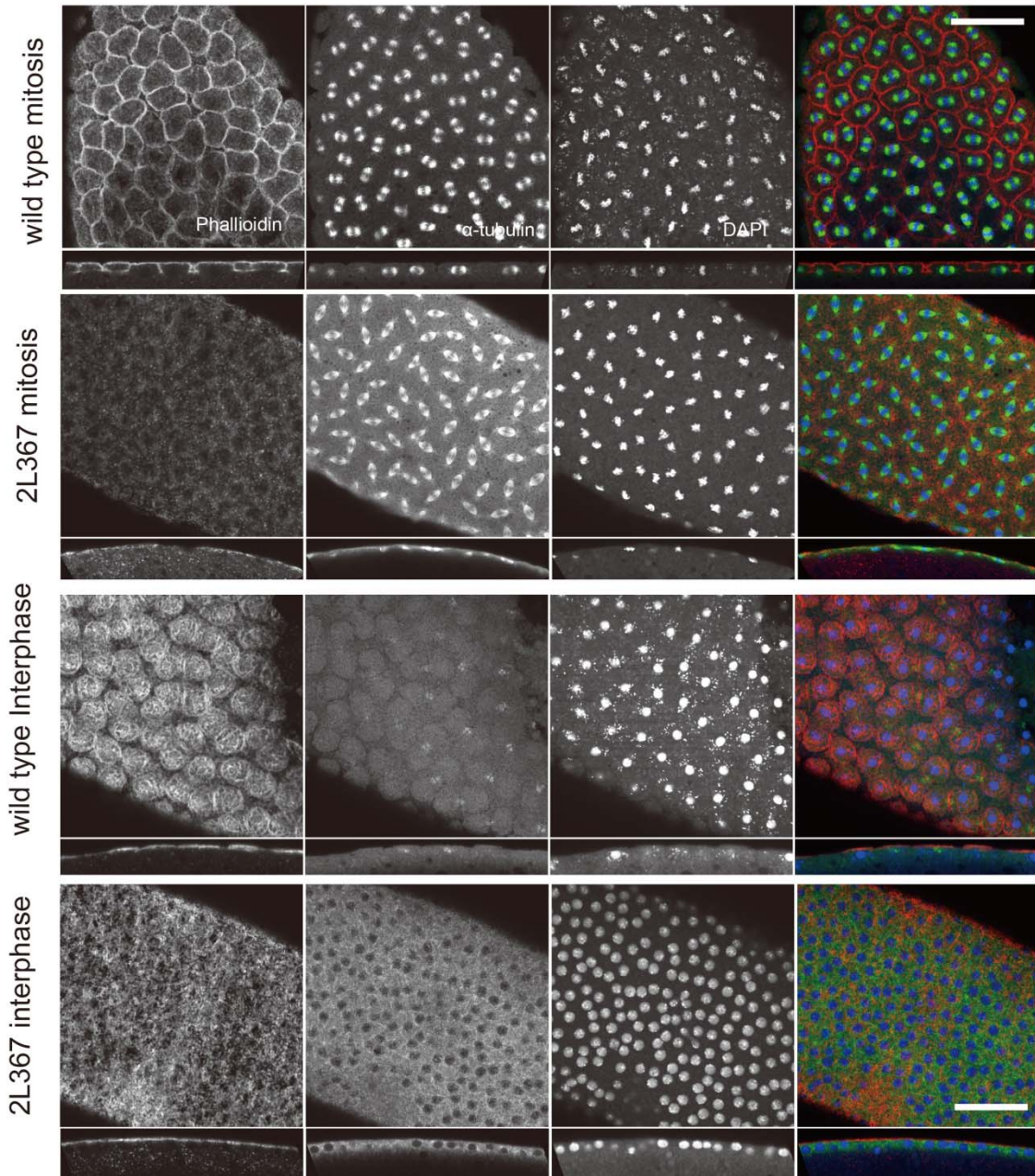**Figure 3.37 Actin caps and metaphase furrow are absent in 2L367 mutant.** Actin caps are formed above nuclear in the interphase, then dissolves and redistributes at metaphase furrows in mitosis. These structures are missing in 2L367 embryos. Scale bar: 20µm
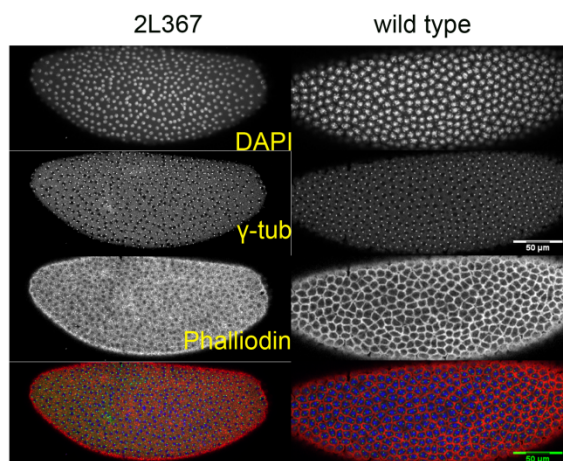
Figure 3.38 The centrosome localization is not affected in 2L367 embryo. The centrosome pair separates in the onset of mitosis. In the 2L367 embryo, the centrosome localization is not affected but couldn't induce actin caps and metaphase furrows. Scale bar: 50μm

3.4.4 Genetic mapping of 2L367

In order to know which gene is mutated in this line, we carried out meiotic mapping with visible markers to narrow down the location of mutated gene and separate other mutations on the chromosome (Figure 3.39). Frt2L2R{w+}/*al dp b pr* Frt2L, 2L367 virgins were crossed with *al dp b pr Bl c px sp*/SM1 males. The recombination between 2nd chromosomes took place during meiosis in oogenesis, and various classes of recombinant showed up in the progeny (Table 3.4).

Table 3.4 The number of progeny with different phenotypes

phenotype		Number of flies	Viable?	Sterile?	Phenotype in germline clone embryo
al	w+	3	Viable	Fertile	-
al dp	w+	6	Viable	Fertile	-
al dp	w+	1	Viable	Sterile	-
al dp	w+	8	Lethal	-	No phenotype
al dp b	w+	17	Lethal	-	With phenotype
dp b	w	7	Lethal	-	With phenotype
b	w	23	Lethal	-	No phenotype
	w	7	Lethal	-	No phenotype
	w	2	Viable	Fertile	-

Because the mutated gene leads to maternal defects, it was termed *fs* (*female sterile*) temporarily. In addition to *fs*, 2 lethal mutants were isolated. According to the number of progeny with different phenotype, the localization of lethal mutations was estimated. The first one (l_1) localizes in the middle of *dp* and *b* (8:6) and the second one (l_2) is between *b* and *pr* but close to *pr* (7:2) (figure 3.39). None of them showed maternal defects. *fs* is lethal mutant according to the progeny from recombinational cross. The location of *fs* was estimated in the similar way, and it locates between *dp* and *b* but close to *b* (32:2) on the chromosome with the range from 2L:10,020,000 to 2L:14,020,000 (figure 3.39).

After narrowing down to this range, we did deletion mapping using different deficiency lines which cover this expected range. After first round of cross, we couldn't find any progeny with genotype of Df(2L)ED761/2L367 and Df(2L)ED775/2L367, suggesting that the overlap of these two deficiency lines contains the mutated gene (Figure 3.39). New deficiency lines covering this overlap range were used in the following complementary test. After the second round of deficiency cross, I got a narrower expected range which contains 10 genes (Figure 3.39).

Next, I did complementary cross using the lines which contain the mutant gene list in the expected range. *Ced-12* ^{c06760} couldn't complement with 2L367, while the others could, indicating the mutant gene in 2L367 is ced-12.
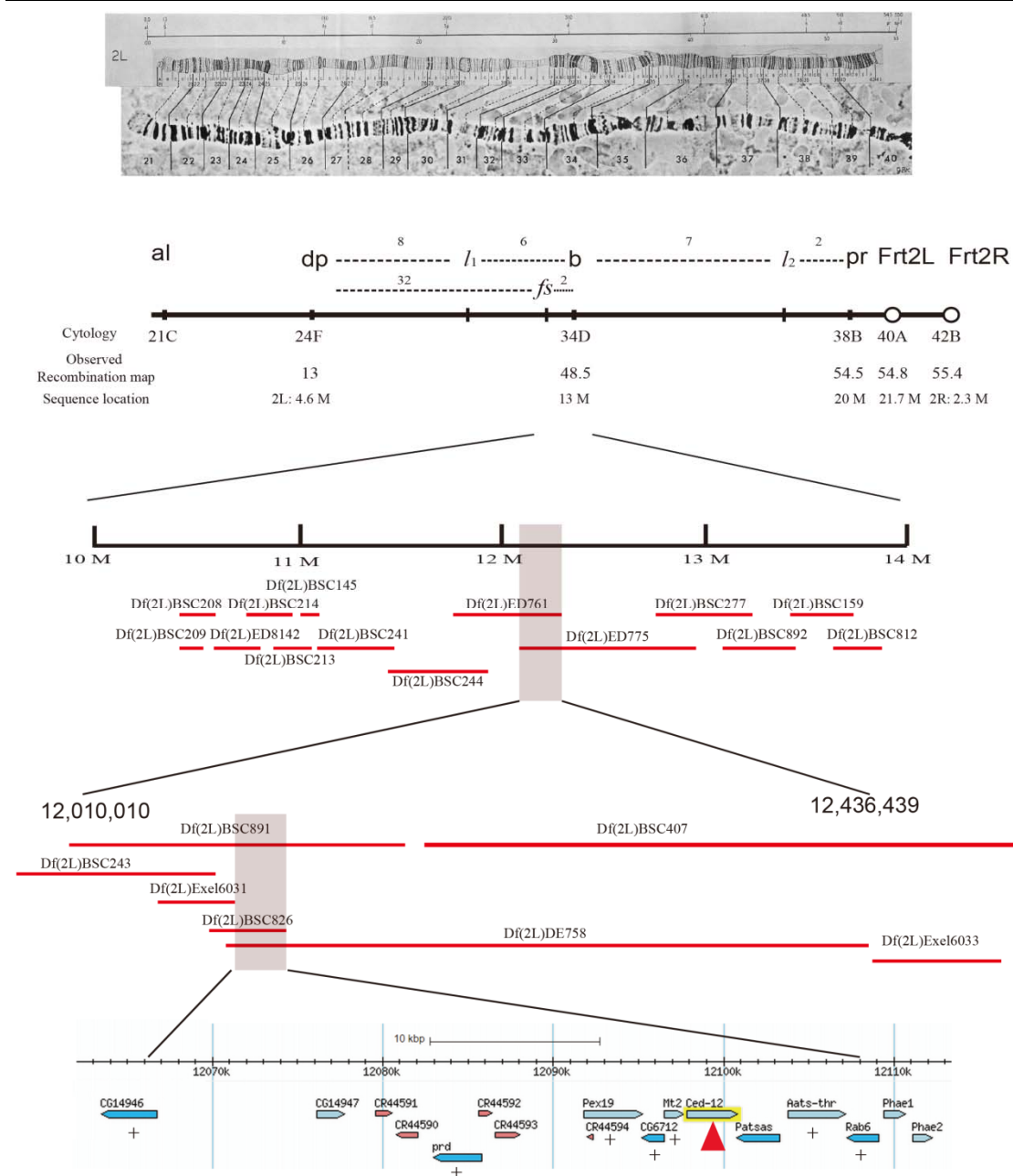
Figure 3.39 2L367 mapping scheme. After meiotic recombinational mapping and complemental test, *ced-12* was found as the mutated gene in 2L367 leading to the phenotype.

3.4.5 Ced-12 colocalizes with Sponge and actin in syncytial blastoderm

Ced-12 (ELMO in mammal) was identified in *C.elengas* as an essential gene involved in the engulfment of dying cells during apoptosis (Hedgecock et al., 1983). Ced-12 is involved in regulation of Rho/Rac GTPase signaling

pathway (Zhou et al., 2001). Western blot showed the reduced amount of Ced-12 in 2L367 mutant (termed *Ced-12^{2L367}* in the following text) (Figure 3.40).

Figure 3.40 Ced-12 protein is reduced in 2L367 embryo. Compared with wild type embryo extraction, the Ced-12 protein is reduced significantly.

Figure 3.41 Ced-12 colocalizes with Sponge and actin. In the interphase, Ced-12 and Spg localize at actin caps, while in the mitosis, Ced-12 and Spg translocate to metaphase furrow with F-actin. Scale bar: 10μm

It has been reported that there is a the physical interaction between Ced-12 and Sponge during *Drosophila* CNS development (Bie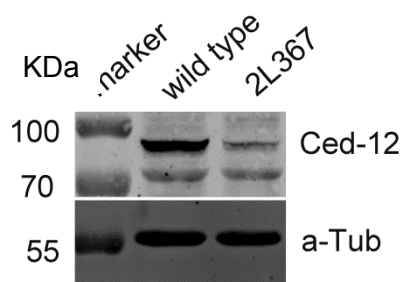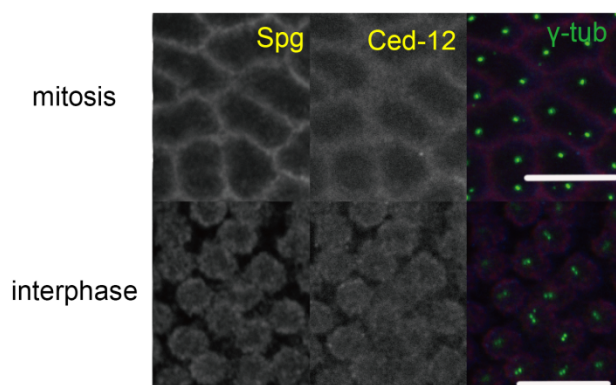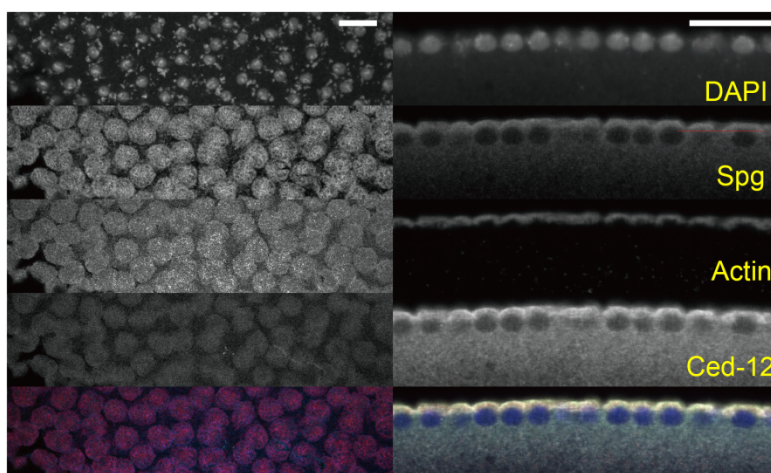rsmith et al., 2011). Maternal effect of *sponge* mutation also leads to a blastoderm phenotype which is similar to *ced-12^{2L367}* (Postner et al., 1992). Sponge is an ortholog of human DOCK3 and DOCK4, and activates Rac as a noncanonical guanine nucleotide exchange factor (Biersmith et al., 2011). Sponge is involved in border cell migration and is controlled by PVR signaling (Bianco et al., 2007). However, DOCK proteins only show GEF activity when they are bound to Ced-12/Elmo (Meller et al., 2005). This could be the reason why *ced-12^{2L367}* and *sponge* show the same defects, and together with the localization of Ced-12 and Sponge, provides the link to actin dynamic regulation in syncytial blastoderm.

In wild type embryo, Ced-12 colocalizes with Sponge and actin caps in interphase. In mitosis, Ced-12 and Sponge colocalize at the metaphase furrow where F-actin localizes (Figure 3.41). In *ced-12^{2L367}* embryo, the localization of Ced-12 and Sponge spreads along the plasma membrane (data not shown). As shown previously, the localization of centrosome is normal in *ced-12^{2L367}* embryos (Figure 3.38), but the actin based structures are missing. Taken together, the current data point to the possibility that Ced-12/Sponge complex acts as a signal linker between centrosome and actin cytoskeleton in syncytial blastoderm in *Drosophila.*

Chapter 4. Discussion

4.1 Molecular mechanism of interaction between Cip4 and Dia in actin polymerization

Purified actin monomers can self-assemble to filaments, but the initiation step is limiting, because formation of actin filament nuclei is kinetically unfavorable. Therefore actin nucleators are employed to overcome the kinetic barrier of actin nucleation (Chhabra and Higgs, 2007). These actin nucleators include Arp2/3 complex, formins and Spire. Arp2/3 complex bypasses the kinetic barrier by mimicking the barbed end of actin filament (Goley et al., 2004). Spire recruits and organizes actin monomers with a tandem of WH2 domains into an actin oligomer, serving as an actin nucleation "seed" (Dietrich et al., 2013). Formins assemble actin filaments using an entirely different mechanism. *In vitro* studies showed FH2 domain is sufficient for actin polymerizing (Chesarone et al., 2010; Grosshans et al., 2005). However, the FH2 domain binds actin monomers with a very low binding affinity and lacks the similarity to actin (Goode and Eck, 2007). Co-crystal structure of the complex of Bnip-FH2 with muscle actin suggests that the FH2 domain can stabilize actin dimers or trimers, as a likely mechanism for polymerization (Otomo et al., 2005).

Overexpression of Cip4 in *Drosophila* embryos lead to a phynocopy of *dia* mutant, suggesting Cip4 antagonizes Dia genetically. From the pyrene assay and TIRF assay, the antagonistic nature between Cip4 and Dia was uncovered at the molecular level. However, the mechanism of Cip4 in inhibiting actin polymerization activity of Dia is less clear. In the *de novo* polymerization process of actin filaments, it is possible that the binding of Cip4 to Dia prevents Dia from stabilizing actin dimer/trimer. On the other hand, it is also possible that Dia can bind the actin dimer/trimer and stabilize them, but the addition of new

actin monomers is blocked by binding of Cip4. Current data are not sufficient to distinguish between the two alternatives. Considering the effect of Cip4 on Dia which is already attached to barbed end of F-actin, we propose 3 models: 1) the binding of Cip4 to Dia makes Dia fall off from the growing barbed end of F-actin, 2) FH1 domain is occupied by SH3 domain of Cip4, and it not accessible for profilin-actin complex. Dia is still sitting on the growing tip of F-actin. 3) The binding of SH3 to FH1 makes Cip4 cover the FH2 domain, obstructing the new addition of actin monomers. The TIRF assay showed Cip4 binding reduced the elongation rate mediated by Dia, suggesting that not all of Dia was taken off from the barbed end by Cip4; otherwise no fast growth (in a reduced rate) would be observed. A recent study on yeast suggested that F-BAR protein Hof1 inhibited actin polymerization activity of Bnr1 (formin in yeast) without displacing the Bnr1 from growing filament ends (Graziano et al., 2014). This is consistent with our explanation. It was reported that dimerization of SH3 domain was important for inhibition of Bnr1, suggesting that the inhibition was not due to competition between the SH3 domain and profilin for binding FH1 (Graziano et al., 2014). From our data and literature, the most likely model of Dia inhibition by Cip4 is that binding of Cip4 to Dia makes the FH2 domain inaccessible to actin monomers. However, the mechanism of inaccessibility is either steric effect caused by any bulky protein with SH3 domain or a conformation-change induced by Cip4, which is still an open question. In order to have a clear explanation, color labeled TIRF microscopy and structure study of actin-Dia-Cip4 will help.
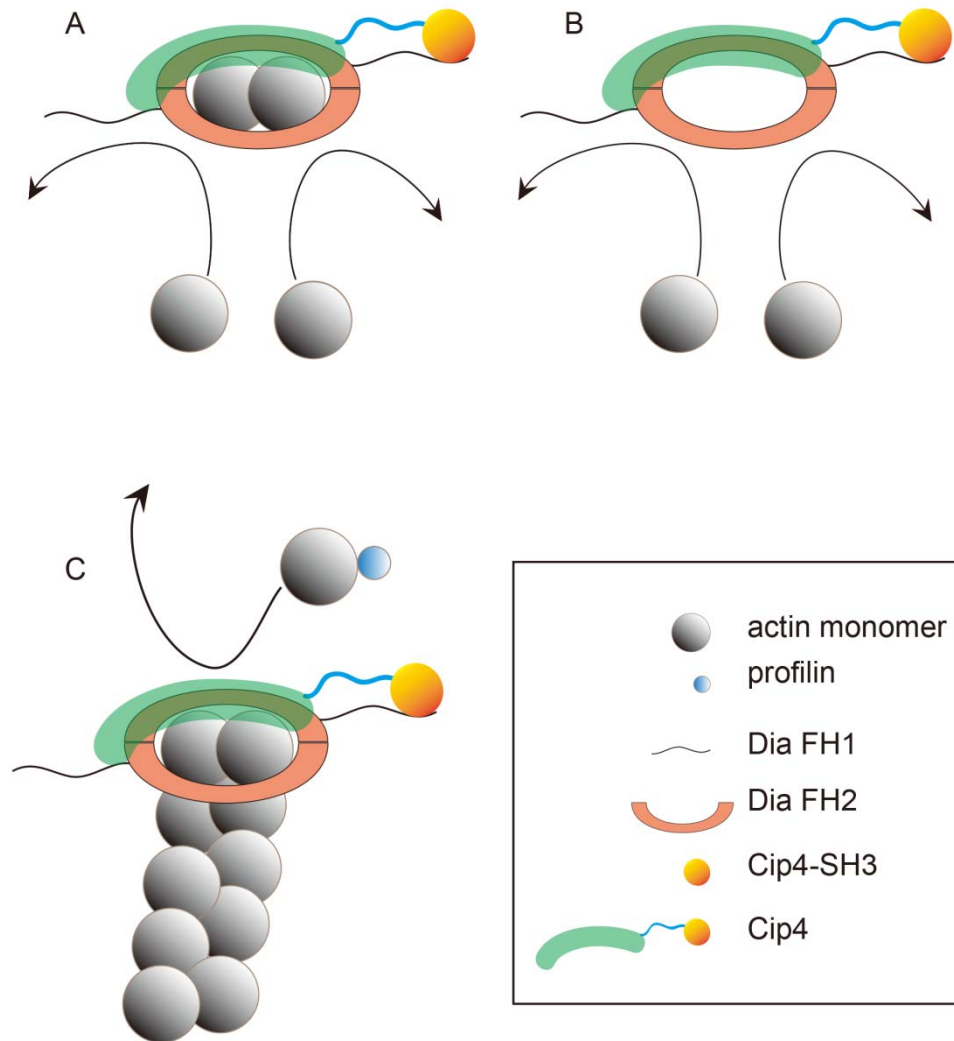
Figure 4.1 The schematic representation of likely mechanisms of Cip4 inhibiting Dia activity. (A, B) The likely mechanisms of Cip4 inhibiting Dia nucleation. (A) Binding of Cip4 to Dia prevents Dia from stabilizing actin dimers/trimers. (B) Binding of Cip4 doesn't affect Dia stabilizing actin dimer, but blocks the addition of new actin monomer to the actin dimer core. (C) Cip4 binds to Dia on the barbed end of actin filament. Due to the steric effect or the conformation changing caused by Cip4, the FH2 domain is not accessible for the addition of new actin monomers.

4.2 Membrane property during cellularization

At the onset of cellularization, the membrane at the furrow canal is highly dynamic, as shown by tubular extensions stained with Amph. When the furrow canal assembly is complete and F-actin accumulates at the furrow canal after 5-10 min, the tubular extensions disappear. F-actin is essential for the stabilization of membranes. Cytochalasin D treatment and loss of function of

Dia in the embryo lead to the persistent tubular extensions (Sokac and Wieschaus, 2008b; Yan et al., 2013).

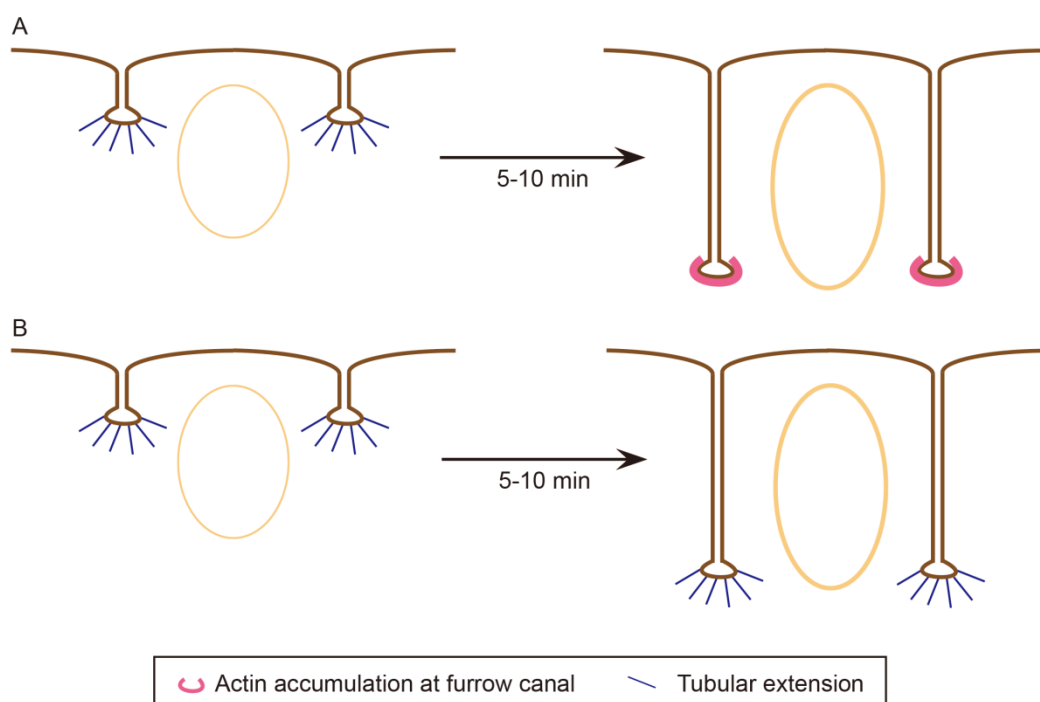**Figure 4.2 The stabilization of membrane at furrow canals needs F-actin.** (A) During cellularization, the membrane at furrow canals is highly dynamic initially, but stabilizes after 5-10 minutes due to the accumulation of F-actin at furrow canals. (B) Loss of Dia or injecting Cytochalasin D in the embryo leads to the persistent membrane tubular extension.

For the mechanism of Dia suppressing tubular membrane extension, we propose that linear actin filaments generated by Dia form a dense cortical layer beneath the membrane, and this cortical layer of linear F-actin increases the membrane rigidity and suppresses membrane remodeling. A clear correlation of reduction of Arp2/3 activity and reduction in membrane tubular extension was observed, suggesting that branched F-actin network promotes endocytic activity, which is in contrast to the linear F-actin cortical layer. Cip4 provides a link between F-actin and membrane remodeling (Itoh et al., 2005; Suetsugu and Gautreau, 2012). Nucleation promoting factors (NPFs) are recruited by Cip4 to endoctyic sites and activate Arp2/3, thus promoting endocytosis (Fricke et al., 2009). In this study, the inhibitory activity of Cip4 on Dia was revealed.

Thus, Cip4 induces branched F-actin network at the membrane remodeling site by interaction with NPFs, which intern activate Arp2/3. Simultaneously, Cip4 suppresses linear F-actin beneath membrane through inhibition of Dia activity. The dual activity of Cip4 may promote efficient membrane remodeling.
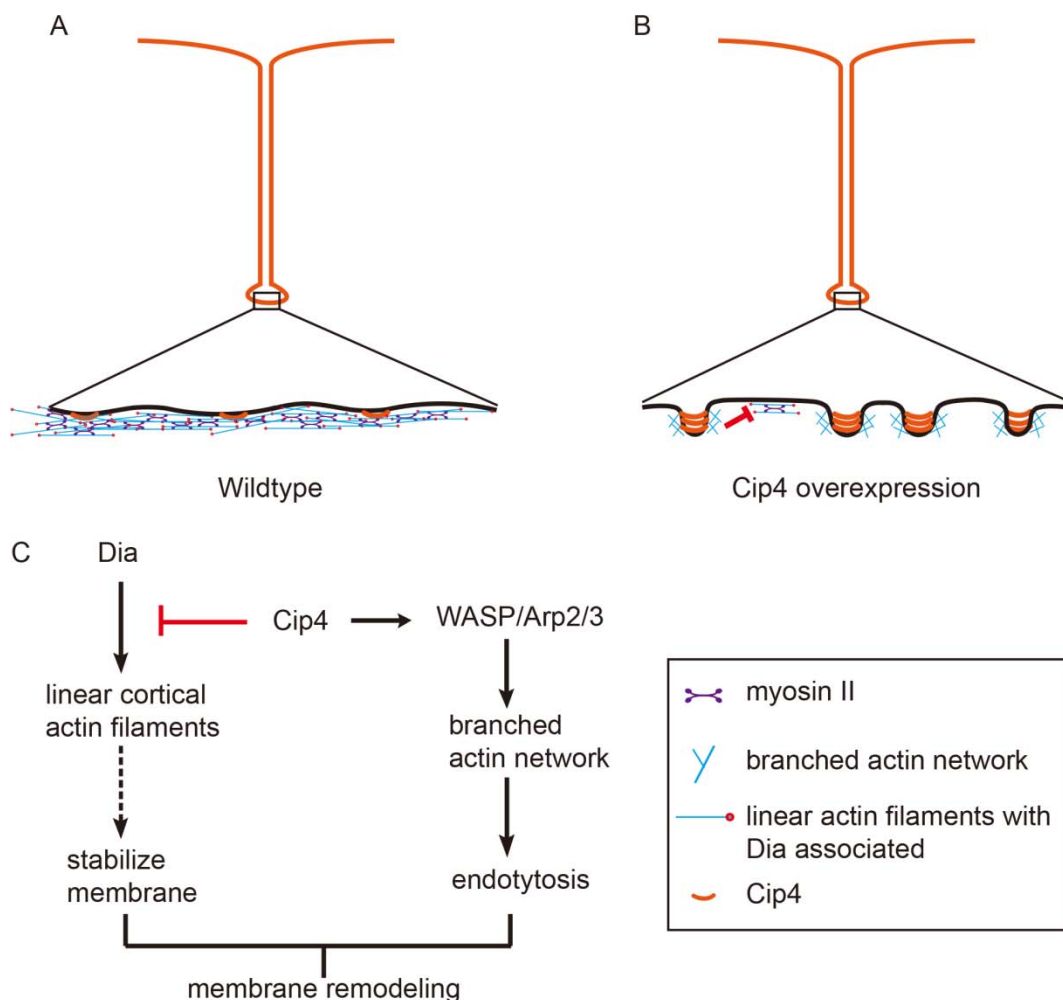
Figure 4.3 The dual activity of Cip4 promotes efficient membrane remodeling. (A) At the mid-stage of cellularization, the furrow canal is stabilized by a cortical layer of linear actin filaments. (B) Cip4 overexpression bends the membrane, and WASPs are recruited to the membrane, which activate Arp2/3 and promote branch actin filament polymerization. Branched actin filaments provide the force for membrane invagination. Cip4 inhibits Dia activity at the plasma membrane, therefore reduces the amount of cortical linear F-actin. The membrane rigidity is reduced by the dual activity of Cip4. (C) Schematic representation of Cip4 promoting membrane remodeling.

The polarity of epithelia is maintained during the course of cellularization. There is a very sharp boundary between lateral and basal domain in epithelia,

as indicated by immunostaining with protein markers for lateral and basal domains. Several mechanisms for maintaining a sharp boundary are considered, 1) a morphologically visible diffusion barrier, e.g. junctional complexes; 2) sorting mechanism by endocytosis and exocytosis and 3) F-actin-dependent resistance of membrane lateral diffusion.

During cellularization, there is a basal junction localizing between lateral and basal domain. However, this basal junction is dispensable for lateral-basal domain separation (Sokac and Wieschaus, 2008b). In *arm* (*β-catenin* in *Drosophila*) mutant embryos the basal junction is missing, but functional furrow canal compartments and the boundary between lateral and basal are established and maintained (Sokac and Wieschaus, 2008b). The sorting mechanism by vesicle trafficking also does not involved in lateral-basal domain separation, as indicated in embryos from *shibire* female.

The polarity of lateral-basal domain is maintained by Dia and F-actin. Discs-large, a marker of lateral domain, spread into the furrow canal in Cytochalasin D injected embryo. Loss of function of Dia and overexpression of Cip4 leads to a phenocopy. How does F-actin contribute to membrane compartmentalization? One possibility is that cortical layer of linear F-actin increases the rigidity and suppresses lateral diffusion. This is confirmed by FRAP experiments. In the GFP-labeled membrane integrated protein 117/Spider embryo, the recovery rate of GFP signal in the furrow canal is slower than in the lateral domain. Furthermore, *dia* germline clone embryos also showed a faster recovery rate in furrow canals compared with wild type embryo. In addition, an *in vitro* study has provided a quantitative correlation between density of actin cortex and lateral diffusion (Heinemann et al., 2013). The same experiment was carried out with Palmitoylated-YFP embryo. In this embryo, the YFP inserts into the membrane via its palmitoyl tail. Besides membrane localization, there is a strong background of YFP signal swimming around in the cytoplasm freely. After bleaching, the YFP signal on the

91

membrane recovered in less than 1 minute and we couldn't see any difference between the lateral membrane and the furrow canal. We reasoned that this was due to a fast exchange between membrane fraction and cytoplasmic fraction. The GAP43-venus embryo was employed in FRAP experiment. GAP43 has two palmitoyl tails and was considered associated with membrane more tightly than one palmitoyl tailed YFP. Indeed, the turnover rate of GAP43 is slower than one palmitoyl tailed YFP. However, no difference between lateral membrane and furrow canal was detected. These FRAP experiments suggest that the F-actin coated furrow canal counteracts membrane mobility and lateral diffusion, but is free for molecular exchange between plasma membrane and cytoplasm.
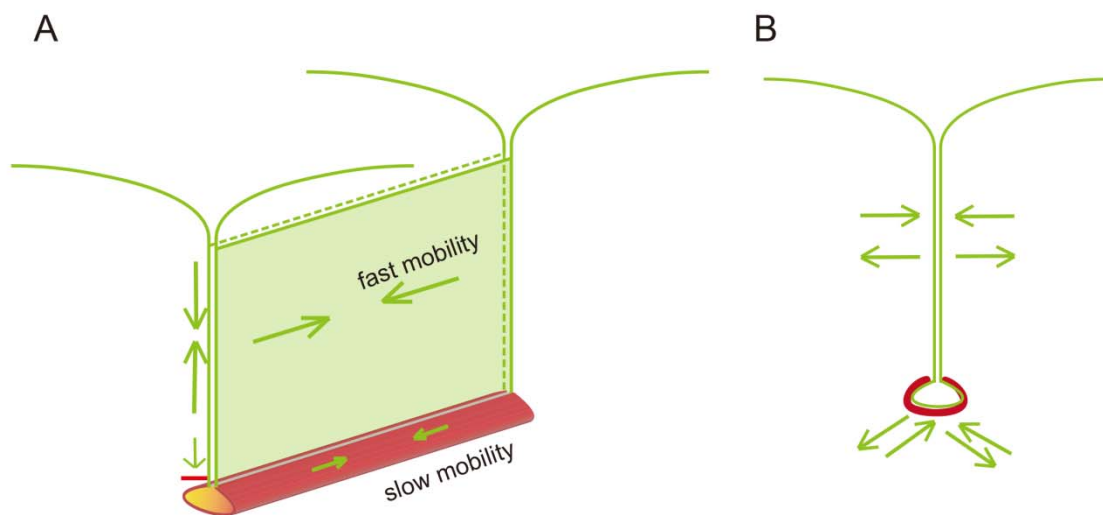
Figure 4.4 Membrane properties in different domain during cellularization. (A) FRAP experiments using 117/Spider-GFP show that the membrane mobility at the furrow canal domain is slower than the lateral domain membrane. The difference between these two domains is due to the F-actin accumulation at the furrow canal. F-actin inhibits lateral diffusion, and this inhibition makes the boundary between lateral and basal domain. (B) The F-actin accumulated at the furrow canal doesn't block the protein exchange between membrane and cytoplasm, indicated by FRAP experiments using membrane attached proteins with palmitoyl tails.

4.3 Ced-12 is required for the formation of actin caps and metaphase furrows

At the onset of interphase of cycle 10 in the syncytial blastoderm stage of *Drosophila* embryo, F-actin forms a dome-like cap above each nuclear and the associated centrosomes. With entry into mitosis, the actin redistributes towards the cap margins and the cap expands until they meet each other, and eventually the metaphase furrow between adjacent nuclei forms. As the daughter nuclei separate the F-actin again forms the cap structure. The mechanism of actin cap formation is not understood yet. In *arpc1^{r337st}* germline clone embryos, the formation of actin caps is not affected, but the actin caps fail to expand and form the metaphase furrow, resulting in the formation of smaller caps compared with wild type (Stevenson et al., 2002). This data suggests that Arp2/3 is essential for actin redistribution. However, the *arpc1 ^{r337st}* allele used was a partial loss-of-function allele, since the stronger alleles of *arpc1* disrupted the oogenesis and blocked egg production (Stevenson et al., 2002). It is possible that the low level of Arp2/3 in *arpc1 ^{r337st}* germline clone embryo is sufficient for actin cap formation. The other possibility is that Arp2/3 is only required for actin cap expansion and that the formation of actin cap is independent of Arp2/3 (Stevenson et al., 2002). To distinguish these two alternatives, injection of high dose of CK666, Arp2/3 inhibitor, may provide new clue.

In addition, in *sponge* germline clone embryos, actin caps and metaphase furrow are not formed (Postner et al., 1992). A later study showed that Sponge was an ortholog of DOCK protein, and bound with Ced-12, regulating embryonic CNS development (Biersmith et al., 2011). DOCK proteins were found to be guanine nucleotide exchange factors (GEFs) which activate Rac and Rho. DOCK proteins only show GEF activity when they are bound to Elmo/Ced-12 (Meller et al., 2005).

In our lab, 2L367 was first found in a screen for mutations from germline clones with a blastoderm phenotype (Rohatgi et al., 1999) (Vogt et al., 2006). In this study, we were able to identify that 2L367 is Ced-12. The phenotype of *ced-12*[2L367] germline clone embryos is similar to *sponge* mutant.

Ced-12 (Ced stands for **ce**ll **d**eath abnormality) was identified initially in *C.elengas* as an essential gene involved in engulfment of dying cells during apoptosis (Hedgecock et al., 1983). Ced-12, together with Ced-5 (ortholog of Dock180), binds to PsdSer receptor, triggering the engulfment (Kinchen and Ravichandran, 2007). One possibility is that Sponge/Ced-12 complex promotes actin caps and metaphase furrows assembly via activating Rac signaling.

It was reported that actin caps are induced by centrosomes. The free centrosomes which are uncoupled from the nuclei by anti-Tubulin antibody treatment or low temperature are sufficient for inducing actin caps above them (Callaini et al., 1991). Furthermore, the free centrosomes are not distributed evenly, and actin caps are not able to form at the space where no centrosome is present. In addition, a clear correlation between the size/density of actin caps and the number/spatial arrangement of free centrosome material was observed (Callaini et al., 1991). Maternal defect of *daughterless-abo-like* (*dal*) shows a defect in centrosome separation, and the metaphase furrow could not form during mitosis (Sullivan et al., 1993), suggesting that centrosome may also be involved in inducing metaphase furrow assembly. However, the signals from centrosomes needed for induction of actin caps and metaphase furrows are less clear.
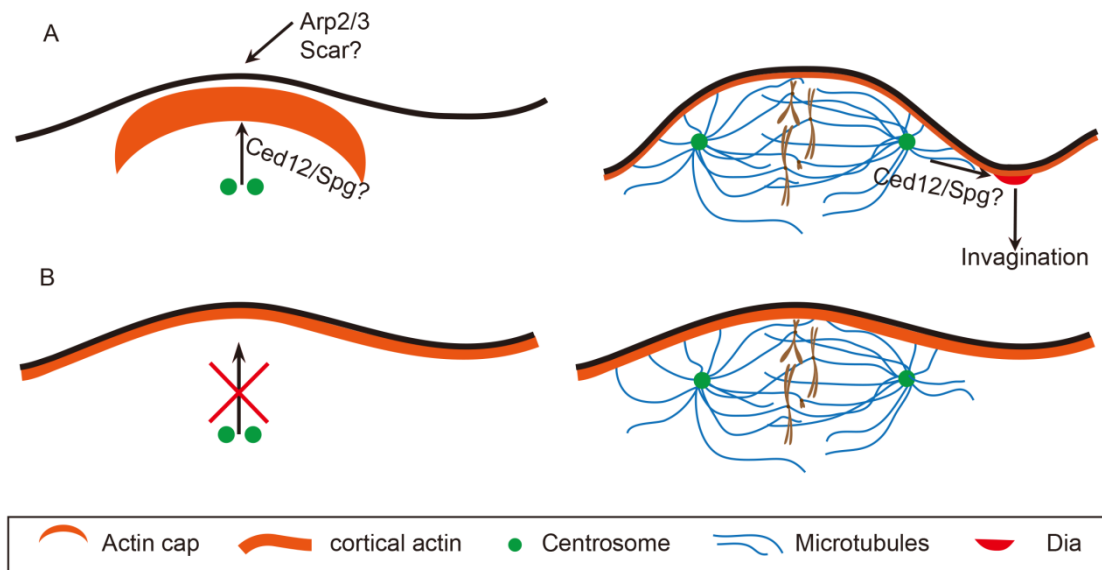
Figure 4.5 Ced-12 is necessary for inducing actin caps and metaphase furrow. (A) In wild-type embryos, the actin caps and metaphase furrows are induced by centrosomes in the interphase and mitosis, respectively. (B) In *ced-12*^{2L367} embryo, the position of centrosomes is not affected, but no actin caps and metaphase furrows are formed. This implies that Ced-12/Sponge is involved in the signal transduction.

In *ced-12*^{2L367} germline clones, the centrosome localization is not affected. However, the actin caps and metaphase furrows are missing. One possibility is that Ced-12/Sponge is involved in the signaling pathway between centrosome signaling and actin-based structure. Dock180, a homolog of Sponge, activates Rac in the presence of Elmo (Wang et al., 2014). And Rac is an important activator for N-WASP/WAVE and PI(4)P-5 kinase (de Curtis, 2014). N-WASP activates Arp2/3 and promotes actin assembly (Rohatgi et al., 1999). PI(4)P-5 kinase increases concentration of PI(4,5)P2, and PI(4,5)P2 is involved in Myosin II assembly (Reversi et al., 2014). The other homologs of Sponge Dock3 and Dock10, are involved in activation of Rho (Laurin and Côté, 2014). Dia is a RhoGTPase effector and is necessary for metaphase furrow formation in *Drosophila* (Grosshans et al., 2005). We could not exclude involvement of other Arp2/3-independent mechanisms. Our hypothesis is that in interphase, centrosome pair induces actin caps above it via Ced-12/Sponge-Rac-Scar-Arp2/3 signaling pathway, and during mitosis, the

centrosome pair separates and migrates to the side of the nuclei, and induces metaphase furrows via Ced-12/Sponge-Rho/Rac-Dia/Arp2/3 signal pathways.
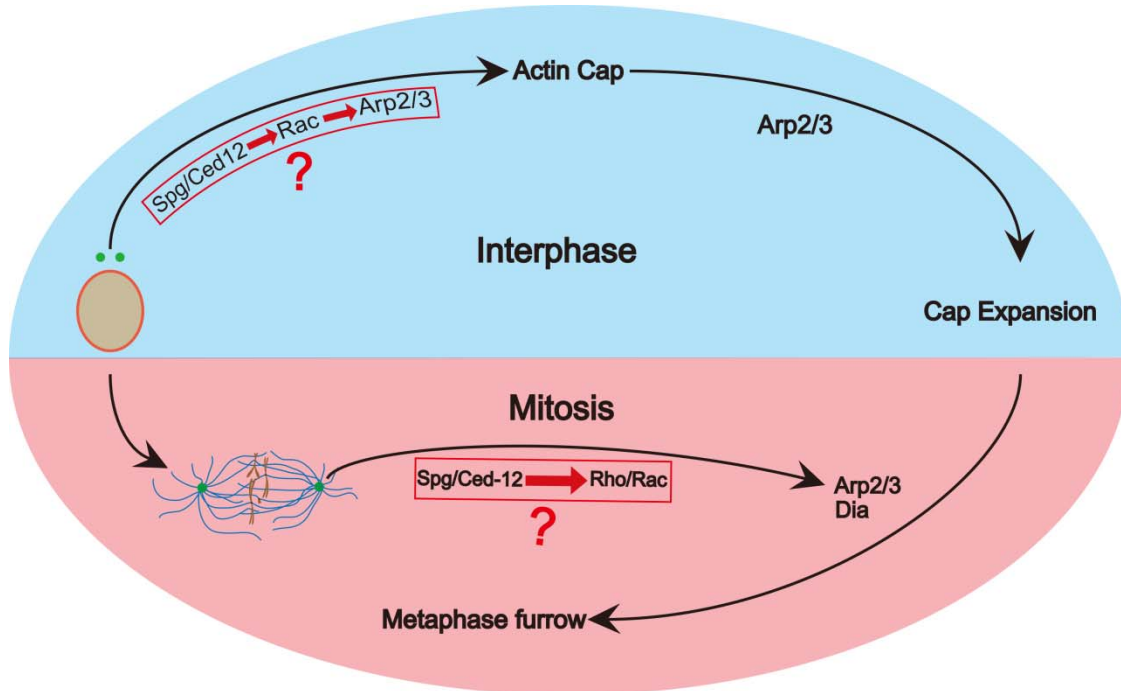
Figure 4.6 Schematic representation of involvement of Ced-12/Sponge in the regulation of F-actin caps and metaphase furrow. In the interphase, the centrosome induces actin cap formation, and Ced-12/Spg complex is essential for this process. Ced-12/Spg activates Rac; then Rac activates WAVE/Scar, which allows WAVE/Scar to activate Arp2/3, causing actin polymerization. At the onset of prophase, the centrosome undergoes duplication and migration, and induces metaphase furrow, probably using a similar pathway: Ced-12/Spg activates Rac and Rho, then Rac activates Arp2/3 and Rho activates Dia, causing actin polymerization and building the metaphase furrow.

References

Abu-Thuraia, Afnan, Rosemarie Gauthier, Rony Chidiac, Yoshinori Fukui, Robert A. Screaton, Jean-Philippe Gratton, and Jean-François Côté. "Axl Phosphorylates Elmo Scaffold Proteins to Promote Rac Activation and Cell Invasion." *Molecular and Cellular Biology*, October 20, 2014.

Acharya, Sreemukta, Philip Laupsien, Christian Wenzl, Shuling Yan, and Jörg Großhans. "Function and Dynamics of Slam in Furrow Formation in Early Drosophila Embryo." Developmental Biology 386, no. 2 (February 15, 2014): 371–84.

Arasada, Rajesh, and Thomas D. Pollard. "Distinct Roles for F-BAR Proteins Cdc15p and Bzz1p in Actin Polymerization at Sites of Endocytosis in Fission Yeast." *Current Biology: CB* 21, no. 17 (September 13, 2011): 1450–59.

Aspenström, Pontus. "BAR Domain Proteins Regulate Rho GTPase Signaling." *Small GTPases* 5 (April 17, 2014).

Baker, J., W. E. Theurkauf, and G. Schubiger. "Dynamic Changes in Microtubule Configuration Correlate with Nuclear Migration in the Preblastoderm Drosophila Embryo." *The Journal of Cell Biology* 122, no. 1 (July 1993): 113–21.

Beltzner, Christopher C., and Thomas D. Pollard. "Identification of Functionally Important Residues of Arp2/3 Complex by Analysis of Homology Models from Diverse Species." *Journal of Molecular Biology* 336, no. 2 (February 13, 2004): 551–65.

Bianco, Ambra, Minna Poukkula, Adam Cliffe, Juliette Mathieu, Carlos M. Luque, Tudor A. Fulga, and Pernille Rørth. "Two Distinct Modes of Guidance Signalling during Collective Migration of Border Cells." Nature 448, no. 7151 (July 19, 2007): 362–65.

Biersmith, Bridget, Ze Cindy Liu, Kenneth Bauman, and Erika R. Geisbrecht. "The DOCK Protein Sponge Binds to ELMO and Functions in Drosophila Embryonic CNS Development." *PloS One* 6, no. 1 (2011): e16120.

Bilancia, Colleen G., Jonathan D. Winkelman, Denis Tsygankov, Stephanie H. Nowotarski, Jennifer A. Sees, Kate Comber, Iwan Evans, et al. "Enabled Negatively Regulates Diaphanous-Driven Actin Dynamics in Vitro and in Vivo." *Developmental Cell* 28, no. 4 (February 24, 2014): 394–408.

Bischof, Johannes, Robert K. Maeda, Monika Hediger, François Karch, and Konrad Basler. "An Optimized Transgenesis System for Drosophila Using Germ-Line-Specific phiC31 Integrases." *Proceedings of the National Academy of Sciences of the United States of America* 104, no. 9 (February 27, 2007): 3312–17.

Bosch, Montserrat, Kim Ho Diep Le, Beata Bugyi, John J. Correia, Louis Renault, and Marie-France Carlier. "Analysis of the Function of Spire in Actin Assembly and Its

References

Synergy with Formin and Profilin." *Molecular Cell* 28, no. 4 (November 30, 2007): 555–68.

Bownes, Mary, Niels Abrahamssen, Claire Gilman, Ross Howden, Alberto Martinez, and Roger Slee. "Drosophila: A Laboratory Handbook. By Michael Ashburner. New York: Cold Spring Harbor Laboratory. 1989.

Breitsprecher, Dennis, Richa Jaiswal, Jeffrey P. Bombardier, Christopher J. Gould, Jeff Gelles, and Bruce L. Goode. "Rocket Launcher Mechanism of Collaborative Actin Assembly Defined by Single-Molecule Imaging." *Science* 336, no. 6085 (June 1, 2012): 1164–68..

Callaini, G., R. Dallai, and M. G. Riparbelli. "Microfilament Distribution in Cold-Treated Drosophila Embryos." *Experimental Cell Research* 194, no. 2 (June 1991): 316–21.

Campellone, Kenneth G., and Matthew D. Welch. "A Nucleator Arms Race: Cellular Control of Actin Assembly." *Nature Reviews. Molecular Cell Biology* 11, no. 4 (April 2010): 237–51.

Chan, D. C., M. T. Bedford, and P. Leder. "Formin Binding Proteins Bear WWP/WW Domains That Bind Proline-Rich Peptides and Functionally Resemble SH3 Domains." *The EMBO Journal* 15, no. 5 (March 1, 1996): 1045–54.

Chesarone, Melissa A., Amy Grace DuPage, and Bruce L. Goode. "Unleashing Formins to Remodel the Actin and Microtubule Cytoskeletons." *Nature Reviews. Molecular Cell Biology* 11, no. 1 (January 2010): 62–74.

Chhabra, Ekta Seth, and Henry N. Higgs. "The Many Faces of Actin: Matching Assembly Factors with Cellular Structures." *Nature Cell Biology* 9, no. 10 (October 2007): 1110–21.

Chitu, Violeta, and E. Richard Stanley. "Pombe Cdc15 Homology (PCH) Proteins: Coordinators of Membrane-Cytoskeletal Interactions." *Trends in Cell Biology* 17, no. 3 (March 2007): 145–56.

Chou, T. B., and N. Perrimon. "Use of a Yeast Site-Specific Recombinase to Produce Female Germline Chimeras in Drosophila." *Genetics* 131, no. 3 (July 1992): 643–53.

Côté, Jean-François, and Kristiina Vuori. "GEF What? Dock180 and Related Proteins Help Rac to Polarize Cells in New Ways." *Trends in Cell Biology* 17, no. 8 (August 2007): 383–93.

Courtemanche, Naomi, and Thomas D. Pollard. "Determinants of Formin Homology 1 (FH1) Domain Function in Actin Filament Elongation by Formins." *Journal of Biological Chemistry* 287, no. 10 (March 2, 2012): 7812–20.

Dawson, John C., John A. Legg, and Laura M. Machesky. "Bar Domain Proteins: A Role in Tubulation, Scission and Actin Assembly in Clathrin-Mediated Endocytosis." *Trends in Cell Biology* 16, no. 10 (October 2006): 493–98.

References

De Curtis, Ivan. "Roles of Rac1 and Rac3 GTPases during the Development of Cortical and Hippocampal GABAergic Interneurons." *Frontiers in Cellular Neuroscience* 8 (2014): 307.

Dietrich, Susanne, Sabine Weiß, Sandra Pleiser, and Eugen Kerkhoff. "Structural and Functional Insights into the Spir/formin Actin Nucleator Complex." *Biological Chemistry* 394, no. 12 (December 2013): 1649–60.

Eisenmann, Kathryn M., Elizabeth S. Harris, Susan M. Kitchen, Holly A. Holman, Henry N. Higgs, and Arthur S. Alberts. "Dia-Interacting Protein Modulates Formin-Mediated Actin Assembly at the Cell Cortex." *Current Biology* 17, no. 7 (April 3, 2007): 579–91.

Farsad, K., N. Ringstad, K. Takei, S. R. Floyd, K. Rose, and P. De Camilli. "Generation of High Curvature Membranes Mediated by Direct Endophilin Bilayer Interactions." *The Journal of Cell Biology* 155, no. 2 (October 15, 2001): 193–200.

Figard, Lauren, Heng Xu, Hernan G. Garcia, Ido Golding, and Anna Marie Sokac. "The Plasma Membrane Flattens out to Fuel Cell-Surface Growth during Drosophila Cellularization." *Developmental Cell* 27, no. 6 (December 23, 2013): 648–55.

Fricke, Robert, Christina Gohl, and Sven Bogdan. "The F-BAR Protein Family Actin' on the Membrane." *Communicative & Integrative Biology* 3, no. 2 (March 2010): 89–94.

Fricke, Robert, Christina Gohl, Elavarasi Dharmalingam, Astrid Grevelhörster, Baharak Zahedi, Nicholas Harden, Michael Kessels, Britta Qualmann, and Sven Bogdan. "Drosophila Cip4/Toca-1 Integrates Membrane Trafficking and Actin Dynamics through WASP and SCAR/WAVE." *Current Biology: CB* 19, no. 17 (September 15, 2009): 1429–37.

Frost, Adam, Pietro De Camilli, and Vinzenz M. Unger. "F-BAR Proteins Join the BAR Family Fold." *Structure* 15, no. 7 (July 2007): 751–53.

Frost, Adam, Vinzenz M. Unger, and Pietro De Camilli. "The BAR Domain Superfamily: Membrane-Molding Macromolecules." *Cell* 137, no. 2 (April 17, 2009): 191–96.

Geisbrecht, Erika R., Shruti Haralalka, Selene K. Swanson, Laurence Florens, Mike P. Washburn, and Susan M. Abmayr. "Drosophila ELMO/CED-12 Interacts with Myoblast City to Direct Myoblast Fusion and Ommatidial Organization." *Developmental Biology* 314, no. 1 (February 1, 2008): 137–49.

Giuliani, Chiara, Flavia Troglio, Zhiyong Bai, Falshruti B. Patel, Adriana Zucconi, Maria Grazia Malabarba, Andrea Disanza, et al. "Requirements for F-BAR Proteins TOCA-1 and TOCA-2 in Actin Dynamics and Membrane Trafficking during Caenorhabditis Elegans Oocyte Growth and Embryonic Epidermal Morphogenesis." *PLoS Genetics* 5, no. 10 (October 2009): e1000675.

Goley, Erin D., Stacia E. Rodenbusch, Adam C. Martin, and Matthew D. Welch. "Critical Conformational Changes in the Arp2/3 Complex Are Induced by Nucleotide and Nucleation Promoting Factor." *Molecular Cell* 16, no. 2 (October 22, 2004): 269–79.

References

Goode, Bruce L., and Michael J. Eck. "Mechanism and Function of Formins in the Control of Actin Assembly." *Annual Review of Biochemistry* 76, no. 1 (2007): 593–627.

Graziano, Brian R., Amy Grace DuPage, Alphee Michelot, Dennis Breitsprecher, James B. Moseley, Isabelle Sagot, Laurent Blanchoin, and Bruce L. Goode. "Mechanism and Cellular Function of Bud6 as an Actin Nucleation-Promoting Factor." *Molecular Biology of the Cell* 22, no. 21 (November 2011): 4016–28.

Graziano, Brian R., Erin M. Jonasson, Jessica G. Pullen, Christopher J. Gould, and Bruce L. Goode. "Ligand-Induced Activation of a formin–NPF Pair Leads to Collaborative Actin Nucleation." *The Journal of Cell Biology* 201, no. 4 (May 13, 2013): 595–611.

Graziano, Brian R., Hoi-Ying E. Yu, Salvatore L. Alioto, Julian A. Eskin, Casey A. Ydenberg, David P. Waterman, Mikael Garabedian, and Bruce L. Goode. "The F-BAR Protein Hof1 Tunes Formin Activity to Sculpt Actin Cables during Polarized Growth." *Molecular Biology of the Cell* 25, no. 11 (June 2014): 1730–43.

Grosshans, Jörg, Christian Wenzl, Hans-Martin Herz, Slawomir Bartoszewski, Frank Schnorrer, Nina Vogt, Heinz Schwarz, and H.-Arno Müller. "RhoGEF2 and the Formin Dia Control the Formation of the Furrow Canal by Directed Actin Assembly during Drosophila Cellularisation." *Development (Cambridge, England)* 132, no. 5 (March 2005): 1009–20.

Habas, R., Y. Kato, and X. He. "Wnt/Frizzled Activation of Rho Regulates Vertebrate Gastrulation and Requires a Novel Formin Homology Protein Daam1." *Cell* 107, no. 7 (December 28, 2001): 843–54.

Hedgecock, E. M., J. E. Sulston, and J. N. Thomson. "Mutations Affecting Programmed Cell Deaths in the Nematode Caenorhabditis Elegans." *Science* 220, no. 4603 (June 17, 1983): 1277–79.

Heinemann, Fabian, Sven K. Vogel, and Petra Schwille. "Lateral Membrane Diffusion Modulated by a Minimal Actin Cortex." *Biophysical Journal* 104, no. 7 (April 2, 2013): 1465–75.

Hetrick, Byron, Min Suk Han, Luke A. Helgeson, and Brad J. Nolen. "Small Molecules CK-666 and CK-869 Inhibit Actin-Related Protein 2/3 Complex by Blocking an Activating Conformational Change." *Chemistry & Biology* 20, no. 5 (May 23, 2013): 701–12.

Itoh, Toshiki, Kai S. Erdmann, Aurelien Roux, Bianca Habermann, Hauke Werner, and Pietro De Camilli. "Dynamin and the Actin Cytoskeleton Cooperatively Regulate Plasma Membrane Invagination by BAR and F-BAR Proteins." *Developmental Cell* 9, no. 6 (December 2005): 791–804.

Jaiswal, Richa, Vince Stepanik, Aneliya Rankova, Olivia Molinar, Bruce L. Goode, and Brooke M. McCartney. "Drosophila Homologues of Adenomatous Polyposis Coli (APC) and the Formin Diaphanous Collaborate by a Conserved Mechanism to Stimulate

References

Actin Filament Assembly." *The Journal of Biological Chemistry* 288, no. 19 (May 10, 2013): 13897–905.

Karr, T. L., and B. M. Alberts. "Organization of the Cytoskeleton in Early Drosophila Embryos." *The Journal of Cell Biology* 102, no. 4 (April 1986): 1494–1509.

Kerkhoff, Eugen. "Cellular Functions of the Spir Actin-Nucleation Factors." *Trends in Cell Biology* 16, no. 9 (September 2006): 477–83.

Kinchen, Jason M., and Kodi S. Ravichandran. "Journey to the Grave: Signaling Events Regulating Removal of Apoptotic Cells." *Journal of Cell Science* 120, no. Pt 13 (July 1, 2007): 2143–49.

Kishino, Akiyoshi, and Toshio Yanagida. "Force Measurements by Micromanipulation of a Single Actin Filament by Glass Needles." *Nature* 334, no. 6177 (July 7, 1988): 74–76.

Kovar, David R., Elizabeth S. Harris, Rachel Mahaffy, Henry N. Higgs, and Thomas D. Pollard. "Control of the Assembly of ATP- and ADP-Actin by Formins and Profilin." *Cell* 124, no. 2 (January 27, 2006): 423–35.

Lammel, Uwe, Meike Bechtold, Benjamin Risse, Dimitri Berh, Astrid Fleige, Ingrid Bunse, Xiaoyi Jiang, Christian Klämbt, and Sven Bogdan. "The Drosophila FHOD1-like Formin Knittrig Acts through Rok to Promote Stress Fiber Formation and Directed Macrophage Migration during the Cellular Immune Response." *Development* 141, no. 6 (March 2014): 1366–80.

Lammers, Michael, Rolf Rose, Andrea Scrima, and Alfred Wittinghofer. "The Regulation of mDia1 by Autoinhibition and Its Release by Rho*GTP." *The EMBO Journal* 24, no. 23 (December 7, 2005): 4176–87.

Laurin, Mélanie, and Jean-François Côté. "Insights into the Biological Functions of Dock Family Guanine Nucleotide Exchange Factors." *Genes & Development* 28, no. 6 (March 15, 2014): 533–47.

Lecuit, Thomas, and Eric Wieschaus. "Polarized Insertion of New Membrane from a Cytoplasmic Reservoir during Cleavage of the Drosophila Embryo." *The Journal of Cell Biology* 150, no. 4 (August 21, 2000): 849–60.

Leibfried, Andrea, Sandra Müller, and Anne Ephrussi. "A Cdc42-Regulated Actin Cytoskeleton Mediates Drosophila Oocyte Polarization." *Development* 140, no. 2 (January 15, 2013): 362–71.

Levayer, Romain, Anne Pelissier-Monier, and Thomas Lecuit. "Spatial Regulation of Dia and Myosin-II by RhoGEF2 Controls Initiation of E-Cadherin Endocytosis during Epithelial Morphogenesis." *Nature Cell Biology* 13, no. 5 (May 2011): 529–40.

Li, Fang, and Henry N. Higgs. "The Mouse Formin mDia1 Is a Potent Actin Nucleation Factor Regulated by Autoinhibition." *Current Biology* 13, no. 15 (August 5, 2003): 1335–40.

References

Maiti, Sankar, Alphee Michelot, Christopher Gould, Laurent Blanchoin, Olga Sokolova, and Bruce L. Goode. "Structure and Activity of Full-Length Formin mDia1." *Cytoskeleton (Hoboken, N.J.)* 69, no. 6 (June 2012): 393–405.

Manseau, L. J., and T. Schüpbach. "Cappuccino and Spire: Two Unique Maternal-Effect Loci Required for Both the Anteroposterior and Dorsoventral Patterns of the Drosophila Embryo." *Genes & Development* 3, no. 9 (September 1989): 1437–52.

Mattila, Pieta K., Anette Pykäläinen, Juha Saarikangas, Ville O. Paavilainen, Helena Vihinen, Eija Jokitalo, and Pekka Lappalainen. "Missing-in-Metastasis and IRSp53 Deform PI(4,5)P2-Rich Membranes by an Inverse BAR Domain-like Mechanism." *The Journal of Cell Biology* 176, no. 7 (March 26, 2007): 953–64.

Matusek, Tamás, Alexandre Djiane, Ferenc Jankovics, Damian Brunner, Marek Mlodzik, and József Mihály. "The Drosophila Formin DAAM Regulates the Tracheal Cuticle Pattern through Organizing the Actin Cytoskeleton." *Development* 133, no. 5 (March 2006): 957–66.

Mavrakis, Manos, Richa Rikhy, and Jennifer Lippincott-Schwartz. "Plasma Membrane Polarity and Compartmentalization Are Established Before Cellularization in the Fly Embryo." *Developmental Cell* 16, no. 1 (January 2009): 93–104.

Meller, Nahum, Sylvain Merlot, and Chittibabu Guda. "CZH Proteins: A New Family of Rho-GEFs." *Journal of Cell Science* 118, no. Pt 21 (November 1, 2005): 4937–46.

Okada, Kyoko, Francesca Bartolini, Alexandra M. Deaconescu, James B. Moseley, Zvonimir Dogic, Nikolaus Grigorieff, Gregg G. Gundersen, and Bruce L. Goode. "Adenomatous Polyposis Coli Protein Nucleates Actin Assembly and Synergizes with the Formin mDia1." *The Journal of Cell Biology* 189, no. 7 (June 28, 2010): 1087–96.

Otomo, Takanori, Diana R. Tomchick, Chinatsu Otomo, Sanjay C. Panchal, Mischa Machius, and Michael K. Rosen. "Structural Basis of Actin Filament Nucleation and Processive Capping by a Formin Homology 2 Domain." *Nature* 433, no. 7025 (February 3, 2005): 488–94.

Otto, I. M., T. Raabe, U. E. Rennefahrt, P. Bork, U. R. Rapp, and E. Kerkhoff. "The p150-Spir Protein Provides a Link between c-Jun N-Terminal Kinase Function and Actin Reorganization." *Current Biology: CB* 10, no. 6 (March 23, 2000): 345–48.

Paul, Aditya S., Aditya Paul, Thomas D. Pollard, and Thomas Pollard. "The Role of the FH1 Domain and Profilin in Formin-Mediated Actin-Filament Elongation and Nucleation." *Current Biology: CB* 18, no. 1 (January 8, 2008): 9–19.

Paul, Aditya S., and Thomas D. Pollard. "Review of the Mechanism of Processive Actin Filament Elongation by Formins." *Cell Motility and the Cytoskeleton* 66, no. 8 (August 2009): 606–17.

Perelroizen, I., J. B. Marchand, L. Blanchoin, D. Didry, and M. F. Carlier. "Interaction of Profilin with G-Actin and poly(L-Proline)." Biochemistry 33, no. 28 (July 19, 1994): 8472–78.

References

Peter, Brian J., Helen M. Kent, Ian G. Mills, Yvonne Vallis, P. Jonathan G. Butler, Philip R. Evans, and Harvey T. McMahon. "BAR Domains as Sensors of Membrane Curvature: The Amphiphysin BAR Structure." *Science (New York, N.Y.)* 303, no. 5657 (January 23, 2004): 495–99.

Pfaendtner, Jim, Edward Lyman, Thomas D. Pollard, and Gregory A. Voth. "Structure and Dynamics of the Actin Filament." *Journal of Molecular Biology* 396, no. 2 (February 19, 2010): 252–63.

Pollard, Thomas D., Laurent Blanchoin, and R. Dyche Mullins. "Molecular Mechanisms Controlling Actin Filament Dynamics in Nonmuscle Cells." *Annual Review of Biophysics and Biomolecular Structure* 29, no. 1 (2000): 545–76.

Postner, M. A., K. G. Miller, and E. F. Wieschaus. "Maternal Effect Mutations of the Sponge Locus Affect Actin Cytoskeletal Rearrangements in Drosophila Melanogaster Embryos." *The Journal of Cell Biology* 119, no. 5 (December 1992): 1205–18.

Pruyne, David, Marie Evangelista, Changsong Yang, Erfei Bi, Sally Zigmond, Anthony Bretscher, and Charles Boone. "Role of Formins in Actin Assembly: Nucleation and Barbed-End Association." *Science* 297, no. 5581 (July 26, 2002): 612–15.

Qualmann, Britta, and Michael M. Kessels. "New Players in Actin Polymerization--WH2-Domain-Containing Actin Nucleators." *Trends in Cell Biology* 19, no. 6 (June 2009): 276–85.

Qualmann, Britta, Dennis Koch, and Michael Manfred Kessels. "Let's Go Bananas: Revisiting the Endocytic BAR Code." *The EMBO Journal* 30, no. 17 (August 31, 2011): 3501–15.

Quinlan, Margot E. "Direct Interaction between Two Actin Nucleators Is Required in Drosophila Oogenesis." *Development (Cambridge, England)* 140, no. 21 (November 2013): 4417–25.

Quinlan, Margot E., John E. Heuser, Eugen Kerkhoff, and R. Dyche Mullins. "Drosophila Spire Is an Actin Nucleation Factor." *Nature* 433, no. 7024 (January 27, 2005): 382–88.

Rasson, Amy S., Justin S. Bois, Duy Stephen L. Pham, Haneul Yoo, and Margot E. Quinlan. "Filament Assembly by Spire: Key Residues and Concerted Actin Binding." *Journal of Molecular Biology*. Accessed September 24, 2014.

Reversi, Alessandra, Eva Loeser, Devaraj Subramanian, Carsten Schultz, and Stefano De Renzis. "Plasma Membrane Phosphoinositide Balance Regulates Cell Shape during Drosophila Embryo Morphogenesis." *The Journal of Cell Biology* 205, no. 3 (May 12, 2014): 395–408.

Rohatgi, R., L. Ma, H. Miki, M. Lopez, T. Kirchhausen, T. Takenawa, and M. W. Kirschner. "The Interaction between N-WASP and the Arp2/3 Complex Links Cdc42-Dependent Signals to Actin Assembly." *Cell* 97, no. 2 (April 16, 1999): 221–31.

References

Roignot, J., D. Taïeb, M. Suliman, N. J. Dusetti, J. L. Iovanna, and P. Soubeyran. "CIP4 Is a New ArgBP2 Interacting Protein That Modulates the ArgBP2 Mediated Control of WAVE1 Phosphorylation and Cancer Cell Migration." *Cancer Letters* 288, no. 1 (February 1, 2010): 116–23.

Romero, Stéphane, Christophe Le Clainche, Dominique Didry, Coumaran Egile, Dominique Pantaloni, and Marie-France Carlier. "Formin Is a Processive Motor That Requires Profilin to Accelerate Actin Assembly and Associated ATP Hydrolysis." *Cell* 119, no. 3 (October 29, 2004): 419–29.

Rouiller, Isabelle, Xiao-Ping Xu, Kurt J. Amann, Coumaran Egile, Stephan Nickell, Daniela Nicastro, Rong Li, Thomas D. Pollard, Niels Volkmann, and Dorit Hanein. "The Structural Basis of Actin Filament Branching by the Arp2/3 Complex." *The Journal of Cell Biology* 180, no. 5 (March 10, 2008): 887–95.

Sagot, Isabelle, Avital A. Rodal, James Moseley, Bruce L. Goode, and David Pellman. "An Actin Nucleation Mechanism Mediated by Bni1 and Profilin." *Nature Cell Biology* 4, no. 8 (August 2002): 626–31.

Schejter, E. D., and E. Wieschaus. "Functional Elements of the Cytoskeleton in the Early Drosophila Embryo." *Annual Review of Cell Biology* 9 (1993): 67–99.

Sokac, Anna Marie, and Eric Wieschaus. "Local Actin-Dependent Endocytosis Is Zygotically Controlled to Initiate Drosophila Cellularization." *Developmental Cell* 14, no. 5 (May 2008): 775–86.

Sokac, Anna Marie, and Eric Wieschaus. "Zygotically Controlled F-Actin Establishes Cortical Compartments to Stabilize Furrows during Drosophila Cellularization." *Journal of Cell Science* 121, no. Pt 11 (June 1, 2008): 1815–24.

Staiger, Christopher J, and Laurent Blanchoin. "Actin Dynamics: Old Friends with New Stories." *Current Opinion in Plant Biology*, Cell Biology / Edited by Laurie G Smith and Ulrike Mayer, 9, no. 6 (December 2006): 554–62.

Stevenson, Catherine, Gonzalo de la Rosa, Christopher S. Anderson, Patrick S. Murphy, Tara Capece, Minsoo Kim, and Michael R. Elliott. "Essential Role of Elmo1 in Dock2-Dependent Lymphocyte Migration." *Journal of Immunology (Baltimore, Md.: 1950)* 192, no. 12 (June 15, 2014): 6062–70.

Stevenson, Victoria, Andrew Hudson, Lynn Cooley, and William E. Theurkauf. "Arp2/3-Dependent Psuedocleavage Furrow Assembly in Syncytial Drosophila Embryos." *Current Biology: CB* 12, no. 9 (April 30, 2002): 705–11.

Stradal, Theresia E. B., Klemens Rottner, Andrea Disanza, Stefano Confalonieri, Metello Innocenti, and Giorgio Scita. "Regulation of Actin Dynamics by WASP and WAVE Family Proteins." *Trends in Cell Biology* 14, no. 6 (June 2004): 303–11.

Stradal, Theresia E. B., and Giorgio Scita. "Protein Complexes Regulating Arp2/3-Mediated Actin Assembly." *Current Opinion in Cell Biology* 18, no. 1 (February 2006): 4–10.

References

Suetsugu, Shiro, and Alexis Gautreau. "Synergistic BAR-NPF Interactions in Actin-Driven Membrane Remodeling." *Trends in Cell Biology* 22, no. 3 (March 2012): 141–50.

Sullivan, W., P. Fogarty, and W. Theurkauf. "Mutations Affecting the Cytoskeletal Organization of Syncytial Drosophila Embryos." *Development* 118, no. 4 (August 1, 1993): 1245–54.

Sullivan, W., and W. E. Theurkauf. "The Cytoskeleton and Morphogenesis of the Early Drosophila Embryo." *Current Opinion in Cell Biology* 7, no. 1 (February 1995): 18–22.

Takei, K., V. I. Slepnev, V. Haucke, and P. De Camilli. "Functional Partnership between Amphiphysin and Dynamin in Clathrin-Mediated Endocytosis." *Nature Cell Biology* 1, no. 1 (May 1999): 33–39.

Takenawa, Tadaomi, and Shiro Suetsugu. "The WASP–WAVE Protein Network: Connecting the Membrane to the Cytoskeleton." *Nature Reviews Molecular Cell Biology* 8, no. 1 (January 2007): 37–48.

Tanaka, Hiromasa, Etsuko Takasu, Toshiro Aigaki, Kagayaki Kato, Shigeo Hayashi, and Akinao Nose. "Formin3 Is Required for Assembly of the F-Actin Structure That Mediates Tracheal Fusion in Drosophila." *Developmental Biology* 274, no. 2 (October 15, 2004): 413–25.

Theurkauf, W. E. "Premature Microtubule-Dependent Cytoplasmic Streaming in Cappuccino and Spire Mutant Oocytes." *Science* 265, no. 5181 (September 30, 1994): 2093–96.

Tomasevic, Nenad, Zhiheng Jia, Alan Russell, Toby Fujii, James J. Hartman, Sheila Clancy, Manping Wang, Christophe Beraud, Kenneth W. Wood, and Roman Sakowicz. "Differential Regulation of WASP and N-WASP by Cdc42, Rac1, Nck, and PI(4,5)P2." *Biochemistry* 46, no. 11 (March 20, 2007): 3494–3502.

Vogt, Nina, Iris Koch, Heinz Schwarz, Frank Schnorrer, and Christiane Nüsslein-Volhard. "The γTuRC Components Grip75 and Grip128 Have an Essential Microtubule-Anchoring Function in the Drosophila Germline." Development 133, no. 20 (October 15, 2006): 3963–72.

Wallar, Bradley J., Brittany N. Stropich, Jessica A. Schoenherr, Holly A. Holman, Susan M. Kitchen, and Arthur S. Alberts. "The Basic Region of the Diaphanous-Autoregulatory Domain (DAD) Is Required for Autoregulatory Interactions with the Diaphanous-Related Formin Inhibitory Domain." *The Journal of Biological Chemistry* 281, no. 7 (February 17, 2006): 4300–4307.

Wang, Jin, Jie-min Dai, Ya-ling Che, Yi-meng Gao, Hui-juan Peng, Bin Liu, Hui Wang, and Hua Linghu. "Elmo1 Helps dock180 to Regulate Rac1 Activity and Cell Migration of Ovarian Cancer." International Journal of Gynecological Cancer: Official Journal of the International Gynecological Cancer Society 24, no. 5 (June 2014): 844–50.

References

Webb, Rebecca L., Meng-Ning Zhou, and Brooke M. McCartney. "A Novel Role for an APC2-Diaphanous Complex in Regulating Actin Organization in Drosophila." *Development (Cambridge, England)* 136, no. 8 (April 2009): 1283–93.

Welch, Matthew D., and R. Dyche Mullins. "Cellular Control of Actin Nucleation." *Annual Review of Cell and Developmental Biology* 18 (2002): 247–88.

Wenzl, Christian, Shuling Yan, Philip Laupsien, and Jörg Großhans. "Localization of RhoGEF2 during Drosophila Cellularization Is Developmentally Controlled by Slam." *Mechanisms of Development* 127, no. 7–8 (July 2010): 371–84.

Xu, Yingwu, James B. Moseley, Isabelle Sagot, Florence Poy, David Pellman, Bruce L. Goode, and Michael J. Eck. "Crystal Structures of a Formin Homology-2 Domain Reveal a Tethered Dimer Architecture." *Cell* 116, no. 5 (March 5, 2004): 711–23.

Yan, Shuling, Zhiyi Lv, Moritz Winterhoff, Christian Wenzl, Thomas Zobel, Jan Faix, Sven Bogdan, and Jörg Grosshans. "The F-BAR Protein Cip4/Toca-1 Antagonizes the Formin Diaphanous in Membrane Stabilization and Compartmentalization." *Journal of Cell Science* 126, no. Pt 8 (April 15, 2013): 1796–1805.

Zallen, Jennifer A., Yehudit Cohen, Andrew M. Hudson, Lynn Cooley, Eric Wieschaus, and Eyal D. Schejter. "SCAR Is a Primary Regulator of Arp2/3-Dependent Morphological Events in Drosophila." *The Journal of Cell Biology* 156, no. 4 (February 18, 2002): 689–701.

Zhou, Z., E. Caron, E. Hartwieg, A. Hall, and H. R. Horvitz. "The C. Elegans PH Domain Protein CED-12 Regulates Cytoskeletal Reorganization via a Rho/Rac GTPase Signaling Pathway." *Developmental Cell* 1, no. 4 (October 2001): 477–89.

CURRICULUM VITAE

Zhiyi Lv

Department of Developmental Biochemistry,
University of Göttingen,
Justus-von-Liebig-Weg 11,
37077 Göttingen – Germany
Phone: +49-(0)551-39-8273
Email: lvzhiyi029@gmail.com

Personal details

Date of Birth: 19.May.1984
Place of Birth: Shanxi, China
Gender: Male
Nationality: Chinese

Education

University of Göttingen, Germany

2010.10-Now	Doctorate, Genes and Development program in Göttingen Graduate School for Neurosciences, Biophysics, and Molecular Biosciences (GGNB)

Northwest A&F University, China

2007.09-2010.07	M. Sc. Developmental Biology
2002.09-2006.07	B. Sc. Biology

Publication list

Shuling Yan,* **Zhiyi Lv,*** Moritz Winterhoff,* Christian Wenzl, Thomas Zobel, Jan Faix, Sven Bogdan, and Jörg Grosshans. 2013. The F-BAR protein Cip4/Toca-1 antagonizes the formin Diaphanous in membrane stabilization and compartmentalization. *J Cell Sci* 126, 1796-1805.
* equally contribution

Gummalla, M., Winkler, F., Kuenneke, L., **Lv, Z**., Zippelius, A., Aspelmeier, T., and Grosshans, J., Fluctuation analysis of centrosomes reveals a suppressive role of Kinesin-1, *J Biophysics* (2014), submitted

Acknowledgements

Acknowledgements

I would also like to thank Chinese Scholarship Council (CSC) to offer me 4 years scholarship.

Finally, I want to thank my parents and brother for their endless support.